Design of a Deployable Tape Spring Half Wavelength Dipole Antenna for the ORCASat Nanosatellite

By

Levente Imre Buzas
B.Eng., University of Victoria, 2019

A Thesis Submitted in Partial Fulfillment
of the Requirements for the Degree of

MASTER OF APPLIED SCIENCE

in the Department of Electrical and Computer Engineering

Supervisory Committee

Design of a Deployable Tape Spring Half Wavelength Dipole Antenna for the ORCASat Nanosatellite

By

Levente Imre Buzas
B.Eng., University of Victoria, 2019

Supervisory Committee

Dr. Peter Driessen, Department of Electrical Engineering and Computer Science
Co-Supervisor

Dr. Afzal Suleman, Department of Mechanical Engineering
Co-Supervisor

Abstract

The focus of this thesis is the design, manufacturing and testing of a deployable radio antenna for the ORCASat nanosatellite. First, the context, motivation, requirements, as well as constraints for this project are introduced. Next, a brief overview of theoretical concepts relevant to the contents of this thesis are presented. After the introduction of the relevant background and theory, a literature review is undertaken, and an experiment-based methodology is established. Prior to conceptualizing a new design, detailed consideration is also given to previous attempts at designing a dipole for ORCASat. The root cause of the problems with these attempts is determined experimentally as the presence of ground planes on the circuit board supporting the antenna. After this preliminary investigation, the blocks required for the ORCASat antenna are introduced as the transmission line feeder, the balun, the impedance matching block, and the antenna arm feed. For each of these components, competing design concepts are developed, and the advantages and disadvantages of each of these concepts are presented. After this, the winning design concept is selected and developed into a manufacturable design. This design is identified as a tunable tape spring half wave dipole antenna featuring a specialized feed with electrically and mechanically optimal characteristics, no impedance matching, and a lossy choke balun wound from the coaxial cable feeder, all mounted on a circuit board in a pre-existing Delrin antenna deployer. Next, the manufacturing and assembly of this design is undertaken, followed by the consideration of an informal commissioning procedure. As part of this, a test article consisting of an incomplete prototype of the dipole is tested, and it is shown to have desirable voltage standing wave ratio, input impedance, and return loss characteristics, as well as excellent tunability. Having established that this test article is a good candidate to meet project requirements, it is updated to include as many of the final components of the antenna as possible. Then, formal test procedures for the verification of the tunability, return loss, VSWR, input impedance, antenna pattern, and absolute gain are established, and executed. Based on the results of this formal verification test campaign, it is concluded that the test article meets the requirements presented at the beginning of this thesis, and it is suitable as a radio antenna for the ORCASat mission. After this, the work is concluded by a set of recommendations for future work to prepare the antenna developed in this thesis for flight.

Table of Contents

List of Tables

List of Figures

Glossary

ADCS – Attitude Determination and Control Subsystem

BER – Bit Error Rate

CAD – Computer Aided Design

CCP – Canadian CubeSat Project

COTS – Commercial Off The Shelf

CSA – Canadian Space Agency

CSDC – Canadian Satellite Design Challenge

CVCM – Collected Volatile Condensable Material

CfAR – Centre for Aerospace Research

C&DH – Command and Data Handling Subsystem

DUT – Device Under Test

EIRP – Effective Isotropic Radiated Power

EOL – End of Life

EPS – Electrical Power Subsystem

FEP – Fluorinated Ethylene Propylene

HF – High Frequency

HQP – Highly Qualified Person

IARU – International Amateur Radio Union

IC – Integrated Circuit

ISS – International Space Station

LEO – Low Earth Orbit

LTCC – Low Temperature Co-Fired Ceramic

LTO – Lithium Titanate

MECH – Mechanical and Thermals Subsystem

NASA – National Aeronautics and Space Administration

ORCAS – Orbiting Configurable Artificial Star

OBC – On-Board Computer

OD – Outside Diameter

PCB – Printed Circuit Board

PLA – Polylactic Acid

PTFE – Polytetrafluoroethylene

RF – Radio Frequency

RL – Return Loss

SMT – Surface Mount Technology

SOLT – Short Open Load Trough

TML – Total Mass Loss

TRL – Technological Readiness Level

TT&C – Telemetry, Tracking and Command Subsystem

UHF – Ultra High Frequency

UVic – University of Victoria

VNA – Vector Network Analyzer

VSWR – Voltage Standing Wave Ratio

List of Mathematical Symbols

D – Directivity

D_0 – Maximum Directivity

U – Radiation Intensity

U_0 – Maximum Radiation Intensity

ϕ – Azimuth Angle

θ – Elevation Angle

I – Electrical Current

R – Electrical Resistance

e_c – Conduction (I_2R) Loss

e_d – Dielectric Loss

e_{cd} – Antenna Radiation Efficiency

G –Gain

G_0 – Maximum Gain

Z_A – Antenna Input Impedance

R_A – Real Component of Antenna Input Impedance

j – Imaginary Constant

X_A – Imaginary Component of Antenna Input Impedance

α – Phase Angle

Z_G – Generator Source Impedance

R_G – Real Component of Antenna Generator Source Impedance

X_G – Imaginary Component of Generator Source Impedance

μ – Scalar Magnetic Permeability

ε – Electrical Permittivity

VF – Velocity Factor

VF_{coax} – Coaxial Cable Velocity Factor

$VF_{microstrip}$ – Microstrip Transmission Line Velocity Factor

Z_{in} – Input Impedance

Z_0 – Transmission Line Characteristic Impedance

β – Wavenumber

l – Physical Transmission Line Length

ε_{re} – Effective Relative Permittivity

λ – Wavelength

c – Speed of Light

f – Frequency

Ω – Ohms

D_{max} – Maximum Antenna Physical Dimension

μ_c – Complex Magnetic Permeability

μ' – Real Part of the Complex Magnetic Permeability

μ'' – Imaginary Part of the Complex Magnetic Permeability

$|S_{12}|$ – Magnitude of Gain of 2-port Network, Forward Direction

$|S_{21}|$ – Magnitude of Gain of 2-port Network, Reverse Direction

L – Transmission Line Electrical Length

Z_L – Load Impedance

$\mathbf{G_{test}}$ – Test Antenna Gain

$\mathbf{L_{path}}$ – Free Space Path Loss

$\mathbf{G_{DUT}}$ – Device Under Test Gain

d – Physical Distance

W – Watt

E – Electric Field Strength

H – Magnetic Field Strength

Γ – Complex Reflection Coefficient

∞ - Infinity

r – Distance From Antenna To Arbitrary Point In Space

$\mathbf{r_{min}}$ – Minimum Distance From Antenna To Far Field

n – Counting Variable

Dedication

Squiddy, thank you for being the most supportive, loving, and caring partner anyone could ever ask for. Without you, my MASC work would not have been possible. I dedicate this thesis to you.

Acknowledgements

I would like to extend my sincere gratitude to the people listed below. Without their motivation, support, patience, contributions, practical guidance, and insights, my graduate studies and the work presented in this thesis would not have been possible.

- Eszter & Ferenc Buzás
- Peter Driessen
- Afzal Suleman
- Roger Graves
- Alexander Doknjas
- Tristan Tarnowski
- Josiah Macleod
- Maarteen Meerman
- Alireza Seyfollahi
- Jens Bornemann
- Deisy Mamedes
- Stefan Bichmaier
- Stephen Harrison
- Mark Wheen
- József Pankaczy

1 Introduction

1.1 Introduction

1.1.1 The Commercialization of Space

The commercialization of space at the advent of the 21st century has brought on an unprecedented rise in spacecraft development. Advances in microelectronics circuits, and the resulting availability of commercial off the shelf (COTS) components, as well as a drastic drop in the cost of launch due to standardization made spacecraft development and operation available to entities which could never consider undertaking such activities. This is illustrated by the contrast between Figure 1 and Figure 2, showing that in the period between 1966 and 2020, satellite development has become a widely proliferated activity.

Figure 1: Countries with satellites in 1966. Adapted from [1].

Figure 2: Countries with satellites in 2020. Adapted from [1].

One key player in this revolution has been nanosatellites, and CubeSats in particular. Nanosatellites are small satellites with a weight of 1-10 kg, while CubeSats are satellites of standardized building blocks, which often fall into the nanosatellite classification [2]. The concept of a CubeSat is illustrated in Figure 3. Taking a cube of 10 cm side (the "1U" building block), a spacecraft of standard dimension is constructed by stacking the cubes in various 3D configurations. CubeSats are often developed by university teams, due to the excellent and affordable learning opportunity they provide to students by exposing them to actual satellite missions, which can be undertaken at a fraction of cost compared what is required to develop large spacecraft.

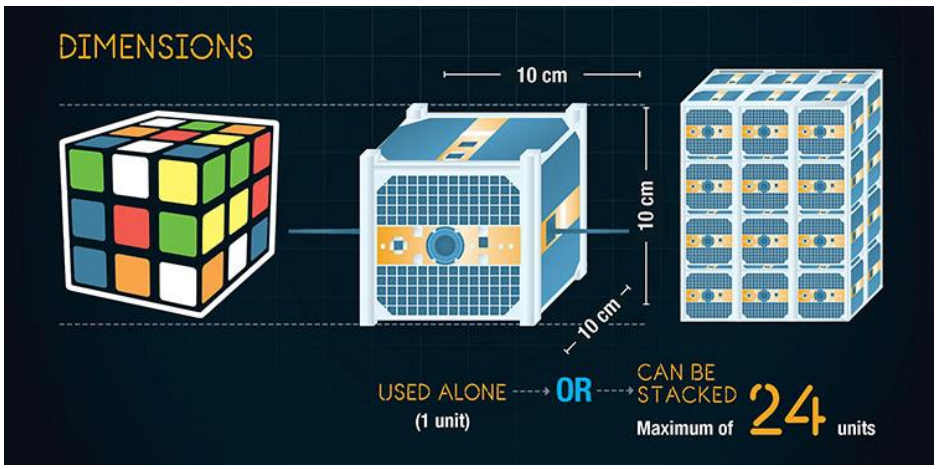

Figure 3: The CubeSat concept – spacecrafts of standard dimensions. Adapted from [3].

1.1.2 Nanosatellite Development in Canada

In Canada, most universities have a student satellite design team. These teams regularly compete in the Canadian Satellite Design Challenge (CSDC), which is a Canada-wide design competition focused on CubeSat development [4]. While a great learning experience, this initiative has not resulted in a successful Canadian CubeSat launch to date.

The only academic organizations in Canada which have successfully launches CubeSats have been the University of Alberta [5], as well as the University of Toronto and York University [6]. To change this, in April 2017 the Canadian Space Agency (CSA) has started a new initiative called the Canadian CubeSat Project (CCP). This offers opportunities and funding for academic partnerships

lead by Canadian universities to develop CubeSats, and train highly qualified personnel (HQP) to supply the Canadian aerospace engineering market with talent [7].

One of such partnerships which has been awarded an opportunity to participate in the CCP has been the academic partnership University of Victoria Centre for Aerospace Research (CfAR) [8]. CfAR's submission, the ORCASat mission, provides the framework in which the antenna design project in this thesis has been undertaken.

1.2 ORCASat

1.2.1 Mission Overview

The ORCASat mission consists of the design, manufacturing, and operation of a nanosatellite conforming to the 2U CubeSat specification. The objectives of this mission are student education and space science. Primarily, the ORCASat project is intended to train HQPs for the Canadian aerospace market by giving students an opportunity to participate an actual space mission as part of their education. To facilitate this learning opportunity, a scientific mission is also undertaken. This is illustrated in Figure 4. As shown, a calibrated light source is provided in low earth orbit (LEO) to selected ground based optical observatories to remove the effect of the atmosphere from their measurements, thus improving the quality of the science they output. The science impact of this mission is notable. This is well illustrated by the fact that the US National Aeronautics and Space Administration (NASA) is planning a mission dubbed Orbiting Configurable Artificial Star (ORCAS), which will tackle the same scientific problem as ORCASat, except without the constraints of a 1U CubeSat [9].

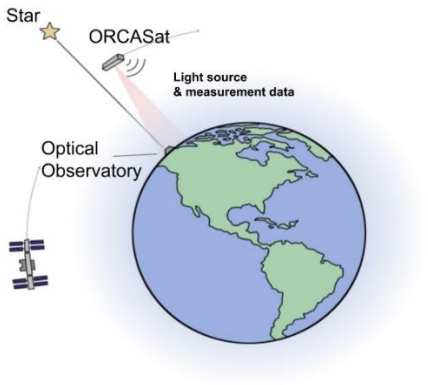

Figure 4: High level illustration of the ORCASat mission concept.

1.2.2 The ORCASat Nanosatellite

1.2.2.1 ORCASat Overview

The ORCASat spacecraft is a nanosatellite conforming to the 2U version of the CubeSat specification. It is illustrated in Figure 5. Externally, it is a 10 cm x 10 cm x 22.7 cm cube, covered in solar panels which are mounted on printed circuit boards (PCB) fastened to an aluminum chassis. Various appurtenances protrude from this body, such as sensors used for determining the orientation of the spacecraft, as well as radio antennas.

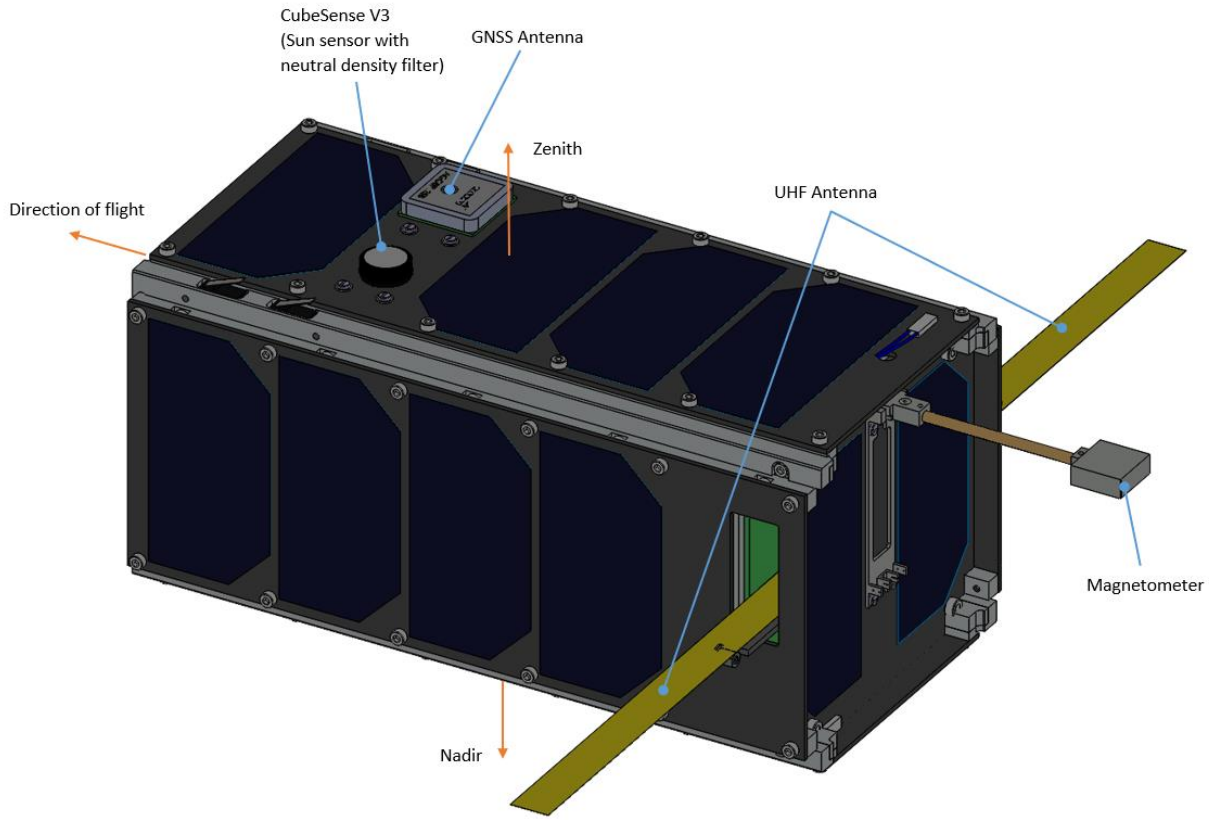

Figure 5: The ORCASat nanosatellite. Courtesy of T. Tarnowski.

Internally, the spacecraft is made up of the payload and the bus modules. These modules and their layout are illustrated in Figure 6. As shown, the payload module is situated near face of the spacecraft which is towards the direction of flight, and it takes up approximately 1U volume. This module contains all the electronic and mechanical components which make up the payload of ORCASat, the calibrated light source. The bus module is situated underneath this, away from the

direction of flight. It also takes up approximately 1U volume. This module contains all the subsystems which are required to enable the operation of the payload in LEO orbit.

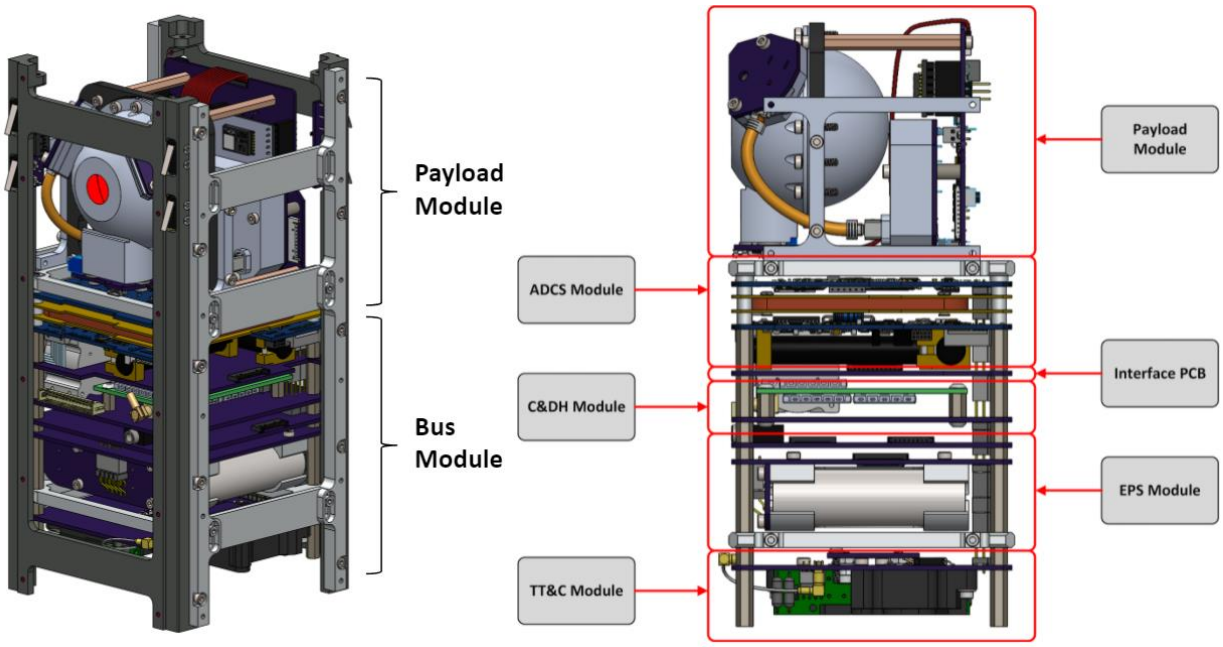

Figure 6: Internal arrangement of the ORCASat spacecraft. Courtesy of T. Tarnowski.

A brief introduction to the electronic subsystems found in the ORCASat bus is given below. They are included for completeness only, their detailed consideration asides that of the Telemetry, Tracking and Command (TT&C) subsystem are mostly irrelevant to this thesis.

- Mechanical and Thermals Subsystem (MECH): MECH is responsible for the mechanical and thermal design of the satellite structure and bus. The satellite structure is machined out of aluminum, and it is used to house the rest of the subsystems. It is designed in house.
- Command and Data Handling Subsystem (C&DH): The C&DH subsystem handles the operations of the satellite. C&DH consists of the On-Board Computer (OBC) and a real-time operating system which executes on the OBC. Both are designed in house.
- Attitude Determination and Control Subsystem (ADCS): Satellite attitude determination and control system, responsible for 3-axis stabilization of the spacecraft. This is a COTS module from CubeSpace, a South African provider of small satellite attitude control

solutions. It is a Y-momentum system consisting of three magnetorquers and one reaction wheel, as well as control software and sensors.

- Electrical Power Subsystem (EPS): Satellite power system. EPS is the hardware that generates, stores, and regulates power. It uses solar cells for power generation, and lithium titanate (LTO) batteries for energy storage. It is designed in house.
- Telemetry, Tracking & Command (TT&C): Satellite communications system, which allows wireless communications between the satellite (specifically the C&DH subsystem in the satellite bus) and the ground segment. This subsystem is considered in its own section due to its relevance to the work in this thesis. It is designed in house by the author of this thesis.

1.2.2.2 The TT&C Subsystem

For this thesis, the key subsystem of interest spacecraft bus module is TT&C. This is responsible for the signal transformations between the on-board computer (OBC) of the spacecraft, and the radio frequency (RF) link to the ground station. An overview of this subsystem is shown in Figure 7. As shown, the key elements of this subsystem are the modem (Texas Instruments CC1110), the RF front end (Qorvo RFFM6406), and the radio antenna (in-house dipole antenna). The entirety of this subsystem is being developed at the University of Victoria (UVic) by the author of this thesis.

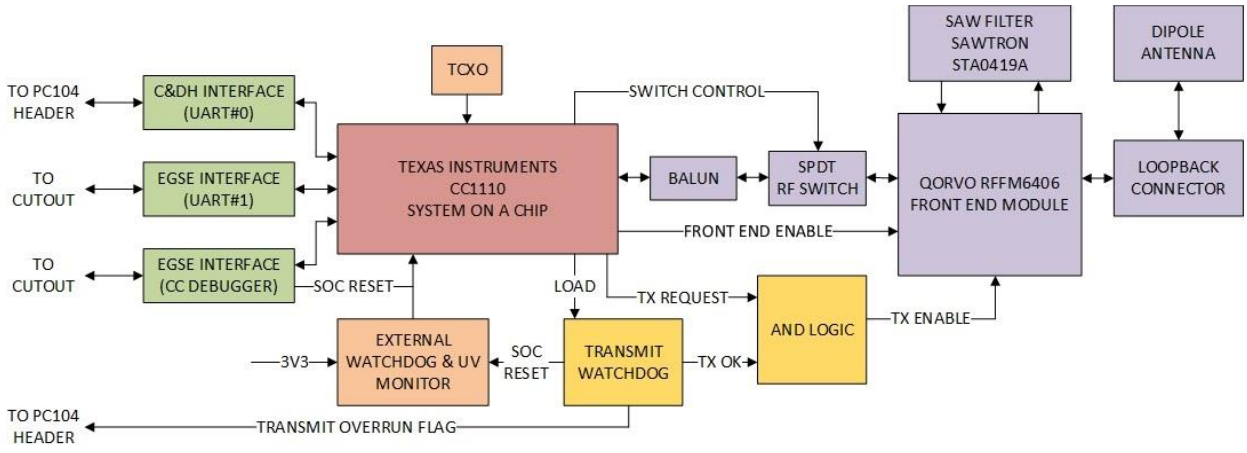

Figure 7: High level block diagram of the ORCASat TT&C subsystem.

1.2.3 The ORCASat Coordinate System

For clarity, consideration must be given to the various terms, directions, and references used to describe direction with regards to the body of ORCASat. To this end, the reference summary in Figure 8 is provided. The terms shown in parentheses along the axes (e.g. (zenith)) are going to be used to refer to direction with respect to the body of ORCASat.

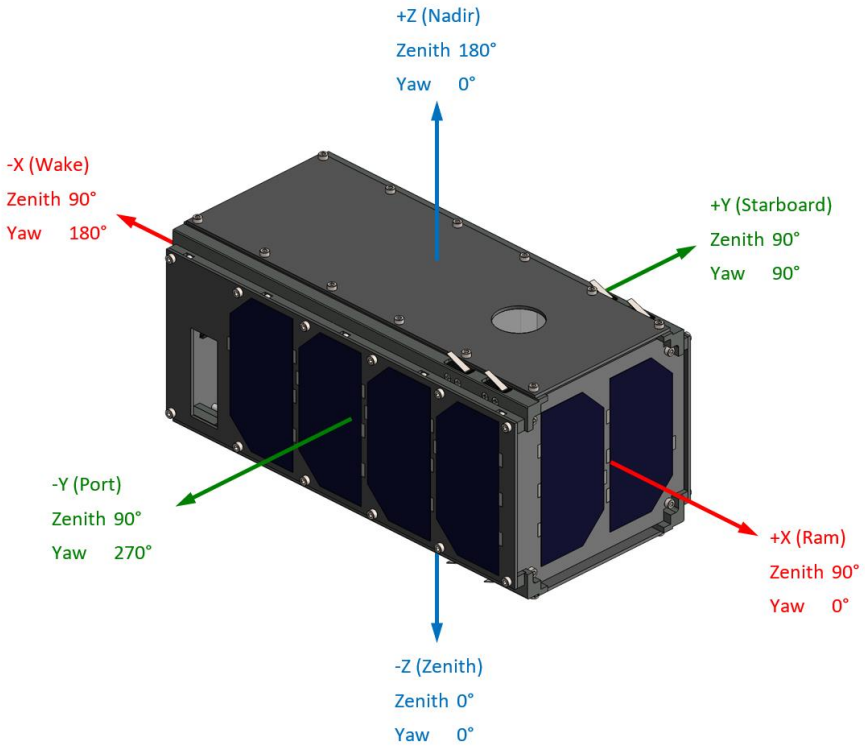

Figure 8: The ORCASat coordinate and reference system. Courtesy of T. Tarnowski.

1.3 Motivation

Since the kick-off of the project in 2018, the development of the ORCASat TT&C subsystem has yielded a working porotype containing the modem, the RF front end, and their supporting components. The design and implementation of the Earth station is also well under way. However, the design of an antenna for ORCASat has not been successful. This has been attempted several times by various members of the ORCASat academic partnership since the project started. Solutions of various complexity and technological readiness level (TRL) have been considered, from dielectric loaded patch antennas with complex geometry (e.g. planar inverted cone) to simple deployables. However, none of these attempts have progressed beyond paper concepts or failed prototypes. It is the need for a simple and reliable radio antenna for the

ORCASat, and the interest of the author in hardware development for amateur radio bands what resulted in the work which is the topic of this thesis.

1.4 Contributions

1.4.1 Overview

The focus of this thesis is the design, manufacturing and testing of a simple and reliable dipole antenna for the ORCASat CubeSat. The key items contributed to the state of the art are explained in the sections which follow.

1.4.2 Antenna Design

The design of a simple, reliable, and physically realizable dipole antenna was conceptualized and developed into a manufacturable design meeting formal requirements and constraints, for operation in the ORCASat bus, which is an environment extremely constrained both from the electrical and mechanical perspective.

1.4.3 Antenna Manufacturing and Assembly

The antenna design was manufactured and assembled into an prototypes of various complexity which were suitable to undergo formal and informal verification testing. As well, special procedures and methods were conceptualised and developed to streamline these manufacturing and assembly.

1.4.4 Antenna Testing

Formal and informal test procedures were developed, tested, and executed to verify that the antenna prototypes are suitable for flight, and meet the formal requirements for the ORCASat antenna. These procedures were developed to make the best use of the facilities at the University of Victoria, and avoid the need for time consuming experimentation and expensive and niche test equipment which are often considered prerequisite for antenna development.

1.5 Thesis Layout

The thesis document has been organized as follows:

- **Chapter 2:** The definition of the antenna design problem, and the introduction of the project requirements and constrains which the final product shall meet to be adequate for flight in ORCASat.

- **Chapter 3:** Explanation of theoretical concepts and vocabulary relevant to this thesis to equip the reader with the subject matter specific knowledge required to fully appreciate the antenna design work presented in this thesis.
- **Chapter 4**: A review of relevant literature to establish a baseline of knowledge related to the state of the art for in-house design of CubeSat dipole antennas for educational missions.
- **Chapter 5:** The conceptualization of the methodology used in the design of the dipole antenna for ORCASat, and a justification for why the practical methodology used is appropriate considering the various considerations impacting the project.
- **Chapter 6:** Investigation of the root cause of the previous ORCASat dipole problems. The previous design is introduced, analyzed, a hypothesis for the suspected cause is established, and an experiment is used to determine the merit of the hypothesis.
- **Chapter 7:** The development of the concept for the dipole antenna. The blocks necessary for the design of a dipole antenna meeting the requirements and constraints are inventoried, and various competing design concepts are generated. For each of these concepts, their advantages and disadvantages are discussed.
- **Chapter 8:** The detailed design of the dipole antenna, yielding a manufacturable product. The winning design concept is selected, suitable electrical and mechanical components are identified, and a manufacturable design is generated.
- **Chapter 9:** The manufacturing, assembly, and commissioning of the first prototype. The antenna design from the previous chapter is manufactured. The manufacturing is divided between in-house, and external sources depending on capabilities needed for the various components. The first prototype is assembled to an extent required for commissioning, and testing is used to evaluate if the design is suitable for a formal test campaign.
- **Chapter 10:** The verification testing of the dipole antenna prototype. The dipole prototype is put trough a formal verification test campaign to determine if it meets the requirements or not. The input characteristics, antenna pattern, and absolute gain of the antenna are verified.

- **Chapter 11:** Conclusions and recommendations for future work to prepare for space flight. It is concluded that the prototype meets the requirements, and it is recommended to undertake another circuit board revision to allow for some minor improvements which will make the antenna a better product. Recommendations about antenna testing in commercial facilities are also presented.
- **Appendix A:** Link budget analysis to explain the origins of a key project requirement.
- **Appendix B:** Supplemental information on the antenna deployer and the TT&C interface.
- **Appendix C**: Market search results for key components of the dipole design.
- **Appendix D:** Supplemental information on the design of the antenna feed.
- **Appendix E:** Raw measurement data for antenna patterns.
- **Appendix F:** Quote for commercial antenna test services.

2 Problem Definition

2.1 Statement of Need

The ORCASat TT&C subsystem needs a reliable antenna which enables it to meet all its requirements while respecting all the constraints which originate from the advanced design and manufacturing status of the spacecraft.

2.2 Requirements and Constraints

2.2.1.1 Overview

The topic of this section are constraints and requirements which must be fulfilled or respected during the design of the ORCASat radio antenna. These non-negotiable constraints and requirements are either mechanical or electrical in nature, and they originate from the ORCASat Mission & System Requirements [10] and the advanced stage of the design of the ORCASat spacecraft and mission.

2.2.1.2 Electrical

1. ***(Requirement)*** *The ORCASat antenna shall meet all its requirements over the 435.0 – 438.0 MHz amateur satellite allocation.*
    a. The ORCASat TT&C subsystem is designed for the 435.0-438.0 MHz amateur satellite frequency allocation. Since the assigned frequency of the spacecraft is not known in early stages of the design, the final product shall be able to work at any assigned frequency within the band of interest.
2. ***(Requirement)*** *The ORCASat antenna shall be a tape spring dipole deployed form the port/starboard faces of the spacecraft.*
    a. The mechanical design and manufacturing of the rest of the ORCASat bus leads the design of the antenna due to problems encountered with earlier design attempts. To prevent catastrophic delays with the project resulting from manufacturing delays , it was decided early on that the antenna will be as required above, and the rest of the bus was designed and manufactured to allow this.

3. ***(Requirement)*** *The ORCASat antenna, when connected to the transmit signal chain, must be able to produce -3.5 dBW effective isotropic radiated power (EIRP) when supplied with the final power amplifier of the ORCASat TT&C subsystem.*
    a. A preliminary downlink budget for a spacecraft with communication system and orbital parameters similar to ORCASat was constructed to confirm that the EIRP above is sufficient to close the link to the Earth station with a margin which is deemed adequate. This link budget is provided in Appendix A.

2.2.1.3 Mechanical

1. ***(Constraint)*** *The ORCASat antenna must use the antenna deployer housing which has already been designed and manufactured by the ORCASat MECH team.*
    a. The antenna deployer housing has already been designed and manufactured by the ORCASat MECH team to prevent catastrophic delays with the project. Their re-design and re-manufacturing is not feasible within the timeline of the project. For the details of this antenna deployer housing, please see Appendix B-1.
2. ***(Constraint)*** *The ORCASat antenna must use the deployment circuit and burn wire mechanism designed by the ORCASat MECH team.*
    a. The deployment circuit and burn wire mechanism has already been designed and manufactured by the ORCASat MECH team to prevent catastrophic delays with the project. Their re-design and re-manufacturing is not feasible within the timeline of the project. For the details of this circuit and mechanism, please see Appendix B-2 and B-3, respectively.
3. ***(Constraint)*** *The ORCASat antenna shall respect the ORCASat TT&C mechanical interface control document (ICD).*
    a. The ICD is the formal record of the characteristics the ORCASat antenna must have to interface with the rest of the bus. Respecting it is critical for an antenna design to be useful. For the ORCASat TT&C mechanical ICD, please see Appendix B-4.

4. ***(Constraint)*** *The antenna shall not utilize any non-metallic materials with a total mass loss (TML) greater than 1.0 percent or a collected volatile condensable material (CVCM) value of greater than 0.1 percent.*
    a. Non-metallic materials outgas in a vacuum, which may result in performance degradation to the outgassing components or their surroundings. Thus, the launch provider does not allow materials which represent outgassing concerns [11].

3 Theoretical Background

3.1 Overview

This section describes the theoretical foundation which is critical to understanding the work which has been presented in the thesis. It is assumed that the reader has a generic background in electrical engineering and radio frequency systems. Coverage is limited to what is essential to the thesis research for conciseness.

3.2 Key Antenna Performance Metrics

3.2.1 Overview

Some of the key antenna performance metrics which have been deemed relevant for this thesis are radiation pattern, bandwidth, gain, directivity, antenna efficiency, and input impedance. While other parameters (e.g. polarization, front to back ratio, antenna temperature) can also be important for other antennas, they have lesser relevance to the work presented, so they are not considered any further.

3.2.2 Radiation Patterns and Directivity

Antennas are devices which guide electromagnetic waves from a transmission structure of some kind to free space, and vice versa. The radiation properties of any antenna are characterized by three closely related parameters – directivity, gain, and radiation efficiency.

Directivity is defined as the *"ratio of the radiation intensity U (in W/unit solid angle) in a given direction from the antenna to the radiation intensity over all directions, U_0"*, and it is defined mathematically as below. If a direction is not given, it is implied that the direction of maximum directivity is under consideration [12].

$$D = \frac{U}{U_0} \tag{1a}$$

Since directivity is a directional parameter, it is sensible to consider it over all directions, in the form of a 3D radiation pattern described by the equation below. According to Balanis, a *"radiation pattern (…) is defined as a mathematical function or a graphical representation of the radiation properties of the antenna as a function of space coordinates"* [12]. This is illustrated in Figure 9.

$$D(\varphi,\theta) = \frac{U(\varphi,\theta)}{U_0} \qquad (1b)$$

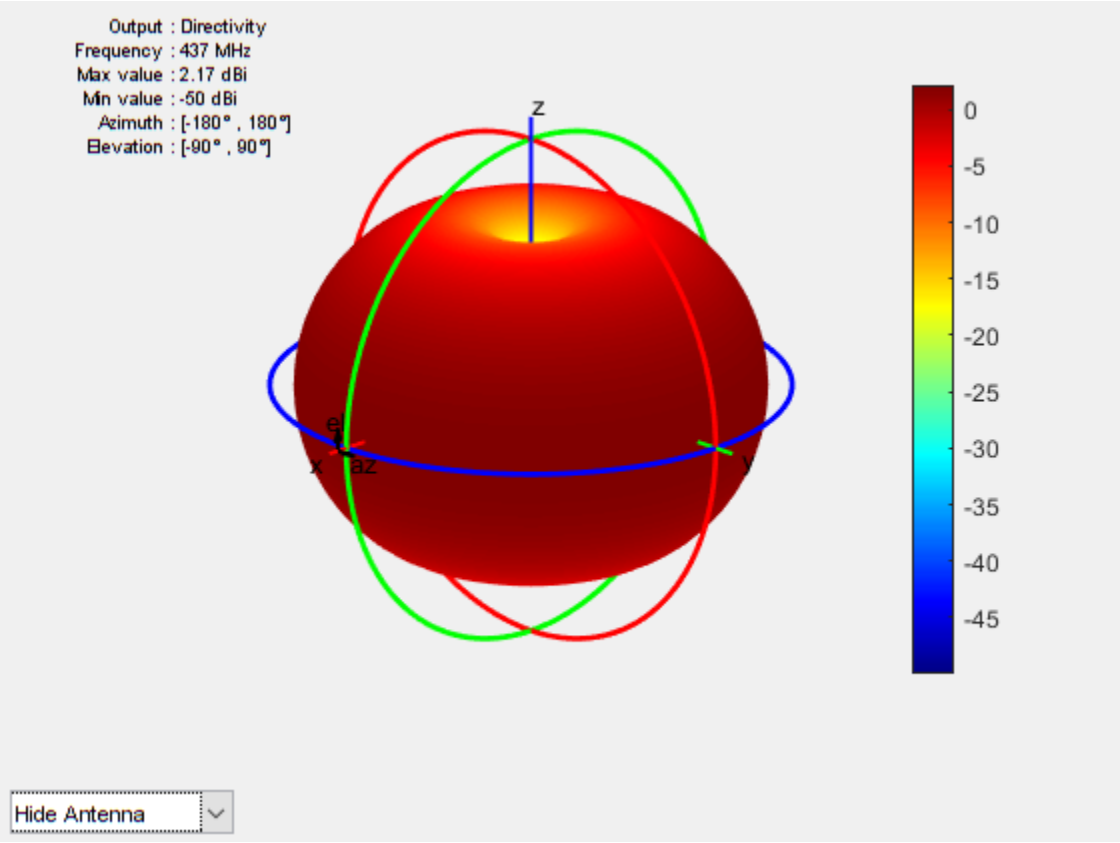

Figure 9: Sample 3D directivity pattern generated by MATLAB for an ideal half wavelength centre fed dipole for 437 MHz.

One simplified way to represent a directivity pattern is as polar cuts of the 3D pattern in the so-called E and H planes. According to Balanis, the E-plane is defined as *"the plane containing the electric field vector and the direction of maximum radiation"*, and the H-plane as *"the plane containing the magnetic-field vector and the direction of maximum radiation"* [12]. These plots may be logarithmic or linear, and they may be normalized to the maximum gain.

For the ideal dipole antenna example of Figure 9 where the dipole is located along the z axis, the E-plane is any plane is the x-z plane, or any other plane which is the rotated copies of this plane around the z axis by the azimuth angle ϕ, while the H plane is the x-y plane. This idea is illustrated in Figure 10 with an E-plane example.

3.2.3 Antenna Gain and Radiation Efficiency

While the 3D properties of an antenna are accounted for by directivity, its efficiency is not. Gain G is another commonly used antenna parameter, which takes both into account. This is defined by Equation 2a, where e_{cd} is the unitless antenna radiation efficiency [12]. Just like for directivity earlier, if a direction is not given, it is implied that the direction of maximum gain is under consideration

$$G = e_{cd}D \tag{2a}$$

Antenna gain, just like directivity can be represented as a 3D pattern, or its E and H plane cuts. For example, since they have been plotted for an ideal dipole, the patterns of Figure 9 and Figure 10 can also be considered gain plots, but assuming that e_{cd}=1 in Equation 2b.

$$G(\varphi,\theta) = e_{cd}D(\varphi,\theta) \tag{2b}$$

One common way to define gain in “decibel over isotropic” or dBi, referencing it as some dB above or below the gain an isotropic antenna would have in the direction of interest. While other definitions also exist (e.g. dBd), this will be adapted for this thesis.

Antennas have various losses associated with them, which give rise to the antenna efficiency e_{cd} considered earlier. This parameter describes how effectively the antenna can transform the electromagnetic waves fed to/from it in a guiding medium to electromagnetic waves in free space. The losses which are commonly considered to be making up the overall antenna efficiency are the mismatch/reflection losses at the antenna terminal, and I^2R losses made up of conduction e_c and dielectric e_d losses in the antenna itself. For the purposes of this thesis, the antenna gain used will not account for the reflection losses as part of the gain, thus the definitions in Equation #2 hold. The reason for this that the requirement for the performance is specified in terms of EIRP, which is calculated in a manner which accounts for reflection losses separately from the gain.

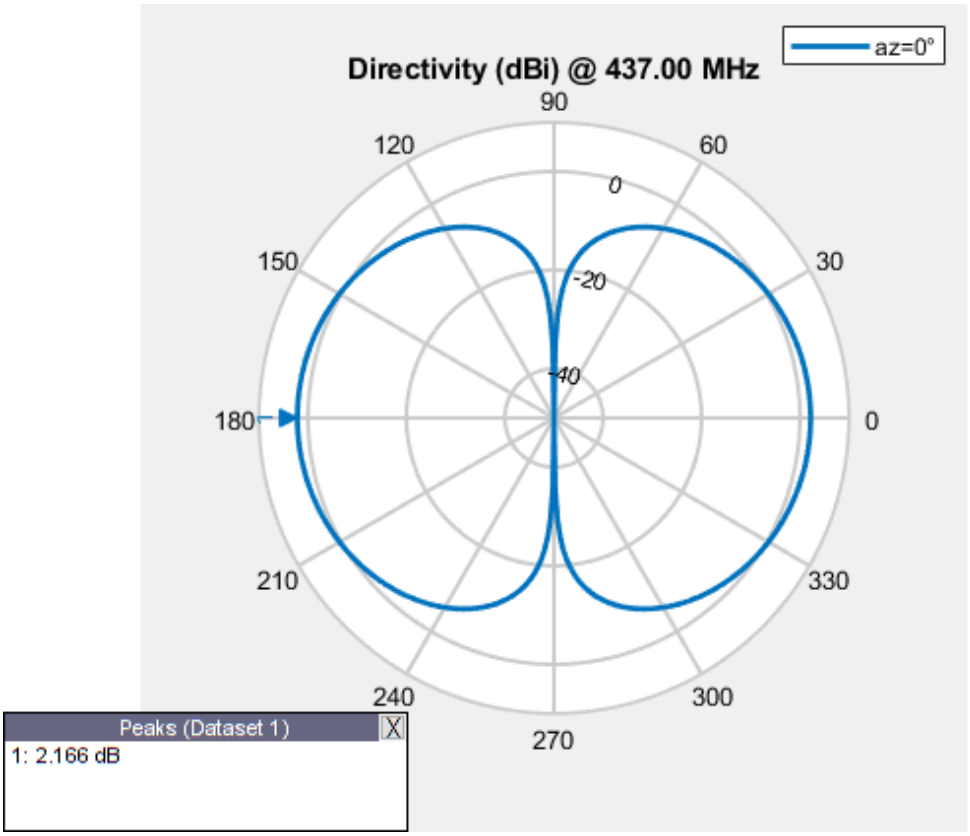

Figure 10: Sample E plane directivity plot generated by MATLAB for the example dipole introduced in Figure 9.

3.2.4 Antenna Bandwidth

Another key antenna parameter is its bandwidth, which is simply the frequency range over which the antenna maintains some performance parameter, such as input return loss, within a prescribed range. Bandwidth is important, because operating frequencies are rarely known exactly at the beginning of the antenna design process, and antennas are often designed for frequency bands which may be extremely wide or narrow. Antenna bandwidth can be defined in many different ways (e.g. % bandwidth). For this thesis, the requirement for bandwidth performance is set in terms of an ability to support a certain EIRP over a given frequency range. This means that the antenna shall be able to produce the target -3.5 dBW EIRP, regardless of the operating frequency in a 3 MHz span centered on 436.5 MHz.

3.2.5 Antenna Input Impedance

In terms of its interaction with the entities interfacing with it, the most critical parameter of an antenna is its input impedance Z_A, which is the ratio of voltage and current at its terminals. This parameter is made up of the antenna resistance R_A and reactance X_A, as shown below.

$$Z_A = R_A + jX_A \tag{3}$$

Two common ways to characterize the interaction of an antenna with entities external to it are power transfer and reflections. For maximum power transfer considering a generator with an impedance of $Z_G = R_G + jX_G$, directly connected to the antenna input terminals, it is desirable for the real part of the antenna and generator impedance to match exactly, and the imaginary parts to cancel each other, in a situation know as conjugate match [12], summarized by the equations below. This ensures that maximum power transfer between the two entities occurs.

$$R_A = R_G \tag{4}$$

$$X_A = -X_G \tag{5}$$

The other way to describe the interaction of an antenna with entities external to it is the extent to which guided radio waves in a feeder with a characteristic impedance of Z_0 incident on the antenna terminals are reflected. The extent of this is given by the complex reflection coefficient Γ, defined in terms of the antenna input impedance Z_A and Z_0 [13].

$$\Gamma = |\Gamma|e^{j\alpha} = \frac{Z_A - Z_0}{Z_A + Z_0} \tag{6}$$

This reflection coefficient gives rise to two other important parameters which are relevant to the practical design of antennas. These are the return loss (RL) and the VSWR, given by the equations below in terms of Γ. These are extremely useful parameters from the perspective of practical antenna design because both are easily measured with a vector network analyzer (VNA).

$$VSWR = \frac{1 + |\Gamma|}{1 - |\Gamma|} \tag{7}$$

$$RL(dB) = -20\log_{10}(|\Gamma|) \tag{8}$$

The interpretation of Γ, VSWR, and RL is as follows. Γ may range from -1 for a short circuit (Z_A=0 Ω), 0 for a perfectly matched antenna (Z_A=Z_0), and +1 for an open circuit (Z_A=∞). VSWR will be a positive number ≥1, with a ratio of 1:1 describing a perfect match. RL will be a negative number, and the greater the magnitude of this number is, the better match it represents.

3.3 Transmission Lines

3.3.1 Overview

While a comprehensive treatment of transmission lines is not relevant for this thesis, the consideration of antennas can not go without the consideration of transmission lines. Every antenna requires a transmission line to guide RF energy to/from it, and transmission lines also have important applications in the constructions of baluns and impedance matching devices.

Transmission lines take many physical forms, but for this the work of this thesis, only coaxial cables and microstrip PCB lines are relevant. Other types of transmission lines (e.g. waveguides) are impractical to be used in a 2U CubeSat in the 435.0-438.0 MHz frequency range due to their size. The key transmission line parameters which are of interest for this thesis are the characteristic impedance Z_0, velocity factor VF, loss per unit length, and input impedance Z_{in} for certain special transmission line lengths. For coaxial cables, the minimum bending radius is also interest.

3.3.2 Characteristic Impedance

The characteristic impedance of a transmission line is a consequence of its geometry. The relationship guiding this can be found on pp. 55 and pp. 145 of Pozar for coaxial cables and microstrip lines, respectively [13]. In practice, coaxial lines are purchased from an established manufacturer with a specified (e.g. 50 Ω) impedance, while microstrip lines are designed using computer aided design (CAD) tools like Altium to have the desired target impedance.

3.3.3 Velocity Factor

When radio waves are propagating in coaxial cables, they are slowed down. As a result, an electrical and as physical length may be distinguished for a transmission line. To quantify this, the so-called velocity factor VF is defined. This describes the speed of the waves in the line as a certain percentage of the speed of light c=299 792 458 m/s, and it is a unitless number between 0 and 1. VF is defined for coaxial cables and microstrip lines as below, where ε_{re} is the effective relative permittivity [14].

$$VF_{coax} = \frac{1}{\sqrt{\mu_r \varepsilon_r}} \tag{9a}$$

$$VF_{microstrip} = \frac{1}{\sqrt{\varepsilon_{re}}} \tag{9b}$$

3.3.4 Line Loss

The loss of transmission lines is also of obvious importance – it determines the "price" which must be paid for their use in terms of power loss. The loss is usually expressed in terms of dB/units of length. The determination of this number is not trivial - the process for that can be found on pp. 79-80 and pp. 145 of Pozar for coaxial cables and microstrip lines, respectively [13]. In practice, the loss is given by the manufacturer for coaxial cable, and it is determined by simulation for the microstrip lines.

3.3.5 Input Impedance

A lossless transmission line will have an input impedance Z_{in} which depends on its characteristic impedance Z_0, the wavenumber β, its electrical length l, and the load impedance Z_L attached to its far end, according to the formula given by Pozar [13].

$$Z_{in} = Z_0 \times \frac{Z_L + jZ_0 \tan(\beta l)}{Z_0 + jZ_L \tan(\beta l)} \tag{10}$$

This is a very important formula, because it has some special cases which are of great practical interest for antenna development. When $l=(n\times\lambda)/2$ with n positive integer, $Z_{in}=Z_L$ – so for transmission lines which are integer multiples of electrical half-wavelength, the load impedance is transformed to the close end of the cable unchanged.

This means, that if the far end of such cable is attached to an antenna feed point with an unknown impedance Z_A which can not be measured directly, that impedance will be available for measurement at the close end of the electrical half wavelength line. The theoretical length L for this line can be determined using the formula in terms of the velocity factor VF below, where f is the intended frequency where the line is to be half wavelength.

$$L = \frac{c}{f} \times 0.5 \times VF \tag{11}$$

In practice, lines of specific electrical length are constructed using measurement instead of calculation. To do this, a basic understanding of the Smith Chart is critical.

3.4 The Smitch Chart

An extremely useful practical tool in the solution of transmission line and impedance matching problems is a Smith Chart. This is a polar plot of the complex reflection coefficient Γ which can be used to convert reflection coefficients to impedances, and vice versa. It can too be used to solve transmission line problems, as Equation #10 can be represented in terms of Γ [13].

Modern VNAs have the capability to display Smith Chart measurements directly, giving a graphical summary of the test article performance without getting lost in the mathematics of the governing equations. Some practical considerations which are utilized later in this thesis to streamline development are explained below.

- Points on the Smith Chart are normalized impedances. If the point is above the x axis, the impedance is inductive, if it is on the x axis it is purely real, and if it is below the x axis it is capacitive.
- On a Smith Chart, an open circuit is shown at coordinates [1,0], a perfect match at coordinates [0, 0], and a short circuit at coordinates [-1,0] if a Cartesian coordinate system considered, centered on the Smith Chart. The closer a point to the centre of the chart is, the better impedance match it corresponds to.
- The input impedance of transmission line segments for various loads can be determined by rotation around the chart. If a point corresponding to Z_L is plotted on the chart, a clockwise rotation of the point around a circle of constant radius, to an extent given by the electrical line length, will reveal Z_{in} at the closer end of the cable. This also implies that a full rotation around the chart corresponds to an electrical length of $l=\lambda/2$ because at that rotation we return to the starting point, and thus $Z_{in}=Z_L$.

3.5 Dipole Antennas

Dipole antennas are a pair of electrical conductors of equal or unequal length which are a certain fraction of the wavelength λ at which the dipole is designed to operate. They are one of the first types of antennas that humans successfully realized in the 19th century. Their most common type is the so-called centre fed half wavelength dipole where the dipole arms are each λ/4 long. This is a highly desirable type of antenna because it is electrically efficient, it is very simple, and its theoretical input impedance has a desirable real component of 73 Ohms [12].

$$Z_{in} = 73 + j42.5\ \Omega \tag{12}$$

This real component is attractive, because common transmission lines often have 50 Ω or 75 Ω characteristic impedances, making it easy to attach dipoles to these types of feed lines, either by pruning the antenna arms until resonance is obtained at the frequency of interest, and the inductive component is eliminated by definition, or employing a matching network to eliminate the inductive reactance.

The radiation pattern (gain or directivity) of a dipole takes the form of a symmetric doughnut – this was already illustrated in Figure 9 and Figure 10. Its maximum gain is normal to the axis of the dipole, and it theoretically measures 2.16 dBi [12].

It is noted that this pattern is measured in the so-called far field or Fraunhofer region away from the dipole, which is the region of space defined as below, where r is the distance from the antenna, D_{max} is the largest dimension of the antenna, and λ is the wavelength of operation [12].

$$\infty \geq r \geq \frac{2D_{max}^2}{\lambda} \tag{13}$$

In theory, centre fed dipole antennas are balanced structures – the impedances of their conductors to the reference plane are equal in magnitude and phase [15]. However, in practice, this will only be true to a limited extent due the impact of the dipole's feed line and surroundings, the latter of which can be very difficult to mitigate. To deal with the impact of the feed line on the imbalance is much easier to deal with– it just needs to be isolated from the antenna to make sure that only the power received or intended to be radiated is transferred between the antenna and the feeder. To better understand this issue, the diagram in Figure 11 needs to be considered [16].

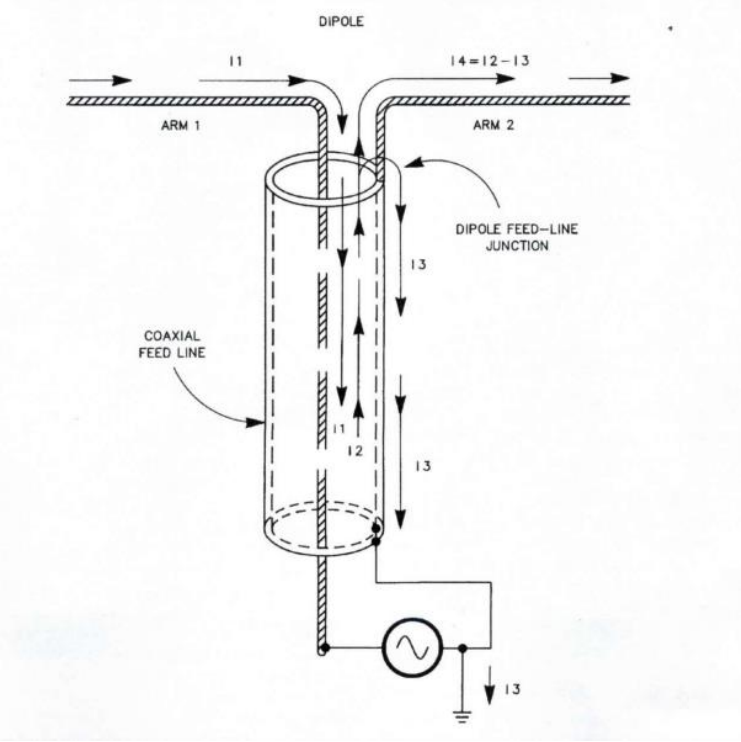

Figure 11: Illustration of the various current paths at the feed point of a dipole. Adapted from [12].

As shown, currents at the feed point of a dipole obey the skin effect, flowing only on or near the surfaces of conductors. However, this results in the common mode current I_3, unequal currents in the dipole arms, and unintended feedline radiation, pattern distortion, and the pick up of noise. To minimize or eliminate this interaction, a balun needs to be used to isolate the feed line from the antenna, or this common mode current I_3 resulting from the skin effect must be reduced as much as possible.

3.6 Ferrite Materials

3.6.1 Overview

Ferrite materials are ceramics of high magnetic permeability made up of various metal oxides. They are often used in the construction of baluns and chokes, so a basic consideration of their properties is of importance. The key concepts to introduce are material mixes, impedance, and resonance.

3.6.2 Material Mixes

Material mixes are various combinations of metal oxides tuned by the manufacturer to exhibit certain electrical characteristics (e.g. NiZn, MgZn). To understand their characteristics, an

understanding of the complex magnetic permeability μ_c is need, which is a tool for dealing with high frequency magnetic fields. This is defined as below [17].

$$\mu_c = \mu' + j\mu'' \tag{14}$$

Mixes can be characterized by a plot of their complex permeability μ_c against frequency, on which the real component defines inductance and the complex component the loss [15]. This is illustrated in Figure 12 with the example of Mix #61, a material which is inductive up to ~25 MHz and lossy above ~200 MHz.

3.6.3 Impedance and Resonance

Since ferrites are often used for suppression in the form of chokes, manufacturers often specify the impedance a single turn choke would have, if it was wound on this material from insulated wire. This specification is based on measurement, and it describes at what frequencies and to what extent the choke can be used for suppression applications. On these graphs, the frequency at which the resistive component is maximum and the reactive vanishes is called resonance – this is where the material is most suitable for suppression. This is illustrated by Figure 13, where the material is resonant around 750 -850 MHz.

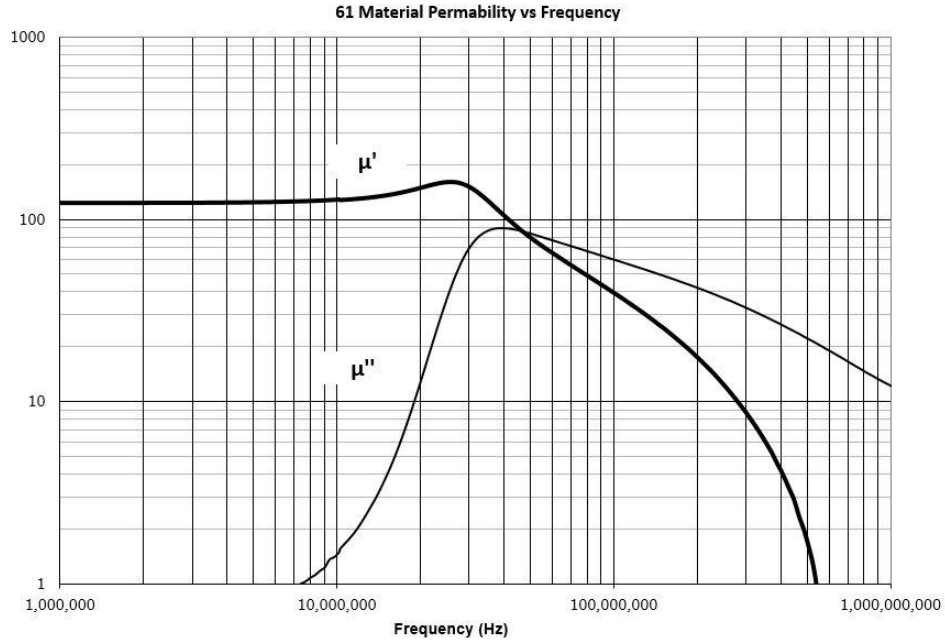

Figure 12: Mix #61 permeability against frequency. Adapted from [18].

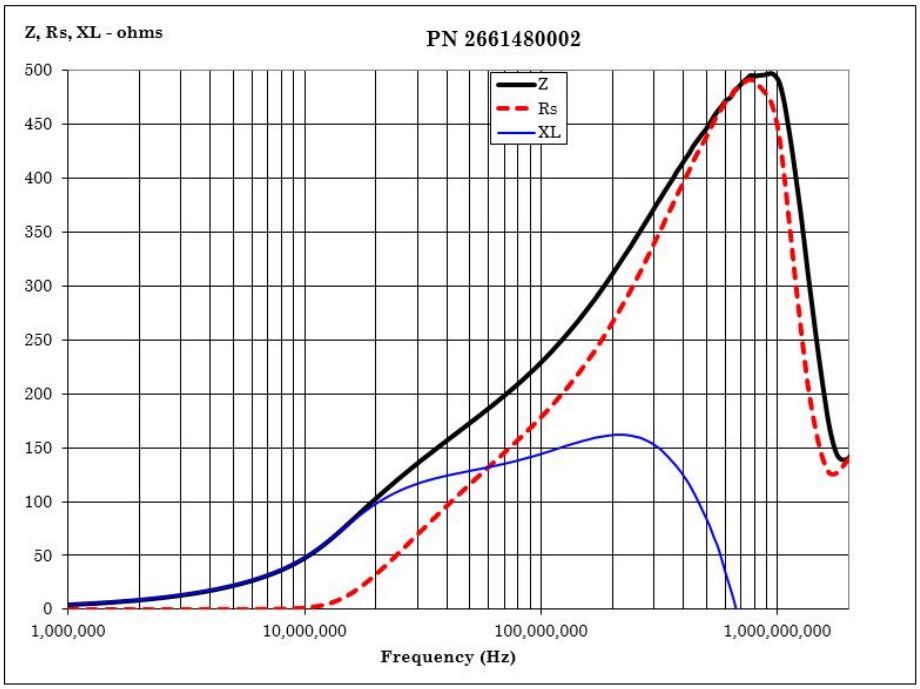

Figure 13: Single turn impedance test results for the 2661480002 Fair-Rite core. Adapted from [19].

For chokes, the choking impedance is approximately proportional to the number of turns from which the choke is wound [15]. This can be beneficial for the construction of chokes with high choking impedance, which is desirable. However, care must be taken as winding multiple turns may shift the resonance downwards in frequency, as illustrated in Figure 14. This is the impact of the change introduced by the increased stray capacitance between the wires used to wind the choke, and it may render the choke useless at the frequency of interest if the initial single turn resonance wasn't high enough in frequency [15].

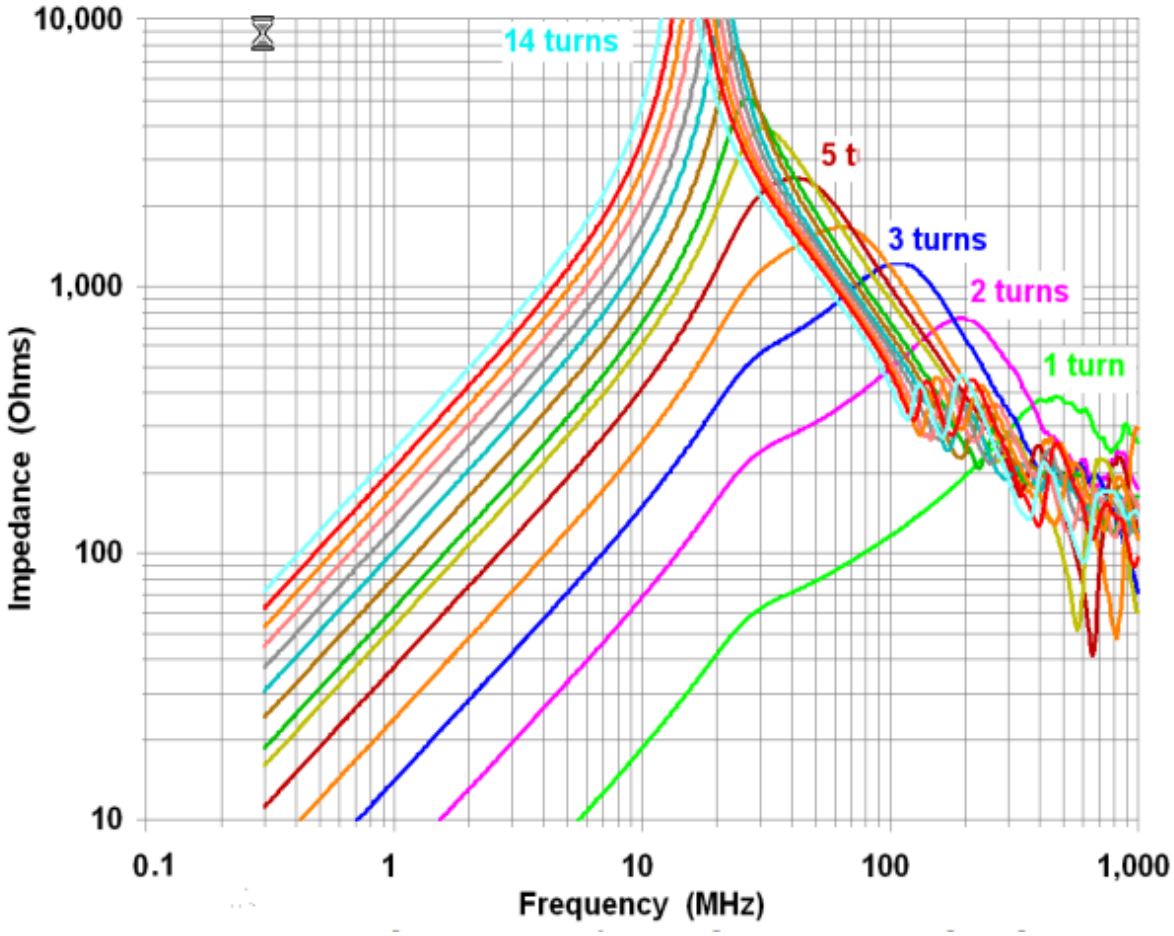

Figure 14: Measured impedance of multi-turn choke on Fair-Rite Type #61 material. Adapted from [15].

4 Literature Review

The topic of this chapter is a brief review of the state of the art for non-commercial deployable dipole antennas for nanosatellite and CubeSat applications. Reviews concerning with antenna types other than dipoles exist (e.g Abulgasem et. al. [20]), but their relevance to this thesis is limited, because the antenna type for ORCASat is constrained to be a dipole. To prepare this review focused on dipoles, an obvious starting point is a survey of CubeSats launched to date. Based on such survey, those missions which have utilized non-commercial dipole antennas can be identified, and literature discussing their design and characteristics can be located.

The most complete databases concerning with CubeSats are those by Krebs [21], Kulu [22], Swartwout [23], Klofas [24], Rupprecht et. al. [25] as well as Wakita [26]. However, only the database by Klofas contains information on the type of antenna used by the catalogued missions. Thus, that is the only one which will be considered here. This database contains a total of 757 CubeSats, considering deployments up to November 23, 2018. Out of these missions, 152 used a dipole antenna of some kind [24].

Out of the 152 CubeSats missions which flown with dipole antennas, only a small sub-set was a source of meaningful antenna design information. This may be attributed to various factors. First, a number of these missions were developed by commercial entities, militaries, or government organizations. This is illustrated by the information in Figure 15. As a result, any design information associated with these spacecraft is likely to be proprietary, and not be released in the public domain. Second, a number of these missions used COTS antennas. Antenna development has a steep learning curve associated with it, and not all organizations developing CubeSats are prepared for to undertake this process. For these antennas, only the integration of the product into the spacecraft is of interest, not the detailed design of the antennas itself. Thus, these types of missions do not produce useful literature either.

The remainder of the missions are those which attempt the design of their antennas in house and publish information about this process. These can be divided into two categories. The first of these categories is comprised of missions where design of custom dipole antennas of various kind (e.g. conventional straight centre fed dipole, V dipole, dipole with reflector element, LC loaded

dual band dipole) are undertaken, but the projects aren't developed further than the concept development [27] or simulation stage [28] [29] [30] [31] [32]. The utility of this literature is limited because experimental validation of the simulation results is missing, and the validity of the presented claims and conclusions can not be independently evaluated.

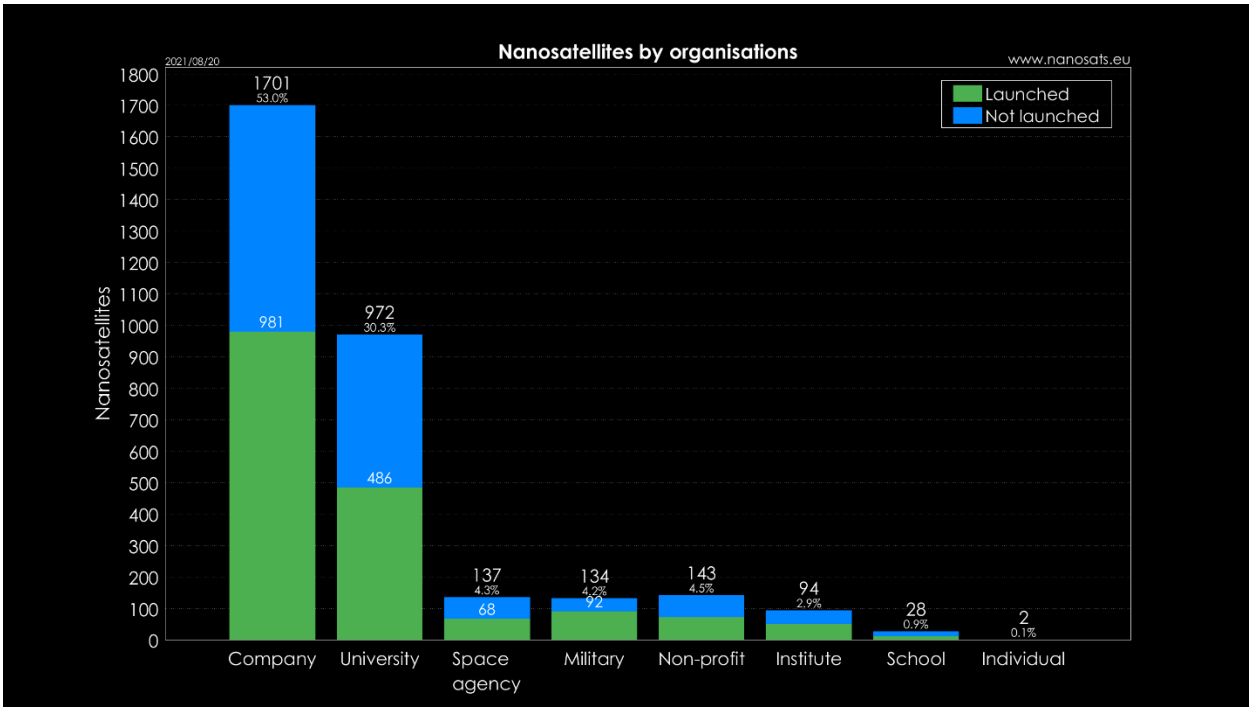

Figure 15: Nanosatellite launches by organisation types. Adapted from [22].

The second category of literature is produced by missions which design their antennas in house, and either use experiments to validate their concepts or simulations or report successful in-orbit operations. These are the most valuable type of literature because they consider the critical implementation details which aren't often considered in the early stages of design but are required for the construction of flight worthy CubeSat antennas. In the following, the literature found for this category will be considered in detail, presenting the sources in order of increasing complexity of the designs they conceptualize.

The simplest design which was found in literature was the center fed half wave ultra high frequency (UHF) dipole antenna design by Mortensen of the Naval Postgraduate School for the NPS-SCAT mission [33]. This design is based on the antennas used by the Cal Poly CP series of CubeSats, an example of which is shown in Figure 16.

Figure 16: CP2 CubeSat by Cal Poly, with dipole antenna. Adapted from [34].

In his master's thesis, he takes the paper concept developed by his colleague Schroer [27], and develops from it a functional antenna prototype which meets the beacon antenna requirements of the NPS-SCAT mission. The design process presented is straightforward because neither Schroer no Mortensen attempt to do electromagnetic simulations of their antenna. Instead, practical, and affordable experiments are used to verify their design after they designed and manufactured a prototype. First, the dimensions of the dipole are defined based on simple antenna theory, and the device is mounted on a corner of the 1U CubeSat, thus minimizing the overlap and interactions between the body and the antenna. They too ensure that the area of the feed is free of PCB ground. Then, a specialized feed supported by a PCB is developed to allow the attachment of the steel piano wire antenna arms to the feeder, and a Pawsey Stub is used as a balun. No impedance matching block is developed. Instead, the antenna arms are pruned until resonance is obtained at the frequency of interest. Lacking a suitable anechoic chamber, Mortensen undertakes makeshift VSWR and gain measurements to validate his design, and reports adequate gain, antenna pattern, and VSWR to close his beacon link with more than sufficient margin.

While the mission of NPS-SCAT was successful with more than two years in orbit [35], Mortensen reports that the tuning of the antenna and the use of the Pawsey Stub as a balun is tedious. This

is unsurprising, due to the frequency dependence of the electrical length of the lines making up his balun, and the manual tuning required to compensate for this. As well, when he undertakes his measurements, a spacecraft mock-up is not used (VSWR test) or the one used is not a good representation of the flight spacecraft from the electrical perspective (antenna pattern test). Nonetheless, Mortensen's work is an excellent example of how a practical design process with minimal resources can yield very desirable results.

Another slightly more complicated, but nonetheless successful design is that of a dipole antenna for the BIRDS3 CubeSat, described by Kishimoto et. al. of the Kyushu Institute of Technology, in their submission for the 34th Annual Small Satellite Conference [36]. In this paper they consider improvements to the design of the communication system and ground station for their not very successful BIRDS2 CubeSat mission. Their design is a centre fed half wavelength dipole as well, mounted in a configuration very similar to that of NPS-SCAT. However, they utilize a more complex feed system, featuring surface mount (SMT) lumped element components, and PCB transmission line technology. They too chose to keep the ground planes around the feed, on both side of their antenna board. This is illustrated in Figure 17.

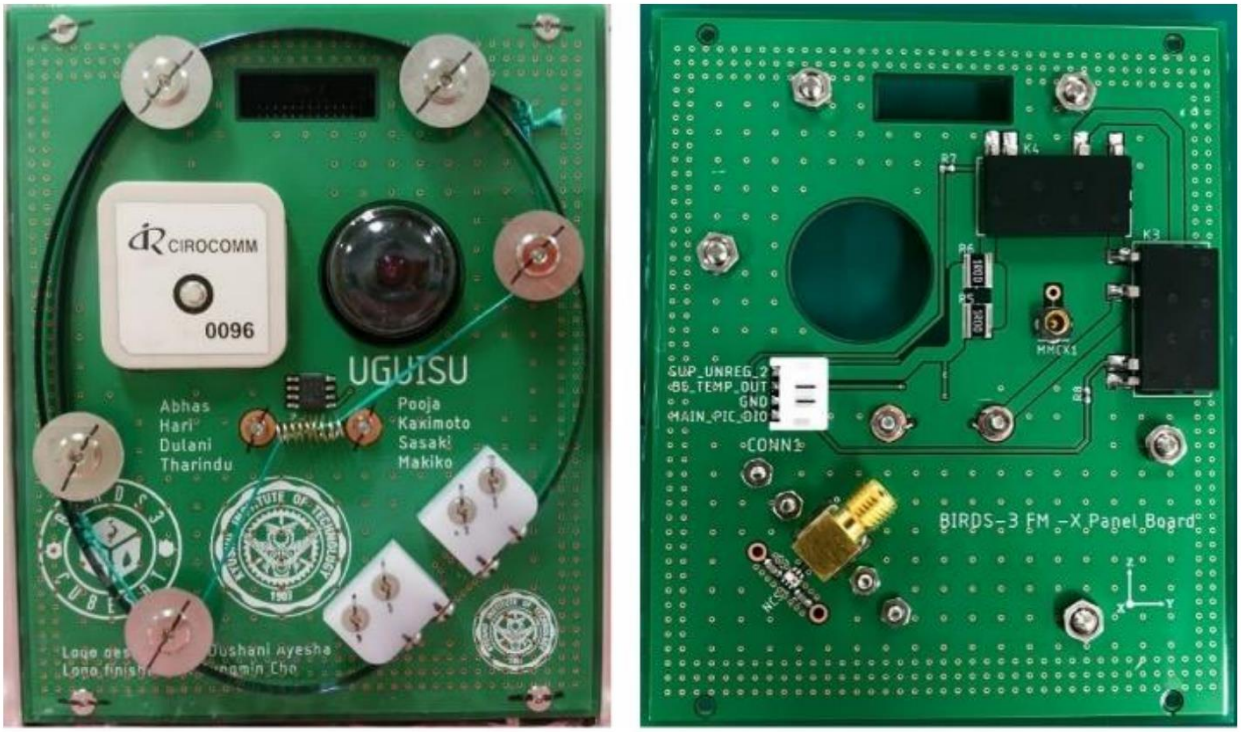

Figure 17: Outside (left) and inside (right) of the antenna board of the BIRDS3 CubeSat. Adapted from [36].

As shown, an SMA connector feeds their antenna via a balun of 1:1.5 turns ratio, followed by a pair of series capacitors in each arm of the balanced side of their circuit. This feed is mounted on the side opposite to the antenna, so RF vias are employed to guide the signal from the capacitors to the antenna, which are pieces of string steel clamped between Delrin blocks and conductors of unknown construction.

Their paper is problematic in many ways. They present no measurements of antenna input parameters, gain or antenna pattern. As well, they do not provide specifications for their circuit components or PCB features. Lastly, they give no consideration to the insertion losses of their balun and matching blocks, and they don't consider the impact of the body of their 1U CubeSat on the antenna. However, they report successful in-orbit performance as well as notable improvements compared to their earlier design, which makes their work worthy of consideration.

Another submission to the 34th Annual Small Satellite Conference by Lyerly and Pachowicz of George Mason University [37] is also of interest. This paper fills a very interesting gap as it is targeted to be formal guidance in the development of flight antennas of academic CubeSats. They take an academic approach where they model the performance of their dipole antenna design using Ansys HFSS, followed by the construction of a prototype and a 0.5U CubeSat mock-up, on which they conduct input parameter measurements.

Their simulated model compares the return loss properties of a centre fed half wavelength dipole in free space to the same dipole mounted on their 0.5U CubeSat body. They report that the dipole must be "cut" to a length longer than what is predicted by theory, to account for detuning caused by capacitive coupling between their antenna and the CubeSat body, and they emphasise the importance of considering the impact of the spacecraft on the antenna electrical parameters.

To support the conclusions of their analysis, they construct a mock-up of their simulated structure from copper clad FR4 PCBs with copper tape covering the edges. They note that Nitiniol memory wire would be ideal for antennas, but for practical reasons they construct their prototype out of copper tubing, and they too include a wire & core 1:1 balun at the antenna feed point. They find that their model matches their measured return loss data from their

experimental setup very closely. Their test article is shown in Figure 18, while a comparison of their measurement results and model predictions are shown in Figure 19.

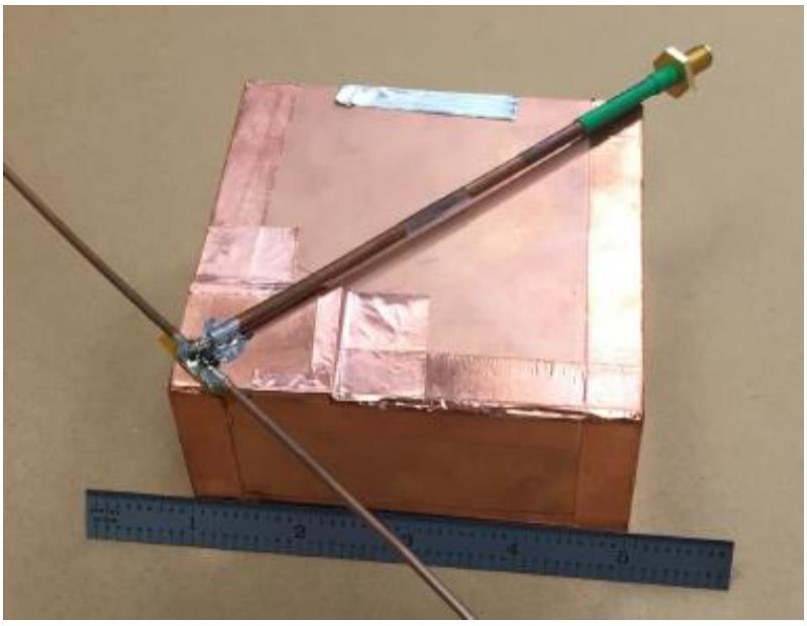

Figure 18: 0.5U CubeSat mock-up with dipole antenna. Adapted from [37].

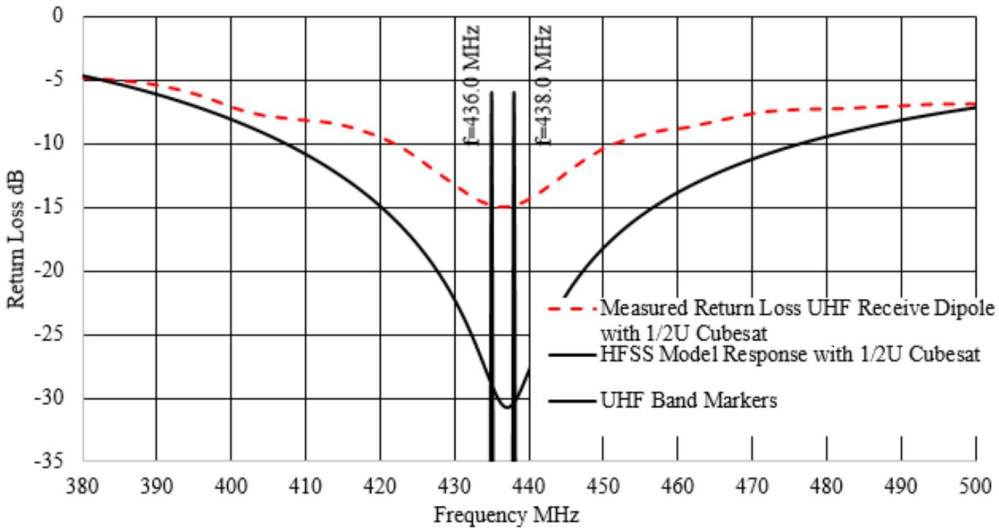

Figure 19: Measured vs. modelled dipole RF for 0.5U CubeSat configuration. Adapted from [37].

Lyerly and Pachowicz does an excellent job of formalizing and documenting the most critical practical design attempts presented in the literature by Schroer, Mortensen and Kishimoto et. al.. However, the simulations that they present are steps which have been shown by Mortensen as steps which may not be required for the delivery of a functional product. This is an important

consideration for academic CubeSat developers, who are often constrained by tight timelines and inexperienced development teams. As well, it is noted the balun choice for their prototype is problematic, as its loss is excessive (2.5dB) and it is not specified to be able to handle the RF power levels (1-2 W) of typical academic CubeSat radio transmitters [38]. Thus, these practical aspects of their work would have to be improved upon before their designs can serve as actual CubeSat antennas.

In his master's thesis, Lankinen of Aalto University [39] takes a similar approach to that presented by Lyerly and Pachowicz. However, he combines an extreme version (no balun) of the simple and easy to develop direct feed successfully employed by Mortensen with the formal modelling and experiment-based process presented by Lyerly and Pachowicz to deliver a functional product. Choosing to opt out of a balun, he connects the splayed ends of his coax feeder directly to his antennas.

Lankinen work presents the design of a pair of V-dipole antennas, each to be used as part redundant half duplex UHF radio communication system. His reasoning for the use of a V dipole in place of a straight dipole is the ability to have nulls not as deep, at the cost of lower maximum gain. He simulates the radiation pattern and S11 log-magnitude response of his proposed antennas in an increasing complex manner. First, he considers them in free space, followed by in the presence of the satellite body. Then, he constructs a prototype and undertakes anechoic chamber measurements to verify his simulation results. For his measurements, he attaches his prototype to a mechanical mock-up of the spacecraft body to make sure that its effect on the antenna parameters is considered. He obtains an S11 log-magnitude response which is better than the simulation in the band of interest. As well, he obtains a reasonable (few dB) agreement between his simulation and his measured antenna pattern data.

With the success of the Aalto-1 CubeSat in orbit, the utility of Laniken's design is clear [40]. His ability to obtain a more omnidirectional radiation pattern because of the V antenna shape is highly desirable, as uncontrolled tumbling for CubeSats is not uncommon. As well, the fact that his work includes careful considerations for the CubeSat body in models as well as input characteristic and antenna pattern experiments is a definite improvement on the process

described both by Mortensen as well as Lyerly and Pachowicz. However, his use of a direct feed system without a balun is problematic, as his does not consider the interaction of his feeder with his antenna, and the potential adverse effects resulting from that.

Given the constraint which demands the use of the existing antenna deployer for ORCASat, the benefits reported by Laniken regarding the desirable antenna pattern can not be directly applied to the work in this thesis. Unfortunately, the existing deployer can not deploy a V dipole. However, his work is relevant nonetheless, because it validates the direct feed system by Mortensen in the context of another mission - even if it does not feature a balun.

In conclusion, a consideration of relevant literature for in-house CubeSat dipole antenna design yielded some very relevant insights. First, it was found based on the work of Mortensen, that simulation and modelling of an antenna is not necessary a pre-requisite for successful in orbit performance. Secondly, it was determined that rigorous testing using prototypes which include a mock-up of the CubeSat body is essential for confidence in, and the delivery of a functional product. However, the availability of anechoic chamber facilities was found to be non-critical, as makeshift, and cost-effective in-house test setups were shown yield adequate confidence in the antenna design for flight. It was also found that none of the literature found reported a need for complex matching networks between the antenna, because pruning was adequate to make the antenna resonant at the frequency of interest. Interestingly, this problem has not been considered in the context of the transmission line electrical length between the antenna and the connection point to the rest of the system. This may be just an omission on behalf of the authors, but it may also indicate that pruning alone was sufficient to obtain near perfect resonance around 50 Ohms – if that is the case, the impact of the transmission line length on the dipole input impedance seen at the end of said line is minimal. Lastly, for baluns, the literature considered was found to be divisive. Some authors recommend their use, while others got away without them. However, no source considered has shown a rigorous treatment for the use or omission of these devices, so the technical and implementation details (e.g. insufficient power rating, difficult construction, need for PCB features) presented for them may make the effort required to implement them a potentially difficult thing to justify in light of precedents for successful flight without them.

5 Methodology

5.1 Overview

The topic of this section is the determination of the optimal methodology for the design, implementation, and verification of a dipole antenna for ORCASat which will enable the success of the mission of this spacecraft. To determine the optimal methodology, the project timeline, other ORCASat-related responsibilities of the author of this thesis, previous efforts on dipole antenna development for ORCASat by others, the project constraints, as well as lessons learned from the literature need to be considered.

At the time when the development of the antenna in this thesis was undertaken (Q3-Q4 2021), timeline of the ORCASat project calls for spacecraft delivery to the launch provider in Q2-Q3 2022, and orbit insertion in Q3-Q4 2022. With the author of this thesis also being responsible for the frequency licensing of the ORCASat satellite communication system, as well as the design, manufacturing, implementation, and testing of the rest of the ground and space station, the development timeline for ORCASat TT&C was very busy. This is illustrated by the ORCASat assembly, integration, and testing (AI&T) timeline shown in Figure 20.

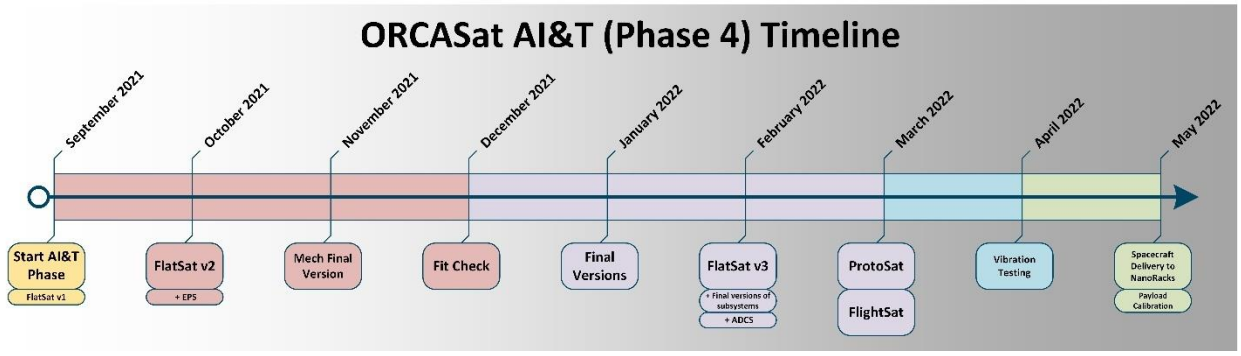

Figure 20: ORCASat AI&T high level timeline. Courtesy of A. Doknjas.

Not considering work on patch antennas which never yielded a prototype, previous antenna development work for ORCASat is considered by the MSc thesis work of Inês Bernardino, who attempted to develop a dipole antenna for this spacecraft [41]. In her master's thesis, she takes a simulation-based approach to come up with a realizable dipole antenna and matching network design for ORCASat, which she manufactures and evaluates in terms of its input characteristics.

However, for reasons which are considered in Section 6 of this thesis, she is unable deliver a functional dipole for ORCASat.

Most of the constraints which have been presented in Section 2.2 are a direct consequence of the roadblock created by Bernardino's lack of ability to deliver a functional product. The design of the mission and the spacecraft had to advance while the antenna was being developed by her. To allow risk free development of the mission and the rest of the spacecraft, it was necessary to constrain the antenna to a dipole. Otherwise, due to long timelines associated with manufacturing the antenna deployer, an unacceptable amount of risk would have been introduced to the project.

5.2 Methodology

Considering the considerations introduced above, as well as the conclusions of the literature review in Section 4, the optimal methodology to tackle the antenna design problem is as follows. First, it is necessary to review and study the work by Bernardino to determine what exactly resulted in inadequate performance for the prototype what she developed. It is deemed optimal to take a practical approach to debugging this problem. This is because the simulations show adequate performance, but the prototype does not, and it needs to be investigated what is it about the prototype which makes it not perform as expected.

After the root cause of the current problem is determined, it is optimal to adapt a practical development process. The decision for this is supported by the fact that the timeline of the ORCASat project is tight, the author of this thesis has many other responsibilities, and literature shows that simulations aren't necessary to deliver a flight-capable antenna. Instead, a simple a practical design methodology is suitable, which is introduced as a high-level step by step process below.

I. Inventory the blocks which are necessary for the dipole antenna to meet the requirements and constraints of this project. If not clear based on the theory in Section 3, briefly explain how each block helps the design meet the requirements and constraints.
II. Conceptualize potential design solutions for each block from a high-level perspective, while considering the advantages and disadvantages of each solution, considering the

requirements, constraints, the conclusions of the literature review, and the lessons learned by reviewing the work of Bernardino.

III. Select the winning design based on its merit against the criteria presented for the previous step and develop it into a manufacturable product in a well documented detailed design process. As part of the product development, consider how the product will be tested, and come up with a draft for verification test plan.

IV. Manufacture and assemble a prototype and commission it to an extent which will reveal if its performance justifies the time and effort required to put it through a formal verification test campaign. This commissioning shall also be a test of the draft verification test plan, revealing if anything needs to be changed to streamline and refine it into the formal verification test plan which will have to be undertaken to determine if the product meets the requirements and constraints.

V. If the prototype shows promising performance, undertake full verification testing, to an extent which is sensible and cost effective considering the facilities available at the University of Victoria. During the test campaign, identify any critical gaps which represent a risk with flying with the design under test, and identify & evaluate measures for the mitigation of this risk, if exist.

VI. If the prototype passes the verification tests in house, and if there are any risks which require further mitigation, execute the measures identified during verification testing to adequately mitigate the risk by further experiments, testing, and design revisions.

6 Preliminary Investigation

6.1 Overview

The purpose of this section is to document the process which was undertaken to find the root cause of the problem with the dipole antenna prototype developed by Bernardino. First, the design produced by her is introduced, followed by a discussion of potential problems which may be responsible for the inadequate performance. Next, a hypothesis is developed, and an experiment is designed to determine the merit of the hypothesis regarding the root cause. This process allows the root cause analysis to be undertaken in a strategic, organized and well

documented manner, generating some important lessons for the subsequent design process for a new dipole antenna.

6.2 Design Description

The design presented by Bernardino consists of two main components - a half wavelength centre fed dipole antenna, and an UHF radio transceiver. These are shown in Figure 21 and Figure 22. As shown, the antenna is co-located with an UHF radio transceiver designed by the author of this thesis based on the Open LST project [42] on the same PC104 compliant 4-layer PCB. Co-location was prioritized, because at the time the design was undertaken, the ORCASat bus did not allow physical space for separate PCBs for the antenna and the radio. Circuitry associated with radio transceiver is confined to one side of the circuit board, while the other side features the antenna in its deployer, and the deployment circuit.

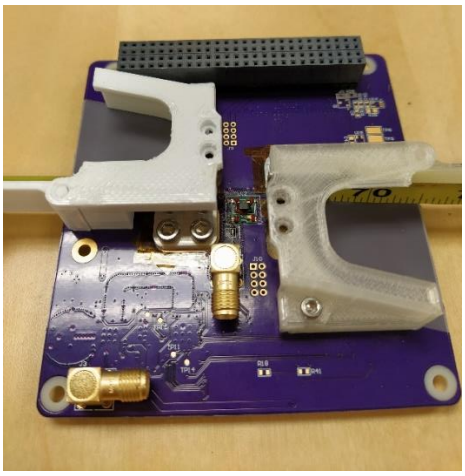

Figure 21: ORCASat TT&C board R1, antenna side.

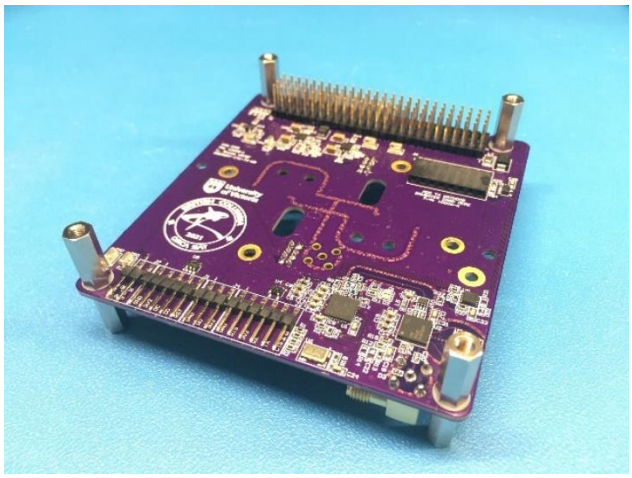

Figure 22: ORCASat TT&C board R1, radio side.

The antenna deployer and the deployment circuit are the same which have been presented as constraints in Section 2.2 of this project. The antenna is fed via an SMA connector, followed by discrete matching components, and a 1:1 COTS wire & core balun. All components prior to the balun are interconnected with microstrip transmission line technology. The balun feeds the antenna via a balanced edge coupled microstrip line arrangement. These lines connect to copper pads on the PCB surface, to which the antenna is mounted by the means of a right-angle bracket made of aluminum. This is illustrated in Figure 23 and Figure 24.

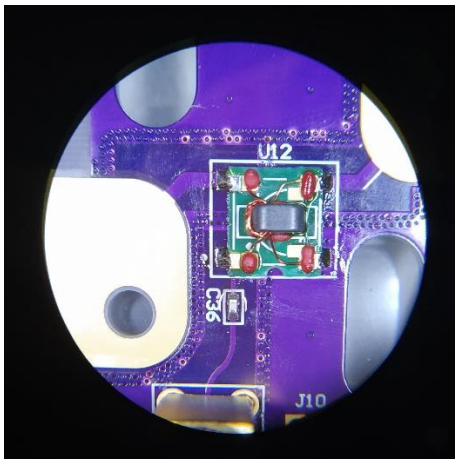

Figure 23: Matching network close-up view.

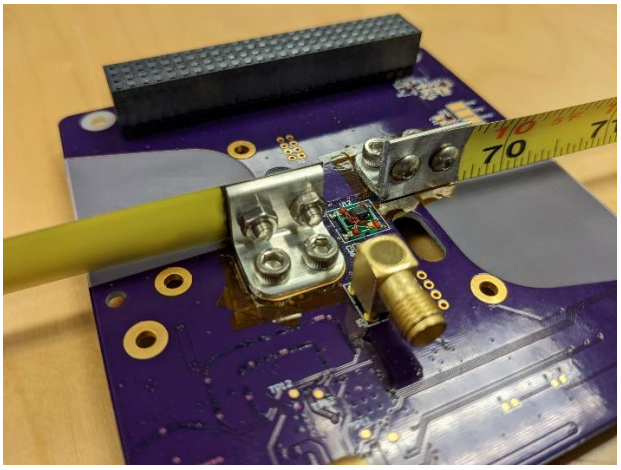

Figure 24: Antenna feed brackets and matching network. Courtesy of T. Tarnowski.

The internal two layers of the PCB feature ground planes to allow the use of PCB transmission line structures. The signals are routed on the top and bottom layers only. The internal stack up of the PCB is configured as shown in Figure 25. This stack up is the standard 4-layer stack up adapted for ORCASat, and it is used for all PCBs which are manufactured by the team.

#	Name	Material	Type	Weight	Thickness	Dk	Df
	Top Overlay		Overlay				
	Top Solder	PSR-4000BN...	Solder Mask		0.0254mm	4	0.03
1	Top Layer	OHS Park 1...	Signal	1oz	0.03556mm		
	Dielectric 2	FR408HR	Prepreg		0.17018mm	3.69	0.0091
2	Layer 1	OHS Park 1/...	Signal	1/2oz	0.01778mm		
	Dielectric 1	FR408HR	Core		1.1938mm	3.69	0.0091
3	Layer 2	OHS Park 1/...	Signal	1/2oz	0.01778mm		
	Dielectric 3	FR408HR	Prepreg		0.17018mm	3.69	0.0091
4	Bottom Layer	OHS Park 1...	Signal	1oz	0.03556mm		
	Bottom Solder	PSR-4000BN...	Solder Mask		0.0254mm	4	0.03
	Bottom Overlay		Overlay				

Figure 25: Standard 4-layer stack up used for all ORCASat PCBs.

6.3 Investigation

The prototype developed by Bernardino was available to the author of this thesis. As the first step, the S11 log-magnitude response of the prototype was re-verified using a calibrated VNA. This prototype was determined to be non-resonant at the frequency of interest, indicating that the final S11 log-magnitude measurements presented in Bernardino's thesis have not been executed correctly.

To better understand what is responsible for the undesirable S11 performance, a decision was made to isolate the various elements of the design and measure their responses individually using a VNA. Using the same PCB technology as the prototype, breakout boards were designed by the author of this thesis for the SMA connector, microstrip line, and series matching capacitor, the balun, as well as the antenna pads with the edge coupled microstrip lines. These are illustrated in Figure 26 to Figure 28. These were then passed on to one of the industry advisers for the ORCASat project, who measured their individual S matrix with a VNA and used that information in an ADS simulations to recommend an update to the matching network, hoping that the problem can be resolved without a re-manufacture of the entire antenna PCB. This update consisted of shorting out the series capacitor and adding another 2pF series capacitor directly at the SMA connector. The details of this analysis were not available to the author, so they are not presented here.

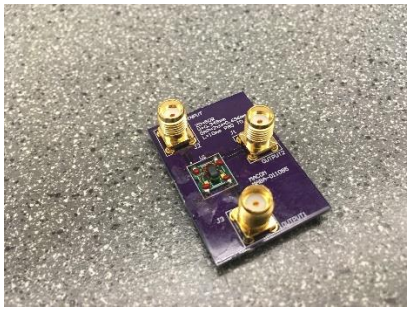

Figure 26: Breakout board for the balun.

Figure 27: Breakout board for the pre-balun circuit.

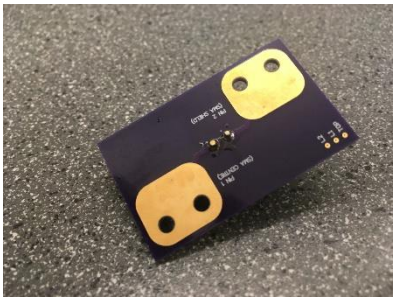

Figure 28: Breakout board for the antenna pads.

These modifications were executed and measured on the VNA, resulting in a response which indicated resonance at a frequency higher than the target. This response is shown in Figure 29. To counteract this, a trial-and-error process was followed, where capacitors and inductors from SMT libraries in the few tens of nH/pF range were substituted in place of the short created earlier, and the response was measured on the VNA. It was determined that series capacitance made the problem worse, by further increasing the resonance frequency of the prototype. However, adding series inductance seemed effective. At the cost of return loss performance, resonance at in the UHF satellite band was obtained. This is illustrated in Figure 30.

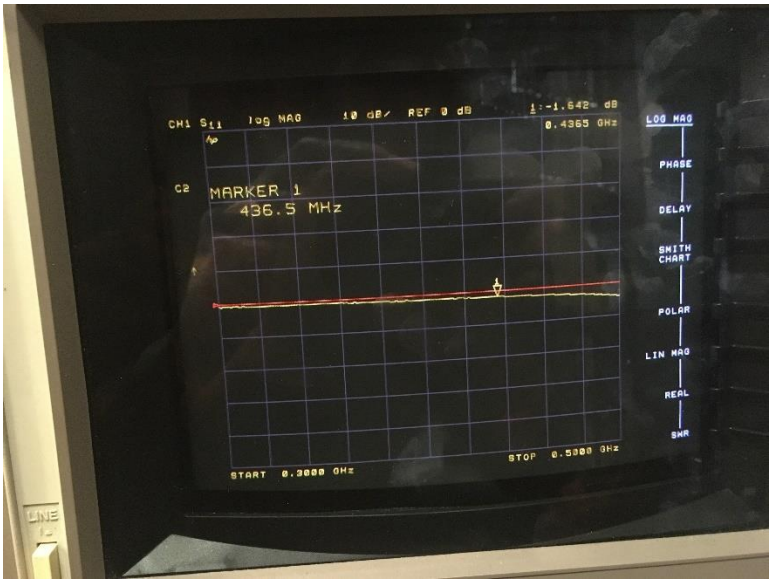

Figure 29: S11 log-magnitude response with updated matching network. Resonance > 436.5 MHz.

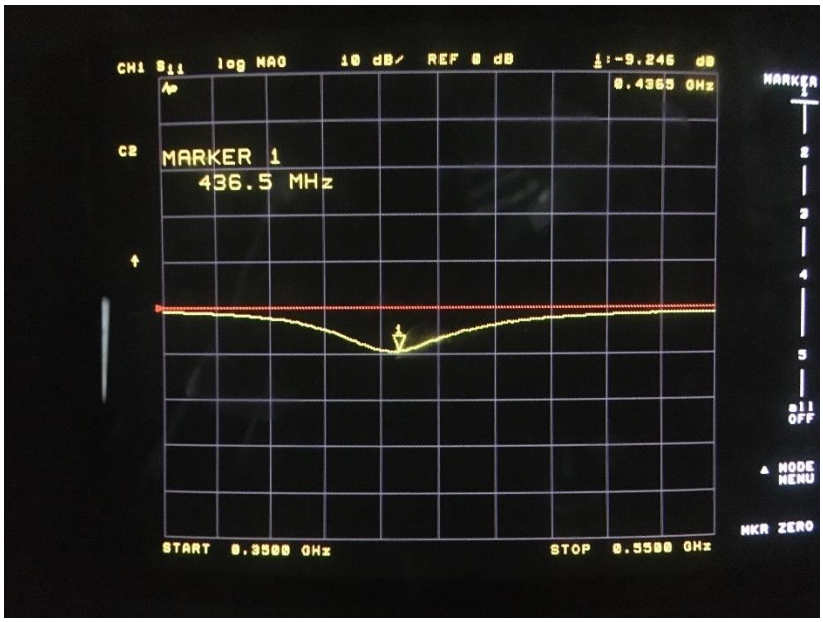

Figure 30: Resonance in the centre of the UHF satellite band.

Unfortunately, the resonance obtained was observed to be very stable. For a functional antenna, it would be expected that the S11 log-magnitude characteristics would change significantly when various objects are placed in the near field of the antenna. This was not the case for the prototype. It was not responsive to tuning as well – lengthening or shortening the arms or removing them entirely did not shift the resonant frequency. This is illustrated in Figure 31 where it is shown that the response of the prototype only changes by approximately 3dB when the

antenna tape measure arms removed. Based on this, it was concluded that instead of an antenna, a matched attenuator incapable of radiation was obtained by incorrect design choices, and any RF power supplied to this device would be dissipated in the dielectric of the PCB .

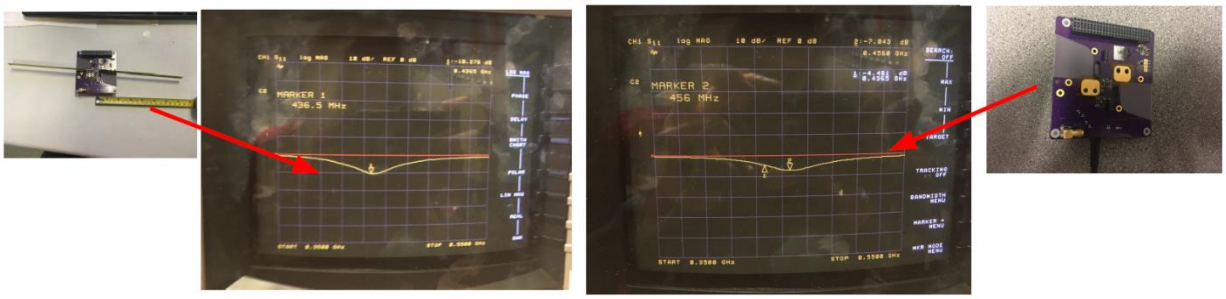

Figure 31: Change in S11 log-magnitude response because of antenna arm removal.

At this point, it was concluded that further experiments involving the prototype developed by Bernardino are not productive. Instead, it was decided to simplify the analysis. A hypothesis was established whereas it was theorized that the dipole would behave like an antenna if only the absolute minimum components (the aluminum brackets, pads, and the edge coupled microstrip line, and the internal ground planes) would be evaluated, in a single-ended configuration. To this end, a simple PCB was designed in Altium, and manufactured, featuring only the components listed above. As a baseline, another PCB was also manufactured, but this did not feature the ground planes, attempting to create a configuration as close to the ideal dipole in free space as possible. These test articles are shown in Figure 32 and Figure 33. It is noted that there is no major visible difference between the boards – they differ only by the presence/absence of ground pours on the two internal PCB copper layers.

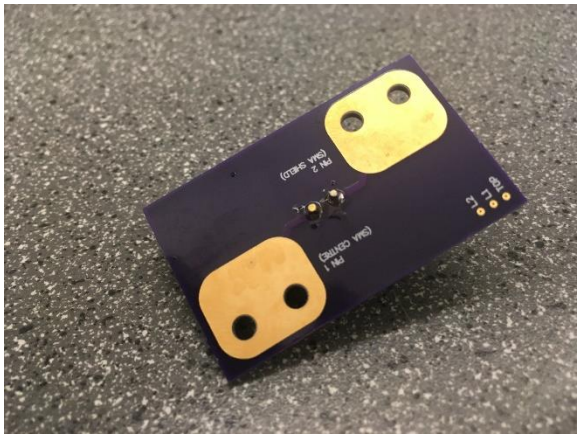

Figure 32: Minimalistic antenna test PCB, pad side.

Figure 33: Minimalistic antenna test PCB, connector side.

The response of the test boards was measured with a VNA, and it was determined that the board with the ground planes mimicked the undesirable behaviour of the prototype, while the control board behaved just like one would expect an antenna. The control board was tunable, and it was very responsive to near field obstacles. This is illustrated in Figure 34 to Figure 41, where it is shown that for the board with the ground planes, the S11 log-magnitude plot is flat regardless of the presence or absence of tape arms, while for the control board, the addition of the tape arms induces resonance of desirable characteristics. Based on this, it was concluded that the problem with the prototype developed by Bernardino is the presence of the ground planes, which were required to allow the use of PCB transmission line features. The use of PCB transmission line features was demanded by the balun and matching technology of choice, as well as the fact that the radio transceiver requires them because microstrip line is used to feed the modem and the RF front end.

After it was determined that the key feature to remove from Bernardino's design was the ground planes, arrangements were made to adjust the TT&C ICD to allow for this. To this end, the ORCASat MECH team was consulted, and they determined that by rearranging the bus electronics stack up, it is feasible to add a constrained but suitable extra PC104 card for the radio transceiver. This was ideal, because this allowed the consideration of various design options which are considered in subsequent sections of this thesis, which may not have been feasible if the co-location was still required.

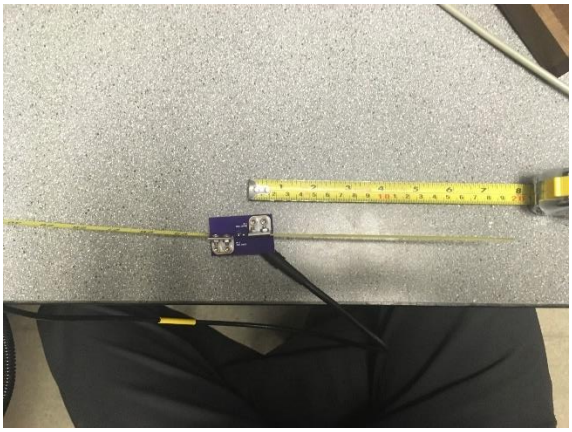

Figure 34: Test PCB with antenna arms, no GND, test setup.

Figure 35: Test PCB, no GND, no antenna arms, S11 log-magnitude response .

Figure 36: Test PCB, no antenna arms, no GND, test setup.

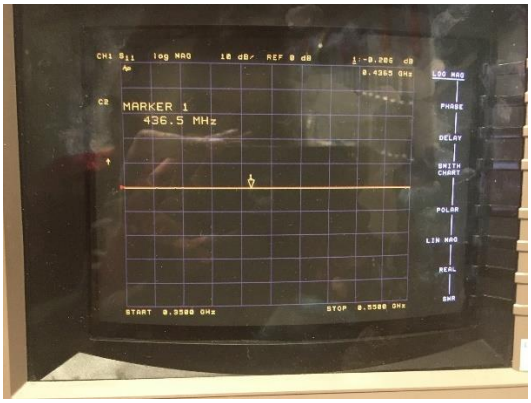

Figure 37: Test PCB, no GND, no antenna arms, S11 log-magnitude response.

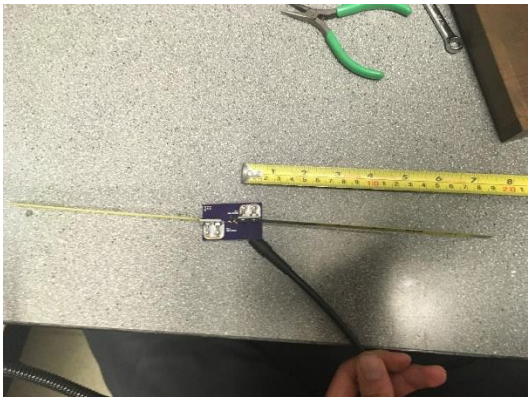

Figure 38: Test PCB with GND, antenna arms, test setup.

Figure 39: Test PCB, with GND and antenna arms, S11 log-magnitude response.

Figure 40: Test PCB with GND, no antenna arms, test setup.

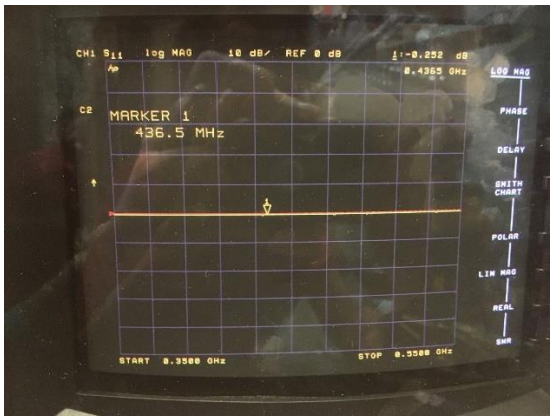

Figure 41: Test PCB, with GND, no antenna arms, S11 log-magnitude response.

The addition of the extra PC104 card for the antenna became a possibility, because of the arrival of the flight model of the COTS ADCS subsystem for ORCASat. Physical access to this allowed the MECH team to reduce the design margins allocated to the physical space in the stack up.

Asides the electrical problems explored above, one key mechanical element which has been determined to be problematic with the prototype developed by Bernardino was the use of the L bracket to support the antenna. This has already been illustrated in Figure 24. With this component not having accommodations for the curvature of the tape spring, during debugging it was found that the material eventually lost its elasticity, making it unsuitable for a deployable antenna. As a result, it was decided to re-design this component as part of the work presented in this thesis.

7 Concept Development

7.1 Overview

The topic of this section is the generation of some competing high level design concepts which may be suitable to meet the requirements and constraints of this project. Considering the constraints introduced in Section 2.2, it is a given that the design of the ORCASat antenna is restricted to a half-wavelength dipole which must fit a pre-existing antenna deployer housing, using the pre-existing deployment circuit. The details of the ICD referenced in this section also reveal that this housing has been designed to fit one width of steel tape measure only. Thus, any concepts which require modifications to the deployer, the deployment circuit, or the tape measure width not an option.

Considering these restrictions and limitations, the blocks of the ORCASat antenna which need to be conceptualized are those which will undertake the signal transformations between the 50 Ω output of the radio transceiver of the TT&C subsystem, and the steel tape measure antenna arms. These consists of the transmission lines & connectors, the balun, any impedance matching circuits which may be required, as well as the antenna arm feed. These are illustrated in Figure 42. The rectangles represent the various blocks, while the arrows indicate the logical order of connecting them. It is noted that the order of the balun and the impedance matching block may be reversed or combined into a single block, depending on the detailed electrical design of these individual elements. It is also noted, that during concept development, it is critical to take the lessons learned in Section 6 into account.

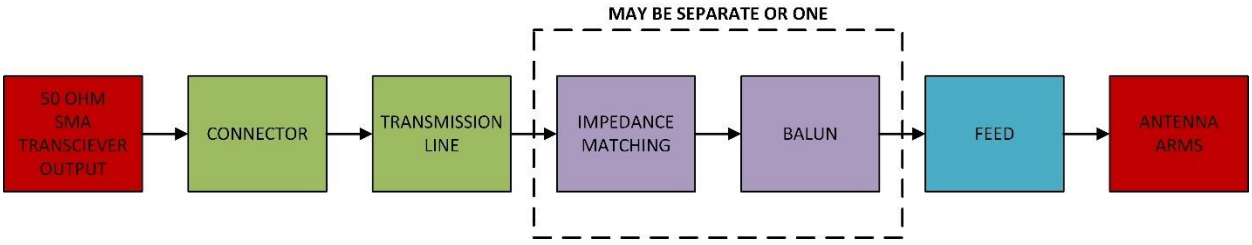

Figure 42: Functional blocks required for a dipole antenna which is suitable for the ORCASat project.

7.2 Transmission Line and Connectors

According to the TT&C Mechanical ICD in Appendix B-4, the ORCASat radio transceiver board is a connectorized product which features an unbalanced 50 Ω microstrip transmission line

terminated in a right angle female SMA connector. Thus, a connectorized transmission line of some kind is needed to guide the electromagnetic waves to/from the transceiver connector to the antenna.

Due to the target operating frequency range, and the mechanical constraints imposed upon the antenna, the only practical option to connect the transceiver board to the antenna board is coaxial cable, which must feature a right angle male SMA connector on one end. This also restricts the impedance of the coaxial cable to 50 Ohms, as SMA connectors are not available in other impedances.

However, the antenna side of the coaxial feeder may be connectorized or not, depending on design decisions made for the rest of the design blocks. For example, the coaxial feeder could be terminated in a PCB mounted RF connector, and PCB transmission line technology could be used to guide the signal from the connector to the blocks upstream, and vice versa. The design choices for this are strongly interrelated with the solutions selected for the rest of the blocks in Figure 42. As a result, the details of this will be discussed later in this thesis, once the rest of the blocks have been conceptualized.

7.3 Balun

Baluns are means by which the adverse interaction of an antenna and its feeder can be minimized. The details of this interaction have already been introduced in Section 3.5 of this thesis. Baluns may take many physical forms and electrical topologies. The considerations of all of them are well beyond the scope of this thesis. To restrict the options, a decision was made to consider current baluns only. This is because based literature by Lewallen [43], current baluns are superior to voltage baluns. Current baluns are all common mode chokes applied to the feed line in some form, aiming at reducing the interaction of the antenna with its feed line by reducing the common mode current I_3 in Figure 11 of Section 3.5. The two types of current baluns which are of interest are inductive and lossy ferrite choke baluns [15]. As well, since the work of Mortensen successfully employed it for a dipole antenna with good flight performance [33], Pawsey Stubs will also be considered.

Most commonly, inductive ferrite choke baluns are wound with insulated wire on a toroidal ferrite core, while lossy ferrite chokes are constructed by passing turns of coaxial cable trough a ferrite bead. This is illustrated in Figure 43 and Figure 44, respectively.

Lossy ferrite choke baluns are cheap and easy to construct, requiring coaxial cable and ferrite materials only. They too are desirable because they have low insertion loss, and they don't introduce any impedance discontinuities in the signal path by alternations to the coaxial cable. They can, however, be physically large and heavy compared to COTS inductive choke baluns, which may be problematic in a space and weight constrained CubeSat electronics stack. For UHF bands, the availability of suitable alternatives for lossy ferrite materials may also be a problem.

Figure 43: Inductive ferrite choke balun for HF amateur radio. Adapted from [44].

Inductive choke baluns are also cheap, and they can be often purchased as a COTS electronic component ready to be installed on a PCB. They are very attractive from the perspective of physical size, as well as weight. However, they come at the cost of more insertion loss than lossy ferrite choke baluns. As well, they may introduce uncertainties to the design, because of lack of outgassing data for the wire insulation used to wind the balun. COTS inductive choke baluns in most cases also require the use of PCB transmission line structures to feed them. This is problematic, because the interaction of the ground planes required for PCB transmission lines with the antenna itself is complex, and based on the experience with the prototype delivered by

Bernardino for her thesis, the use of ground planes may introduce a problems and uncertainties into the design.

The operation Pawsey Stubs is based on the same concept as the balun designs introduced so far. To isolate the antenna and the feeder, current I3 from Figure 11 must be reduced as much as possible. However, the physical arrangement which is used to achieve this is very different. At the antenna feed point, a quarter wavelength electrical length shorted transmission line stub is attached in parallel with the feeder, as shown in Figure 45. This, according to Equation #10 in Section 3.3.5, represents in infinite input impedance, when inspected from the end at the antenna feed. The common mode current I3 sees this, and in the presence of the high input impedance, it does not travel on the shield of the coax, thus eliminating the mismatch. However, this device has narrow bandwidth, and it requires accurate tuning – the electrical length of the cable used for the stub changes with the operating frequency, and so does the input impedance presented by it.

Figure 44: Lossy ferrite choke balun for HF amateur radio. Adapted from [45].

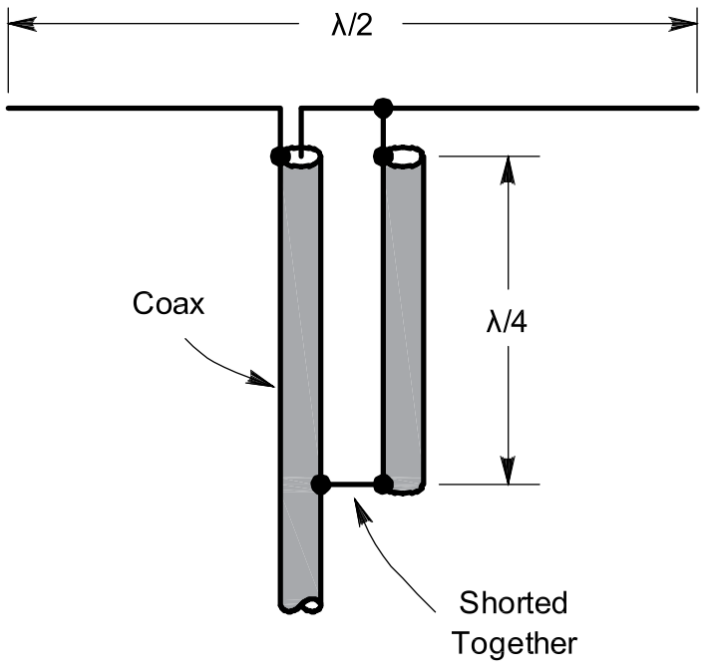

Figure 45: The construction of a Pawsey Stub balun. Adapted from [46].

7.4 Impedance Matching

A method of impedance matching between the complex input impedance of the dipole and the 50 Ω impedance of the coaxial cable from radio transceiver of the ORCASat TT&C subsystem will be required to ensure optimal power transfer between the two. While baluns can be constructed to undertake this, they don't have to – often there are separate impedance matching circuits are used for this.

Impedance matching circuits come in a wide variety of configurations, which can not be all considered as part of this thesis. Those which are deemed suitable for the antenna design for ORCASat are the use of no matching at all, the use of a lumped element matching network, or a matching network furnished out of transmission lines.

Avoiding the matching problem altogether is a simple and desirable concept which is well supported by the literature in Section 4. The antenna may be pruned to a resonant length which is different from its theoretical length once mounted in the spacecraft, resulting in a real input impedance which negates the need for a matching network. A small mismatch may result from the 73 Ω dipole being attached to the 50 Ω transmission line, but this is a small price to pay for the simplicity of this solution

Alternatively, a lumped element matching network may be used, in the form of L, T or π network, or passives in some other topology. However, this method requires the accurate determination of the antenna input impedance looking into the feed, which may be time consuming to determine by simulation. As well, due to the changes in impedances for the passives as a function of frequency, a lumped element balun may only operate well over a narrow bandwidth. Lastly, the impact of anything not well captured by the simulation must be compensated by a manual tuning process. This entails using passive component (L, C) libraries and VNA measurements to determine the optimal values for the passives. This is a cumbersome process, and it is limited in utility as it can not be undertaken in the fully assembled spacecraft, the presence of which impact the antenna input impedance to which the match needs to be tuned.

Matching networks furnished out of transmission lines are a compromise between lumped elements and no matching at all. The impedance measured at the end of an electrical half wavelength coaxial cable can reveal the antenna feed point impedance, to which a transmission line match can be designed without a circuit board re-spin. However, construction of these matching networks out of coaxial cables which are physically suitable for use a 2U CubeSats is not trivial, as the cables are extremely thin. They are also problematic as they may have a narrow bandwidth because line electrical lengths and impedances seen at the ends of line segments making up the matching network change with frequency. As well, transmission line matching networks are difficult to tune, and they can only be tuned as part of a cumbersome process, which can not be undertaken in the spacecraft. On top of this, excess lengths of cable must be too secured somewhere inside of the CubeSat in a manner which will survive the vibrations of a rocket launch.

7.5 Antenna Arm Feed

The guided electromagnetic waves in the transmission line feeding the antenna must somehow enter the antenna arms to be able to become electromagnetic waves in free space. A specialized electromechanical structure is required for this, which does not degrade the electrical properties of the antenna while providing the mechanical integrity which is required to survive vibration during launch to orbit. Based on the lessons learned with the feed in Bernardino's thesis work, it is also important to come up with something which respects the curvature of the tape measure.

The details of this will be considered later in this thesis, because the design choices for the other blocks in Figure 42 strongly influence this.

8 Detailed Design

8.1 Overview

The topic of this section is the detailed design of the ORCASat antenna. In the sections which follow, competing concepts for various blocks of the antenna shown in Figure 42 in the last section will be developed into a physically realizable design which meets the requirements and constraints outlined earlier in this thesis.

8.2 The Design of the Pre-Feed Blocks

The most suitable options for the various blocks of the ORCASat antenna can not be selected alone, because the design of the various block influence each other. The block which most fundamentally impacts the rest of the blocks is the selection of the balun because that will determine if PCB transmission lines will be needed on the antenna board. As a result, this balun block will be considered first.

Due to the difficulty associated with tuning and manufacturing a Pawsey Stub, it was decided to consider only inductive and lossy choke baluns for the ORCASat antenna. To gain a detailed insight into the feasibility of using an inductive choke balun and allow concrete comparisons of design parameters to that of a lossy choke balun, an exhaustive market search for COTS inductive choke baluns was conducted. The requirements for this search are outlined and explained below.

1. *The candidate shall be an active component in production which is easy to source with a reliable supply chain which has a stock of >1000 pieces at the time of the market search.*
    a. Esoteric or end of life (EOL) components may have desirable properties, but they represent a risk as the spacecraft can not be constructed if they aren't available.
2. *The candidate shall be specified to operate over the 435.0-438.0 MHz frequency.*
    a. The antenna has a requirement to operate over this frequency range.
3. *The candidate shall have a continuous RF power rating of 2W (33 dBm) minimum.*
    a. The RF front end of the TTC subsystem is specified to produce at most 32.5 dBm when saturated [47], so the balun must be able to withstand this with some margin.
4. *The candidate shall feature a characteristic impedance of 50 Ohm with a turn ratio of 1:1 to 1:1.5 or 75 Ohms with a turn ratio of 1:1.*

a. These ratios allow the matching of the real part of the ideal dipole input impedance (73 Ohms) to the microstrip line from the RF front end with the least amount of mismatch loss.

5. *The candidate shall feature an insertion loss which is 1dB or less.*
    a. This is an arbitrarily determined requirement to help narrow down the search to those baluns which will not impact the EIRP significantly.
6. *The candidate shall be an inductive choke current balun.*
    a. Current baluns are superior to voltage baluns.

The results of this market search are included in Appendix C-1. The winner was determined to be the Qorvo RFXF0009H, featuring 75 Ohm characteristics impedance, 2 W continuous RF power rating, 1:1 turns ratio, 45-1200 MHz frequency range, and a stable supply chain via RFMW [48].

However, all COTS baluns considered suffered from a key disadvantage, which has only been realized after the search was completed. The antenna is constrained by outgassing specifications for its non-metallic components and obtaining outgassing data from manufacturers for the insulation of the wire used for winding the baluns proved to be very difficult. Just to determine the existence or absence of this information, extensive correspondence with the manufacturer is required. Depending on the manufacturer, the information may not be available, may only be available upon special request, or may be only produced upon request at the end of a costly up screening process, for which the customer is expected to pay for. For the RFXF0009H, the data was simply not available – the Application Engineering Team for Qorvo could not produce it when the author requested of them.

This problem is compounded by the requirement to use PCB transmission line structures with these types of baluns. This is problematic because these structures need ground planes, which may adversely interact with the antenna. While it is possible to have ground plane only over a select area of the antenna PCB, this was decided to be avoided, as the effort required for the characterization of the optimal ground plane width which is needed to ensure correct operation of PCB transmission line structures was deemed too great given the development timeline of this project.

Thus, it was decided to use a lossy choke balun, as that may easily be realized without any electrical requirements for the antenna PCB, and without any outgassing concerns. The lossy choke balun consists of two main components – coaxial cable and the ferrite bead on which it is wound. The selection of ferrite had to be undertaken first because this was going to determine the diameter of coax which can be used to wind the choke. The requirements for the ferrite for the ideal ferrite are listed below, along with their explanations.

1. *The candidate shall be an active component in production which is easy to source with a reliable supply chain which has a stock of >1000 pieces at the time of the market search.*
    a. Same justification as for COTS inductive choke balun.
2. *The candidate shall exhibit a Z response with the largest possible R component at or above the highest possible operating frequency range which may be assigned to ORCASat, 438.0 MHz.*
    a. To maximize the effectiveness of the choke and allow it to be wound with more than one turn if needed, the maximum loss is needed at or above the intended operating frequency of the antenna.
3. *The candidate shall be a bead type ferrite which physically fits the electronics stack.*
    a. If the ferrite does not fit into ORCASat, it is useless, and bead type ferrites are easier to fit onto a PCB with the use of a slot in the PCB than a toroid.

After extensive research, it was found that the 2661480002 bead from Fair-Rite Products Corp. [19] is the reasonable option for the ferrite. This was due to size – there were other products with desirable electrical properties, but they were too large for the stack. The 2661480002 is a product made of high frequency Type #61 NiZn ferrite material which has its peak R at around 4-500 MHz, with the real part of the impedance being around 450-500 Ohms. This was illustrated in Figure 13 in an earlier section.

Lossy choke baluns work under the principle that they suppress the common mode current (I_3 in Figure 11) on the antenna feed line while leaving the differential mode current unchanged. The extent to which they can do this depends on the choking impedance, so the question which naturally arises is whether the 450-500 Ohms provided by a single turn on the 2661480002 is

sufficient to isolate the feed line from the antenna. There is some debate around the amount of choking impedance required to achieve this– various sources claim 500 Ohms to thousands of Ohms [15]. References for UHF frequency ranges for this are especially difficult to find, because the most common application of these chokes is high frequency (HF) amateur radio. Thus, to conclusively answer how much choking impedance is enough, it was decided to execute two practical tests with the full assembled antenna prototype instead of literature review and complex choke impedance measurements. They are explained below:

- The extent to which touching the feed line impacts the return loss and VSWR will be evaluated for a choke with a single turn as well as two turns. If the choke serves an effective balun, this impact will be minimal because the antenna will be isolated from the feeder by the choke.
- The antenna pattern will be measured with a single and a double turn choke and compared against that of an ideal dipole. If the higher choking impedance is necessary (and the stray capacitance between turns does not negate this) the double turn choke will yield a measured pattern more similar that of an ideal dipole.

The selected ferrite bead has an internal diameter of 4.95 mm [19] which was one of the determining factors in the selection of the coaxial cable which was used to wind the choke. The requirements for the ideal cable are given below, along with explanations:

1. *The candidate shall have a jacket outside diameter which allows the construction of at least a two-turn choke using the 2661480002 core from Fair-Rite Products Corp. with an internal diameter of 4.95 mm.*
    a. Without the ability to construct a choke with ≥2 turns, higher impedances for the choke can not be realized.
2. *The candidate shall not feature a solid inner conductor or a shield.*
    a. Solid conductors make the cable rigid and difficult to bend, and a solid outer conductor (e.g semi-rigid types) does not work with the antenna arm feed explained later in this thesis.

3. *The candidate shall be an active component in production which is easy to source with a reliable supply chain which has a stock of >1000 pieces at the time of the market search.*
    a. Same justification as for COTS inductive choke balun.
4. *The candidate shall respect the outgassing constraints introduced earlier in this thesis.*
5. *The candidate shall feature as low insertion loss as possible.*
6. *The candidate shall offer the lowest possible minimum bend radius.*

The results of the coaxial cable selection are included in Appendix C-2. The best option was found to be RG-178B/U, a 50 Ohm 1.8 mm outside diameter (OD) jacket cable with a polytetrafluoroethylene (PTFE) dielectric and a fluorinated ethylene propylene (FEP) jacket. This offers an optimal combination of loss, materials from the perspective of outgassing, flexibility, and availability. The suitability of PTFE and FEP in terms of the outgassing constraints was determined by the NASA Outgassing Data for Selecting Spacecraft Materials reference publication [49].

For the construction of the first prototype, was decided to buy this coax in a connectorized format, as a pre-made jumper. This streamlined development and reduced development costs as no special tools and expertise for crimping connectors were required. The selected product for this was part number 415-0027-036 from Cinch Connectivity Solutions Johnson, a 914.4 mm SMA to SMA RG-178 coaxial cable assembly [50]. The decision to use this was made based on the reasonable price of this product, it solid availability trough Digi-Key, and its adequate length which allowed the manufacture of at least two electrical half wavelength jumpers with SMA connectors on one end for 437 MHz.

8.3 Antenna Feed Design

With the detailed design of the coaxial cable feeder, the balun, and impedance matching blocks known, the antenna arm feed was considered. As explained earlier, the re-design of this was decided because the L brackets proposed by Bernardino did not account for the curvature of the tape measure, which introduced a risk related to the tape loosing is elasticity. Another consideration for re-design originated from the decision to use a lossy ferrite choke balun. The fact that the output of this balun is a coaxial cable made it sensible to connect this directly to the

feed, without the use of any PCB features. However, since the antenna was tuned by pruning the arms, it was necessary to accommodate for easy antenna arm replacement, without disturbing the coax soldered to the feed. On top of this, it was also necessary to create a method by which the coax could be soldered to the feed – something which was not feasible to do directly on the steel antenna arms.

The requirements for the new feed were as follows. This block had to be mechanically suitable to withstand the vibrations from a rocket launch, but also electrically suitable to guide the signal from the coaxial cable to the antenna arms with minimum degradations. As well, it had to allow easy replacement of the tape arms without disturbing any solder joints, and it had to accommodate for challenges associated with soldering to steel. Lastly, it had to accommodate for the curvature of the tape measure to mitigate the risk of the tape losing its elasticity.

Based on the requirements above, and the expert advice of one of the ORCASat project industry advisors, a specialized feed system consisting of a Delrin and an aluminum block sandwiching a copper foil was conceptualized. This is shown in Figure 46.

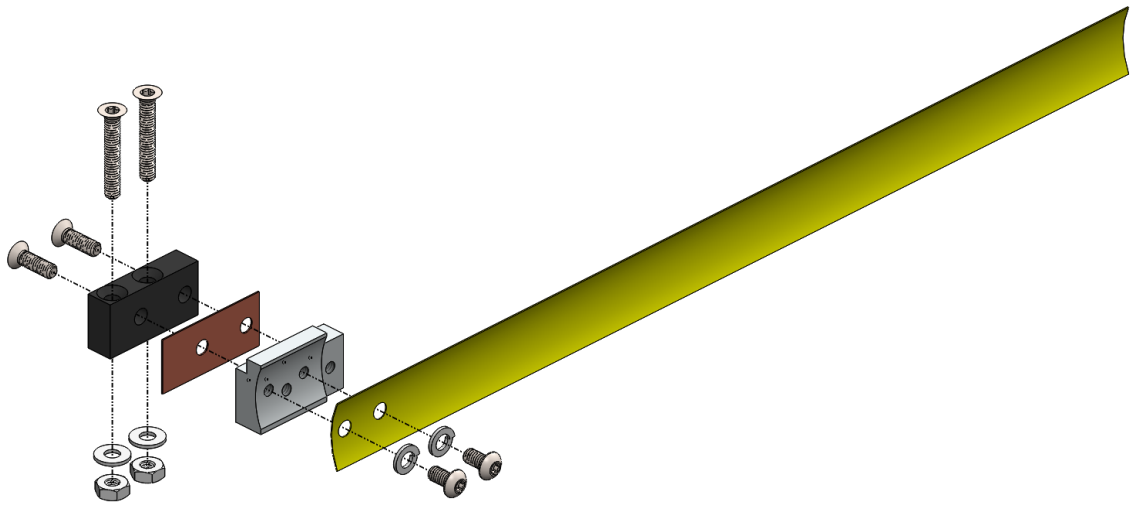

Figure 46: Exploded view rendering of the antenna arm feed concept. Courtesy of T. Tarnowski & ORCASat MECH team.

As shown, the block consists of a Delrin block bolted to the circuit board, which sandwiches a 0.01” thick copper foil with an aluminum block featuring a flat back and curved front. This is the foil to which the centre and shield conductors of the coax are soldered. Then, the tape measure dipole arm bolts to the front of this metal block, to a surface which matches their curvature.

It is noted that asides meeting the requirements outlined above, one key advantage of this design is that the PCB is not part of the circuit. The design of this feed was undertaken by the ORCASat MECH team, under the guidance of the writer of this thesis. The finalized drawings are included in Appendix D-1 for reference.

To bring together the electrical and mechanical components introduced up to this point, a 4-layer PCB was designed in Altium, to the specifications given by the ICD introduced in Section 2.2. This is illustrated in Figure 47 and Figure 48 with 3D captures from Altium. This board provides mechanical support for the antenna deployer, feed, and the antenna itself, and it also features the antenna deployment circuit and the PC104 backplane interface to the rest of the spacecraft. The manufacturing files for the circuit board itself can be found in the ORCASat TT&C design GitLab repository [51].

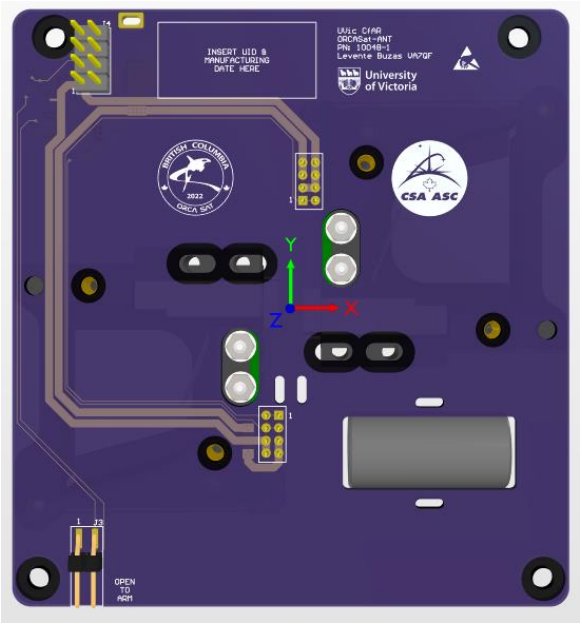

Figure 47: Altium capture for the antenna PCB with components, top side.

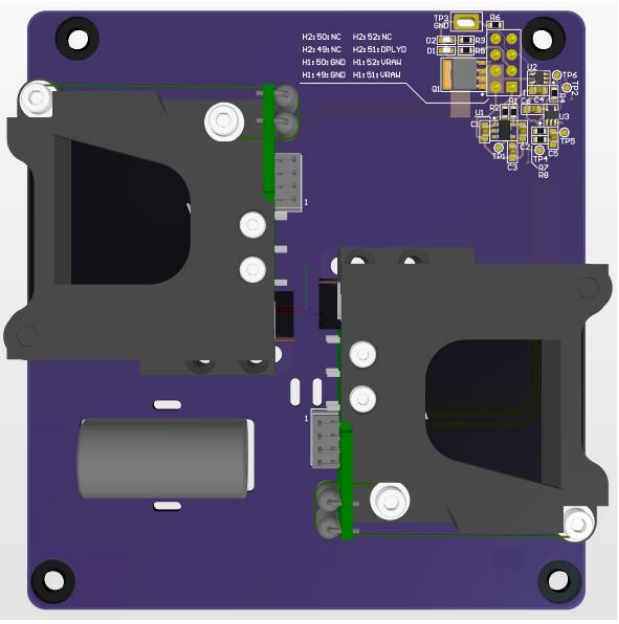

Figure 48: Altium capture of the antenna PCB with components, bottom side.

The PCB has some special features which require further consideration. First, the PCB is designed to be a 4-layer board. This was not because of the need for the extra copper layers, but the availability of the FR408HR Isola substrate by the manufacturer for 4-layer boards. This substrate is desirable because it has better high temperature properties (higher glass transition

temperature), thus making PCB delamination a lesser concern compared to regular FR4. The stack up used was the same ORCASat default which has already been introduced in Figure 25.

Second, there was a lot of extra care taken to avoid the use of ground planes. No ground pours were used anywhere in the design, a choice which was enabled by the lack of use of PCB transmission line structures. This is illustrated by a capture of the copper layers on the board from Altium in Figure 49. The use of ground pours was avoided to prevent difficult to characterize interactions between the antenna and the PCB ground planes, which have been shown to be able to degrade the performance of a PCB mounted antenna to a catastrophic extent in Section 6.3. To ground the electrical components in the deployment circuit which required it, traces were used in a star configuration. This is illustrated by the routing for the deployment circuit section on the bottom layer, shown in Figure 50. As shown, the ground (highlighted traces) is routed with traces to each components from a central location, instead of the industry standard practice of using dedicated vias for each component to ground planes on internal layers.

Asides this, care was also taken to avoid any copper, silkscreen or solder mask in the area directly underneath the antenna deployer. This can be partially seen in Figure 48 as the black area in the deployer opening. This was to avoid the antenna arms shorting to copper or be hindered by PCB features during deployment. A better illustration of this is provided in the next section in Figure 55, where the images of the manufactured bare boards are presented.

Lastly, the PCB was designed in a way to allow the adjustment of the feed gap of the dipole, by using slots as mounting features for the dipole arms. The details of this are shown in Figure 51 and Figure 52. As shown, the Delrin blocks are mounted in slots, which allows them to be slid closer and further apart, thus allowing the feed gap to be varied.

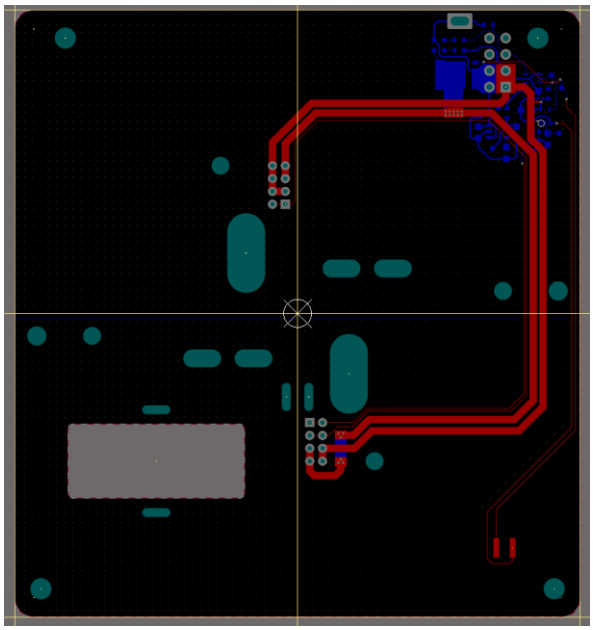

Figure 49: Copper layers on the antenna PCB. Ground planes are not used.

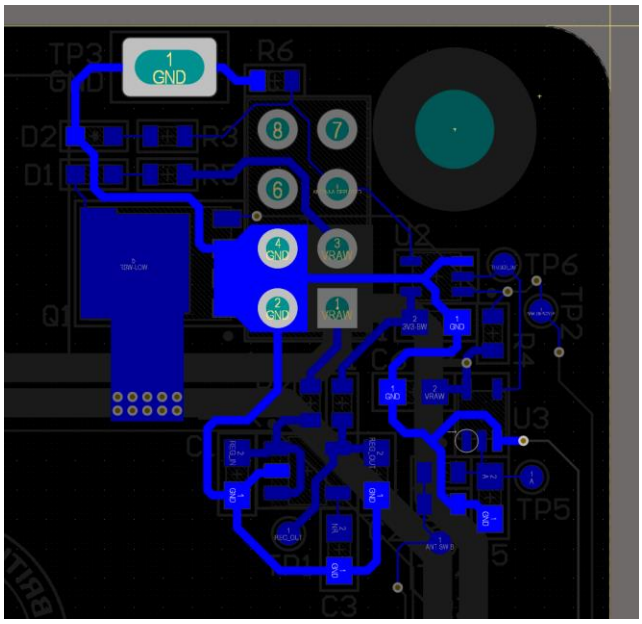

Figure 50: Ground layout for the antenna deployment circuit. The ground trace is highlighted, the use of planes is minimized.

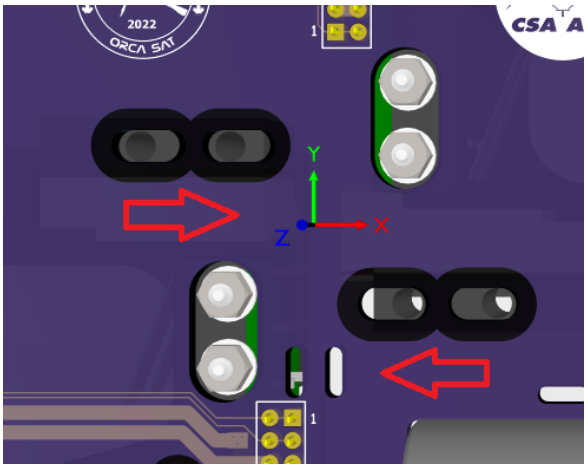

Figure 51: Dipole feed gap adjustment features, top side.

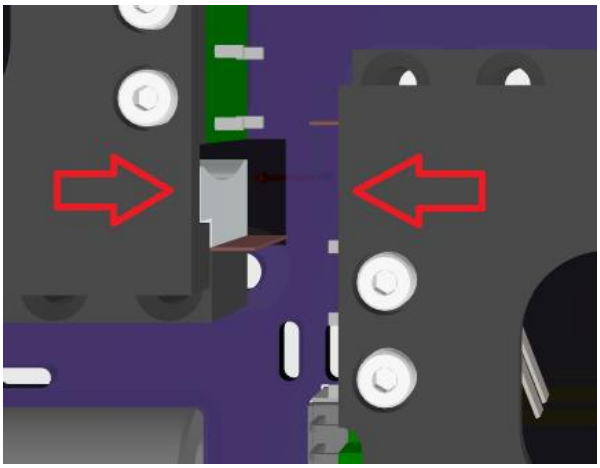

Figure 52: Dipole feed gap adjustment features, bottom side.

This feed gap adjustment feature was thought as a practical way which may aid in the matching of the dipole to 50 Ohms. This is theoretically feasible, as if the feed gap of a dipole is changed, its resonance frequency changes. The feasibility is illustrated by Figure 53, where an Ansys simulation of an ideal dipole with various feed gaps is shown.

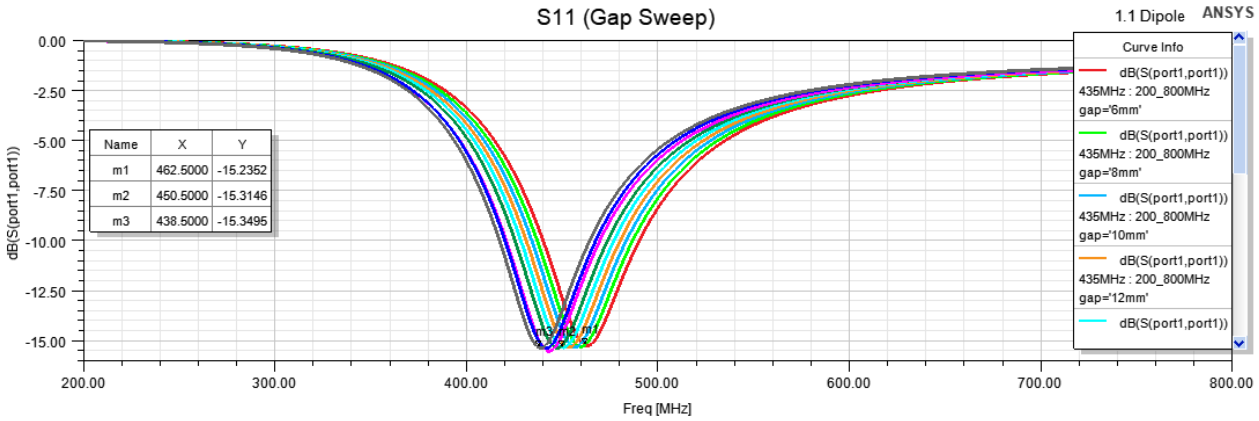

Figure 53: S11 log-magnitude plot of simulated resonance frequencies for an ideal dipole for feed gaps between 6 mm and 12 mm in 2mm increments. Courtesy of I. Bernardino.

8.4 Design Summary

The antenna design selected for implementation is shown in Figure 54. It is a half-wavelength deployable steel metal tape spring dipole with an adjustable feed gap, mounted on a 4-layer PCB, inside of a Delrin antenna deployer housing. The dipole is fed by RG-178 B/U coaxial cable, soldered to the 0.01” thick copper tabs inside the specialized feed. This coaxial cable is terminated in a right angle SMA connector on the side away from the antenna feed. Between the antenna feed and the SMA connector, a lossy choke balun is featured, wound on a Type # 61 ferrite bead, with the option of using >1 turns, if needed to increase the choking impedance. A separate block for impedance matching between the dipole and the coaxial cable is not used, with the intention being that the dipole will be made resonant tuned by pruning its arms, and any mismatch loss between the real dipole input impedance and the transmission line will be accepted. The PCB supporting the dipole features minimal ground to avoid undesirable interactions between the ground and the antenna, and it features a deployment circuit, which is responsible for the deployment of the antenna arms under the control of the OBC. The PCB is manufactured out of FR408HR Isola high temperature substrate, using the standard ORCASat PCB stack up.

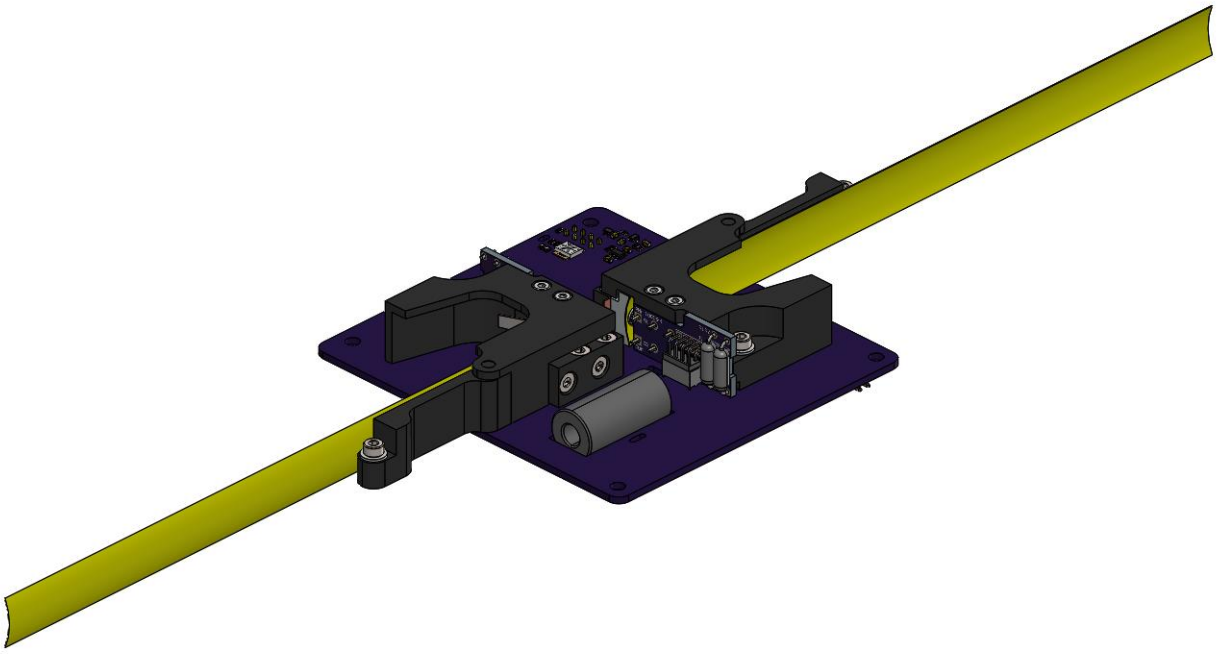

Figure 54: Antenna design isometric view. Courtesy of T. Tarnowski.

9 Manufacturing and Assembly

9.1 Manufacturing

The components which needed to be manufactured for the dipole antenna design introduced in the last section were the PCB, the feed components in Appendix D-1, the tape measure antenna arms in Appendix D-2, as well as a coaxial feeder of appropriate electrical or physical length. The antenna deployer housing and the burn wire resistor PCBs were already available as they were manufactured by the ORCASat MECH team earlier in the project to mitigate manufacturing risks to the project.

The manufacturing of the PCBs was done at OSH Park, an American PCB house. This manufacturer was selected because of their pricing and their default use of the Isola FR408HR substrate. The minimum quantity of 3 PCBs were manufactured. A sample from these board is shown in Figure 55 and Figure 56.

The manufacturing of the mechanical components was undertaken at a local machine shop (NorthWest FabWorks of Parksville, BC) as sponsorship to the ORCASat project. The manufacturing was overseen by the author of this thesis under technical advice from the ORCASat MECH team.

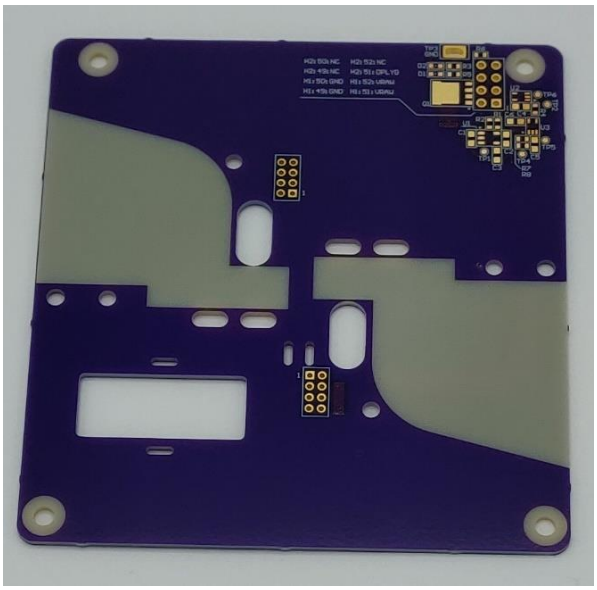

Figure 55: Manufactured antenna PCB without ground planes, bottom side.

Figure 56: Manufactured antenna PCB without ground planes, top side.

The manufacturing of the antenna arms was also undertaken by the ORCASat MECH team. These were cut to length in house and drilled using a 3D printed template to be compatible with the drawing in Appendix D-2. Their length was standardized at 25 cm, because that allowed generous extra length for tuning, should an arm length above the minimum possible theoretical half wavelength value for 435.0 MHz be needed. The coating was only removed from the antenna arms in the are where they overlap with the aluminum. This was appropriate because launch provider, NanoRacks, confirmed to the team during a video conference that outgassing from the coating on the tape measure is not a concern.

The coaxial jumper and copper tabs were manufactured by the author of this thesis. The tabs were cut to size from 0.5" wide 0.01" thick copper tape, and they were drilled out with 3D printed templates as well, based on the drawing in Appendix D-1. The coax was cut to the desired length, which was either determined by physical measurement based on specifications by the MECH team, or by Equation #13 if an electrical half wavelength cable was needed. For later iterations of the jumper, the latter was also verified by VNA measurement. It is noted that due to the extremely small cross section of the RG-178B/U coax, a razor blade was required to cut the coax to length. The use of wire cutters was found to be deforming the cuts and making the cable ends difficult to work with. It is also noted, that to avoid damage to the shield, a wire stripper pre-set to an opening marginally larger than the outside diameter of the shield was used, to avoid damage to the individual strands in the shield. The assembled coax with the copper tabs is illustrated in Figure 57. It is noted that the silver covering on the white cable is a metal liner made of HVAC tape, to prevent damage to the coax by the sharp edges on the spacecraft mock-up during testing.

Figure 57: An early prototype of the feeder assembly.

9.2 Assembly

The assembly of the antenna board required three iterations until a full prototype was obtained. This was due to the various components of the antenna arriving sporadically, and test facilities becoming available in a sporadic manner as well. The various configurations are outlined below. Only features which are different from the design described earlier are considered. The features which are not mentioned were as designed in each configuration. To aid with the assembly of the feed, the most delicate block of the antenna port, a step-by-step procedure was devised. This is included in Appendix D-3.

<u>Initial commissioning (Configuration #1):</u>

- Single turn choke
- Electrical half wavelength feeder
    - Cut by physical measurement using metal ruler, based on Equation #13
- No antenna deployer
- No deployment circuit
- 3D printed PLA feed support block instead of Delrin
- No burn wire PCB

<u>Verification testing (Configuration #2):</u>

- Single or double turn choke (for different tests)

- Electrical half wavelength feeder
    - Cut by VNA measurement or by physical measurement using metal ruler based on MECH team specification
- Full antenna deployer
- Deployment switch PCBs
    - No solder on board-to-board connectors
- No deployment circuit

Full prototype (Configuration #3):

- Single turn choke
- Maximum length feeder (~18”)
- Full deployment circuit
- Full antenna deployer
- Markings and serialization

9.3 TinSat

To allow the evaluation of the electrical performance of the antenna, a mock-up of ORCASat was prepared. This was designed to be electromagnetically like the final spacecraft, and it was required because solar panel PCBs were not available at the time testing described in this thesis was conducted. This article, named ‘TinSat’, consists of the actual satellite flight structure, covered by sheet metal plates, and outfitted with a 3D printed pipe adapter mountable on the nadir and port side of the mock-up. It is illustrated in Figure 58 and Figure 59.

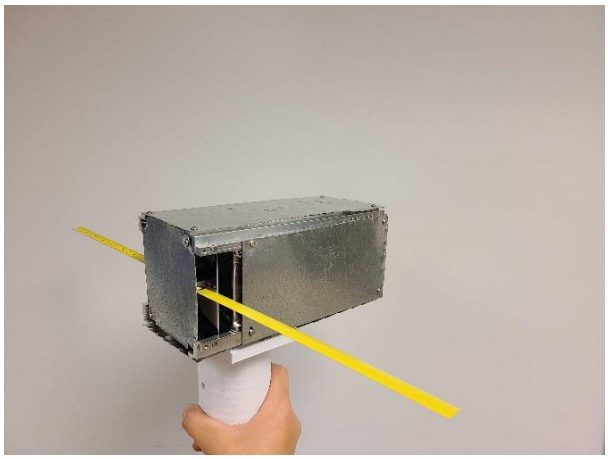

Figure 58: TinSat wake/starboard view, with antenna board installed.

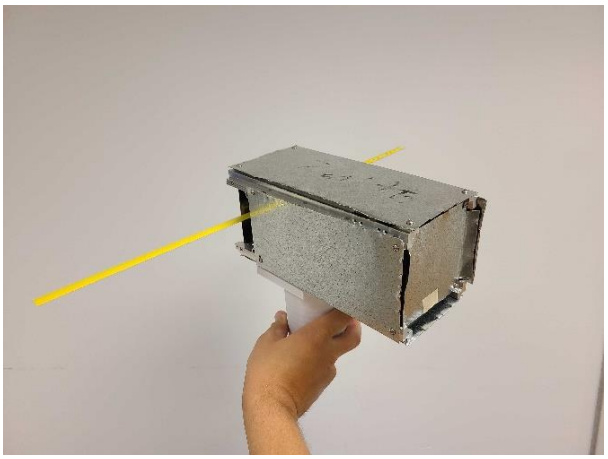

Figure 59: TinSat ram/starboard view, with antenna board installed.

9.4 Antenna Commissioning

9.4.1 Overview

The commissioning of the antenna consists of a set of informal measurements to verify that the antenna interacts with its environment, it is tunable, and it can be made to resonate at the frequency of interest with adequate bandwidth. The commissioning isn't focused on perfecting the antenna response, or its accurate characterization by measurement. Instead, it intends to investigate the trends the antenna response follows. It is undertaken primarily to ensure that no time is wasted by putting a non-functional test article trough a formal verification test procedure. This commissioning was undertaken using Configuration #1 from the last section.

9.4.2 Indoor Measurements

The initial measurements were undertaken indoors, using a HP8720C VNA. First, the test article was connected to the VNA calibrated over a wide frequency range and it was held at an arms length distance away from everything in the lab. Then, the S11 log-magnitude response on the VNA was displayed. It was observed that the test article was very responsive to its surroundings in terms of its S11 log-magnitude performance. Variations on the order of 10-20 dB were seen. It was also observed that the test article was resonant around 250 MHz. This is illustrated in Figure 60.

It is noted that for the purposes of this thesis, resonance is arbitrarily defined as a return loss RL < -10dB, because that means that at most 10 % of the incident power is reflected from the antenna due to the mismatch.

Based on these observations, it was concluded that the test article behaved like an antenna because it displayed resonance, and it interacted with its surroundings to a measurable extent.

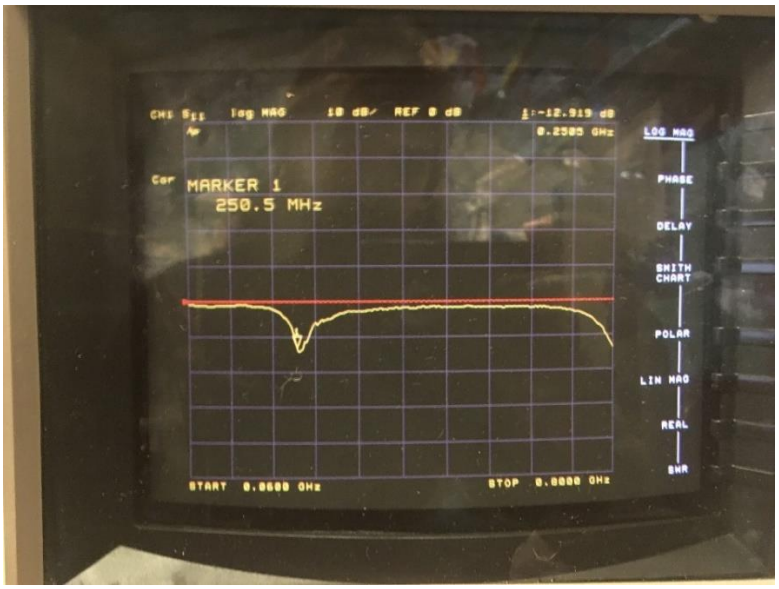

Figure 60: S11 log-magnitude performance for the standalone antenna board.

Next, sheet metal scissors were used to prune the tape arms of the test article to determine if it was tunable. The outcome of this is shown in Figure 61. It was determined that the test article was tunable, as its resonance was successfully moved from around 250 MHz in Figure 60 to the to the UHF amateur satellite allocation by shortening the arms. The ideal arm length in terms of return loss at the frequency of interest was determined to be 155 mm. While S11 log-magnitude and input impedance measurements were taken, quantitative conclusions were not drawn about the performance of the test article at this point, due to the high variability (10-20 dB) in the readings due to the surroundings. This measurement was also taken in the same manner as before, holding the test article at arms length in the lab, while connected to the calibrated VNA.

After the tuning was undertaken, measurements were also taken with minimum and maximum feed gap to determine if this experimental feature was useful for tuning the antenna. However, it was found that adjusting the feed gap put stress on the solder joints between the coaxial cable and the copper tabs, which defeated one of the main advantages of the feed – the fact that the coax solder joints could be left undisturbed after an initial initial installation. Therefore, it was

decided to configure the gap for the maximum for all subsequent measurements (chosen as it made the assembly the easiest) and stop any further investigation of this feature.

9.4.3 Preparations for Outdoor Measurements

To be able to obtain meaningful quantitative results for return loss, VSWR, and input impedance, and evaluate the impact of the spacecraft body on the antenna electrical performance, improvements to the test procedure were required. To this end, it was decided to conduct the rest of the measurements outdoors, with the test article mounted inside of TinSat, on a fibreglass pole. This was to ensure that the near field of the antenna contained as little ferromagnetic material as possible.

However, for these outdoor measurements the HP8720C VNA had to be replaced with an alternative. This VNA is very heavy, fragile, and static sensitive device, thus it is not suited for outdoor measurements. In its place, a RigExpert AA-1000 antenna analyzer was selected. This is a hand-held battery-operated antenna test device designed for the amateur radio market, which can undertake much of the same measurements as a VNA, but with lesser accuracy, and in a much more rugged, portable, and affordable form factor.

To verify that this instrument has adequate capabilities for the measurements, a benchtop comparison between the performance of the VNA and the antenna analyzer was undertaken. For this, both the antenna analyzer and the VNA were calibrated, and they were used to measure the response of the test article as it was left at the end of the previous test. As an improvement, the test article was mounted on a length of PVC pipe on the benchtop to increase the stability of the readings in both cases. This is illustrated in Figure 62.

The results obtained are shown in Figure 63 to Figure 66. It is noted that the antenna analyzer does not have return loss against frequency display capabilities, so the analyzer data is presented in terms of a VSWR graph. Comparison of the graphs indicates that the frequency of resonance (RL of -10 dB is VSWR of 1.925:1) is similar. The difference between the 425 MHz measurement on the analyzer and the 419 MHz measurement by the VNA can be explained as follows. First, the wider the measurement span of the antenna analyzer, the wider the frequency range over which the same number of measurement points are distributed, and the wider the resulting gap

is between them. As well, the analyzer does not have a minimum search functionality like a VNA. This means that finding the exact location of a minima for a full span measurement like the one shown in Figure 64 not always possible, which can explain the 6 MHz offset observed. This isn't problematic, however – once the location of minima is approximated, the span can be decreased to get a higher resolution reading, if required.

Figure 61: Tuned standalone antenna board in Configuration #1, with resonance around the ORCASat operating frequency.

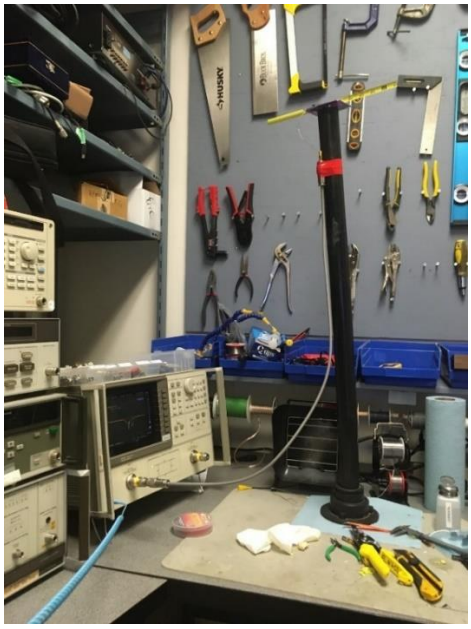

Figure 62: Test setup for baseline measurements.

When the comparison of the VNA and antenna analyzer was undertaken, quantitative measurements of the input impedance and return loss of the test article were also collected by both devices, as the readings were deemed stable enough to be of value. As shown by Figure 63 to Figure 66, there are discrepancies between the measurements taken by these two instruments. The measurements show RL=-20.6 dB and Z_{in}=54.2+8.8j Ωfor the antenna analyzer at 425 MHz, and RL=-13.7 dB and a Z_{in}=51.6+21.0j Ω for the VNA at 419MHz. This can be explained by the narrow minima on the graphs, as well as the 6 MHz difference between the measurement frequencies between the two instruments. Thus, the discrepancy has little relevance, because it originates from how the data was collected, and not how the test article performed.

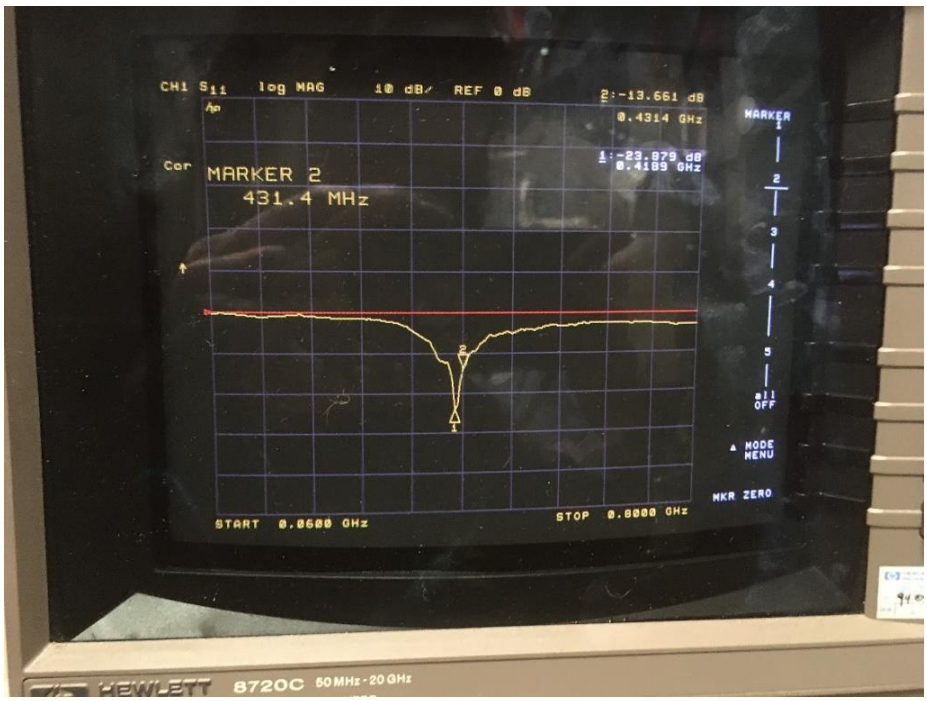

Figure 63: Baseline test measurement results with the VNA.

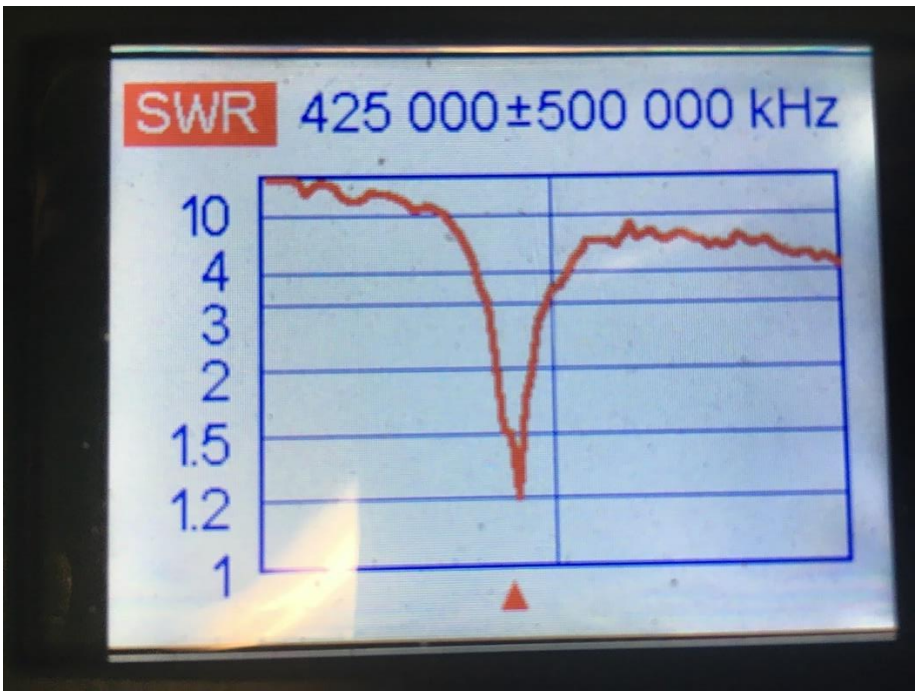

Figure 64: Baseline test measurement results with the antenna analyzer.

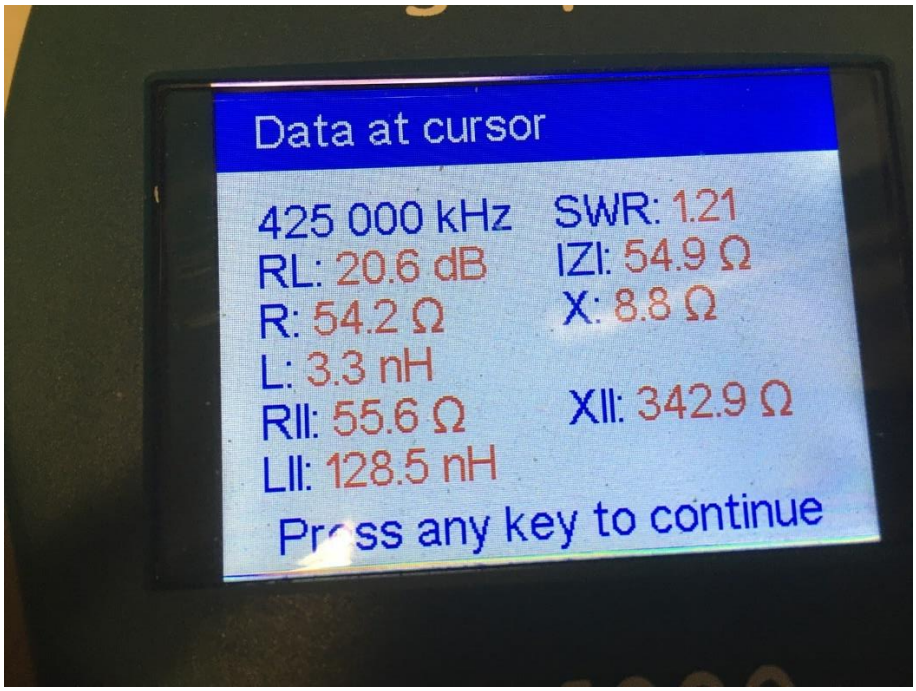

Figure 65: Zin results for the antenna analyzer baseline measurement.

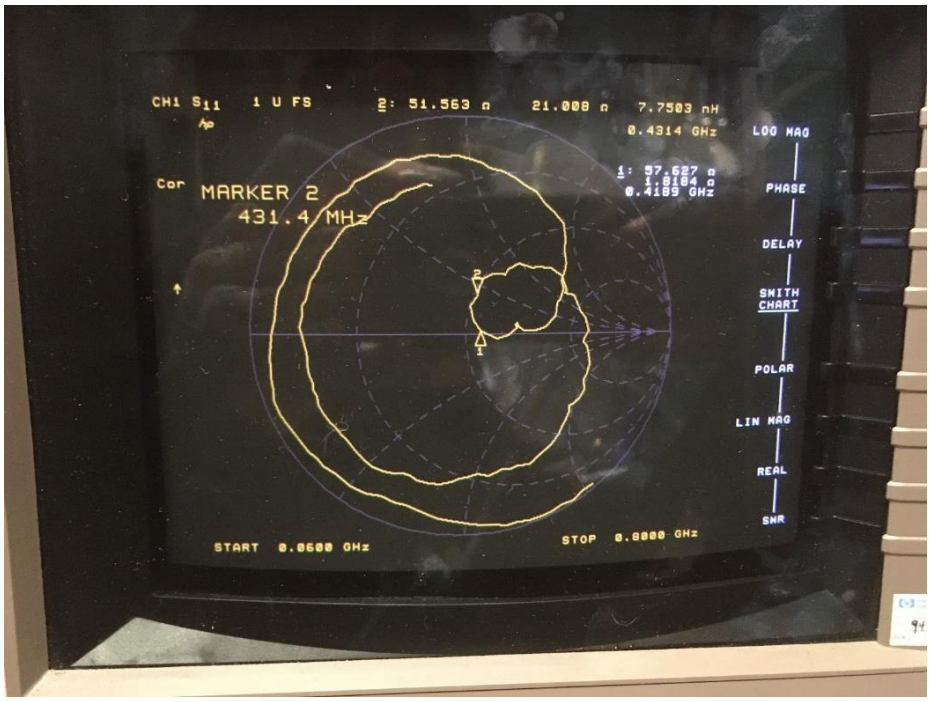

Figure 66: Zin measurement results for the VNA baseline measurement.

9.4.4 Outdoor Measurements

Having established the suitability of the AA-1000 antenna analyzer as a replacement of the VNA, now consideration can be given to the outdoor measurements. For these, the test setup in Figure 67 was used. As shown, a heavy-duty tripod was employed to support TinSat with the antenna board, at the end of a fiberglass pole with a coaxial cable running inside the pole to allow measurements away from the test article. The distance to far field was determined using Equation #13, reproduced below

$$\infty \leq r \leq \frac{2D_{max}^2}{\lambda} \tag{13}$$

For a half wavelength dipole at 437.06 MHz (the ORCASat assigned frequency), the wavelength λ and the larges physical antenna feature D_{max} can be determined as below. It is noted that D_{max} is simply λ/2, the length of the antenna itself. This gives the minimum distance to far field as 0.34 m.

$$\lambda = \frac{c}{f} = \frac{299792458}{437060000} = 0.686\ m \tag{14}$$

$$\mathrm{D} = \lambda = \frac{\lambda}{2} = \frac{0.686}{2} = 0.343\ m \tag{15}$$

$$r_{min} = \frac{2D^2}{\lambda} = \frac{2 \times (0.343)^2}{0.686} = 0.34\ m \tag{16}$$

The length of the fiberglass pole was made longer than this distance r_{min}. As well the antenna analyzer was calibrated at the end of the long test cable. This was to move the measurement plane right up to the SMA terminated coaxial feeder soldered directly to the antenna feed. For this test, new 250mm arms were installed in the antenna board as well, to allow the tuning of the antenna to the spacecraft body in the "free space" provided by the outdoor environment.

Figure 67: Test setup for the outdoor commissioning measurements.

Measurements were undertaken over two ranges. First, 435 +/- 200 MHz was used to tune the antenna coarsely to the 435.0-438.0 MHz frequency range, and then over 436.5 +/- 25 MHz to obtain accurate measurements. The results are shown in Figure 68 to Figure 71. Consideration only given to the data which was collected over the narrower span, as that provides more accurate results. As shown, the test article performance was found to be promising. A return loss of -23.5 dB was measured, along with an input impedance of 45.3 + 4.2j Ω. As well, a desirable

VSWR (better than 1.5:1) was observed almost the entire measurement range. This results suggests that the test article performs as designed, meaning that it is worthwhile to be put trough a formal verification test campaign, which is the topic of the next section.

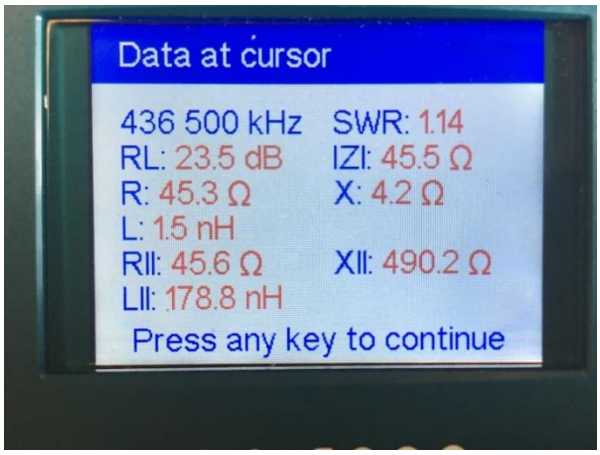

Figure 68: Data snapshot from the outdoor commissioning test.

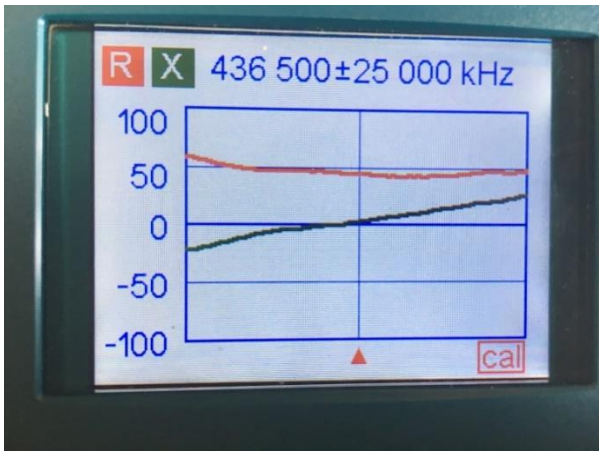

Figure 69: R/X over frequency graph from the outdoor commissioning test.

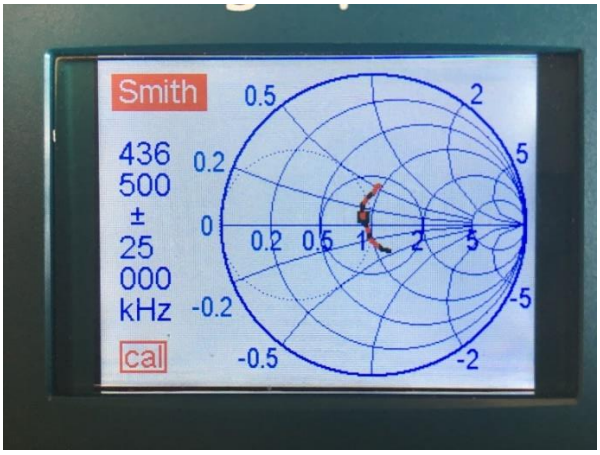

Figure 70: Smith Chart capture from the outdoor commissioning test.

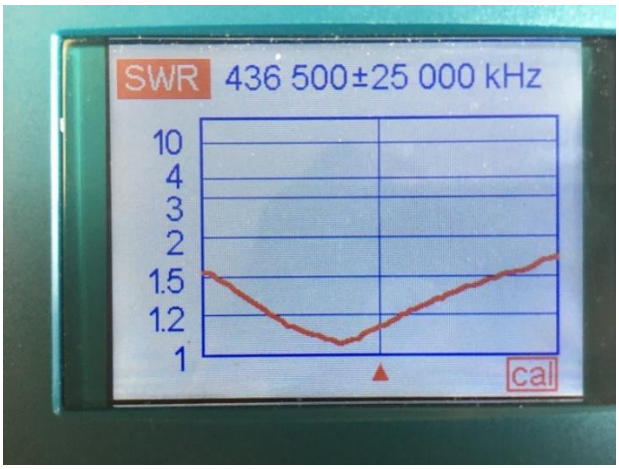

Figure 71: Capture of VSWR over frequency from the outdoor commissioning test.

10 Testing and Validation

10.1 Overview

The purpose of verification testing is to formally evaluate the performance of the ORCASat antenna prototype and determine if it meets the requirements which have been introduced at the beginning of this document. The verification test campaign consists of three experiments. These are the return loss, the coarse gain pattern, and the coarse absolute gain tests. These have been devised as the optimal compromise between available resources, time, and result quality. Their detailed consideration is the topic of the sections which follow.

10.2 Return Loss Test

10.2.1 Test Objective

The main objective of this test is to characterize the return loss and input impedance of the ORCASat antenna as a function of frequency over the 435.0-438.0 MHz amateur satellite allocation. As well, the formal verification of the tunability of the antenna is also of interest.

10.2.2 Equipment Used

The equipment required for the return loss test is listed below:

- Satellite mock-up with ground lead (TinSat)*
- Pipe mounting adapter for satellite mock-up
- Coaxial adapters
- Coaxial jumpers
- HP8720C vector network analyzer
- RigExpert AA-1000 antenna analyzer
- SMA short open load trough (SOLT) 50 Ω calibration kit
- Sheet metal scissors
- Heavy duty tripod
- Fiberglass pole, 60”
- Blade type screwdriver
- Hose clamps
- PVC pipe with flanged end
- Multimeter

- Multimeter leads
- Duct tape

*To make this and subsequent tests more realistic, a method allowing the grounding of the mock-up to the test equipment ground was devised. This was deemed necessary as in the flight satellite, the solar panel PCBs covering the ORCASat chassis will feature internal ground planes bonded to the negative terminal of the batteries in the EPS.

10.2.3 Test Setup

The test setups needed are those illustrated in Figure 72 for VNA calibration, in Figure 73 for the calibration of the antenna analyzer, and in Figure 74 for the return loss measurements. The base configuration of the device under test (DUT) is Configuration #2. It is noted that for various steps in the test, the configuration of the choke may be varied to evaluate the effectiveness of using more than one turns. The details of this are provided as part of the test procedure.

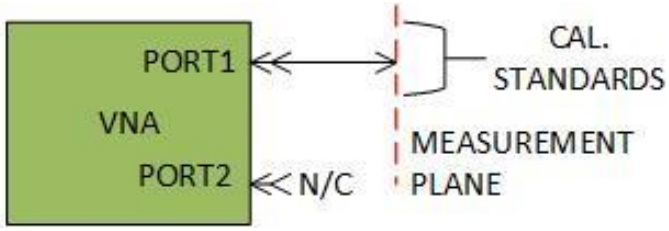

Figure 72: Test setup for VNA calibration.

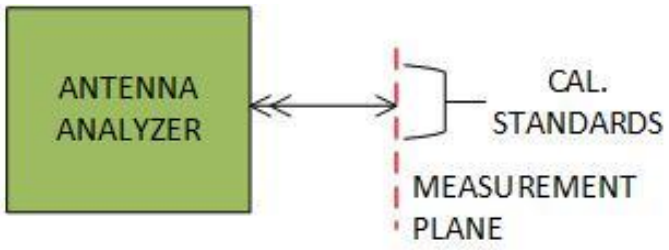

Figure 73: Test setup for antenna analyzer calibration.

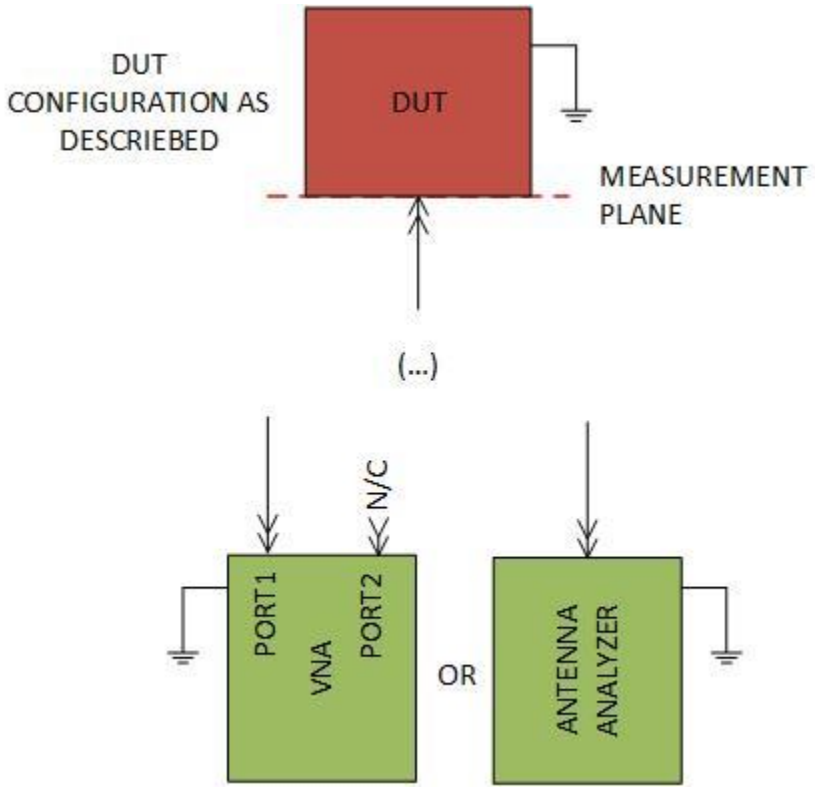

Figure 74: Test setup for return loss measurement.

10.2.4 Test Procedure

1. Construct the test setup in Figure 72. Calibrate the VNA for S11 log-magnitude measurements up to 1GHz.
2. Ensure that the DUT has a single turn of coax over the ferrite, wound from a coaxial cable which is electrical half wavelength by VNA measurement. Also ensure that the DUT has 250mm arms attached with the tape coating removed in the area where the tape bolts to the aluminum block.
3. Connect the DUT to the VNA. Observe if the touching the DUT at various locations or holding the DUT in the vicinity of other objects impacts the return loss observed. Record your observations.
4. Tape the flanged PVC pipe to the centre of the work bench using the duct tape. Rest the DUT on it. Strain relive the VNA test cable by taping it to the PVC pipe.
5. With the DUT resting on the PVC pipe and connected to the VNA, prune the antenna arms with the sheet metal scissors until resonance is observed at approximately 437 MHz. Use a marker to record the return loss at this frequency and take a capture of the

VSWR, S11 log-magnitude, and Smith Chart graphs. Make sure that the Smith Chart shows the impedance measured, and all text on the captures is readable.

6. Attach a coaxial cable of some arbitrary but reasonable length to the pigtail of the DUT. Observe and capture the Smith Chart response of the DUT.
7. Repeat the previous step with a coaxial cable of different length.
8. Construct the test setup for calibration of the antenna analyzer in Figure 73 and calibrate it for 437 MHz +/- 25 MHz.
9. Measure the response of the DUT and take capture of R/X, VSWR and Smith Chart views, as well as a snapshot at 437 MHz.
10. Compare the Z_{in} and the return loss observed in the last step at 437 MHz to the VNA measurements, and make sure that they agree. This is to formally very that the VNA can be replaced by the antenna analyzer for the outdoor test.
11. Set up the for the outdoor test.
    a. Mount the DUT in the satellite mock-up, after having made sure that it has been outfitted with a set of new 250 mm dipole arms. (From here onwards, the DUT refers to the antenna PCB inside of the mock-up.)
    b. Mount the pipe adapter on the nadir face of the spacecraft.
    c. Run a test coaxial lead from the antenna analyzer through the fiberglass pole and calibrate the analyzer at the end of this for its full frequency range after the coax has been run, but before the pole is erected.
    d. Ground the mock-up to the test equipment ground. Measure continuity between these two points to ensure that a good ground connection has been established. Make a record of this.
    e. Erect the heavy-duty tripod. Select a location which will allow maximum distance from surrounding objects.
    f. Mount the fiberglass pole on to the heavy-duty tripod using the hose clamps and the screwdriver.
12. With the DUT mounted on the mechanical supports, prune the tape arms until resonance is observed around 437 MHz.

13. Recalibrate the antenna analyzer for 437 +/- 50 MHz. Fine tune the arm length by pruning so the minimum SWR occurs at 437 MHz.
14. Configure the analyzer for real time SWR measurements. Measure SWR in real time and see if the reading is stable or variable. Observe if touching the feeder of the DUT or the analyzer impacts this. Record your findings.
15. Measure the response of the DUT and take capture of R/X, VSWR and Smith Chart views, as well as a data snapshot at 437 MHz.
16. Attach a coaxial cable of some arbitrary but reasonable length to the pigtail of the DUT. Observe and capture a data snapshot of DUT at 437 MHz.
17. Repeat the previous step with a coaxial cable of different length.
18. Disassemble the mock-up and record the optimal dipole arm lengths determined for the test cases with, and without the satellite mock -up.

10.2.5 Expected Outcomes

The expected outcomes for the return loss test are listed below:

- Agreement between VNA and analyzer measurements
- Antenna resonance at around 437 MHz
- RL of <-10 dB or less over 435.0-438.0 MHz
- Antenna impedance near 50 Ωresistive
- Impact of extending cable length by an arbitrary amount is minimal
- Antenna is tunable by pruning

10.2.6 Limitations and Assumptions

The limitations and assumptions for this test are listed below:

- The measurements in this test are made outdoors instead of a true anechoic chamber so the measurement accuracy may suffer due to the lack of the “free space” provided by a true anechoic chamber.
- The LMR-400 coaxial line used to connect the DUT to the test equipment during the outdoor measurements has metal inside it which may impact the results.

- The satellite mock-up is not an exact representation of the flight version of ORCASat, so discrepancies between the two can result in discrepancies in the measurement results.
- The electronics of the deployment circuit were not installed on the PCB during the test due to shipping delays for electronic components. Having this circuit in place may impact the result of the measurements.

10.2.7 Test Results

The result of this test are shown in Figure 75 to Figure 91, as well as in Table 1 and Table 2.

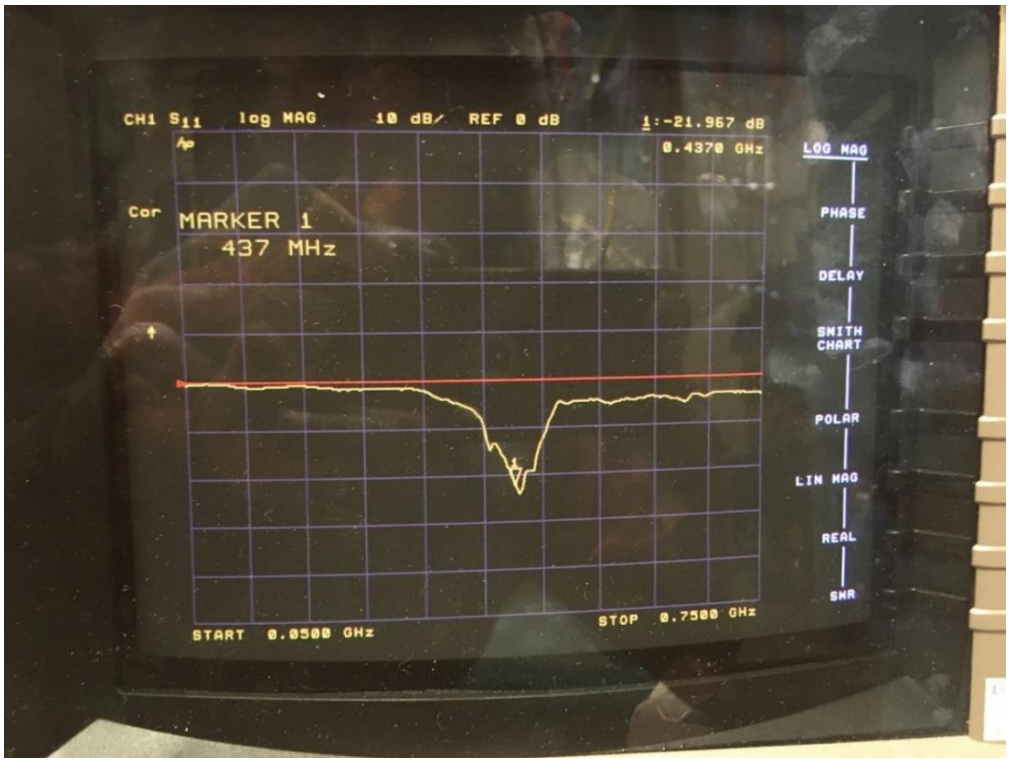

Figure 75: S11 log-magnitude response, λ/2 cable, indoor, VNA.

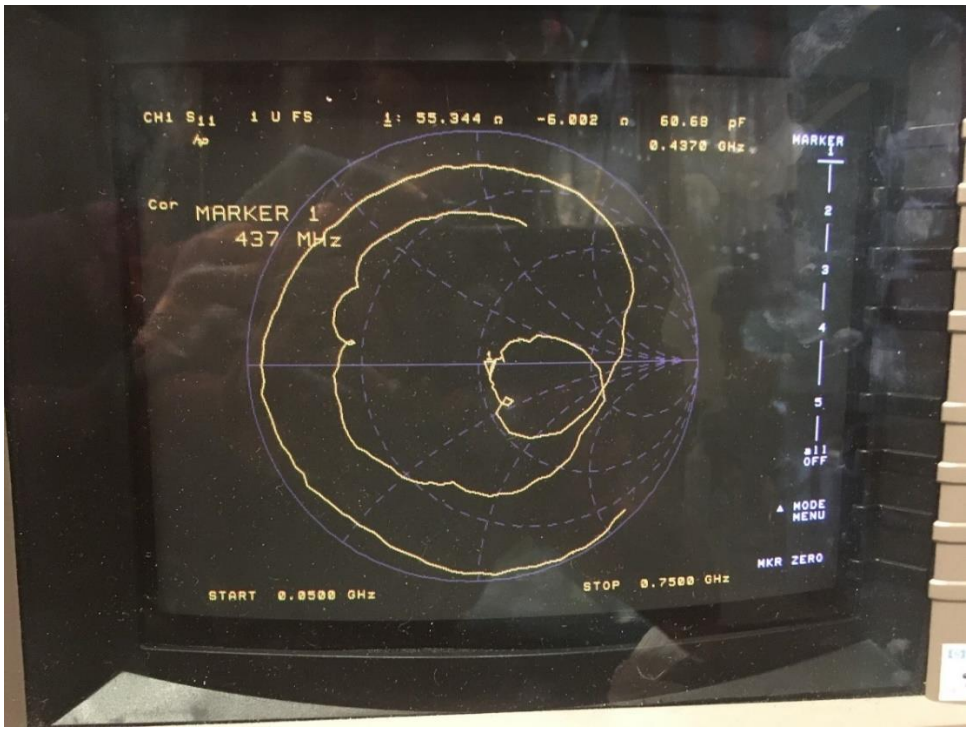

Figure 76: Smith Chart response, λ/2 cable, indoor, VNA.

Figure 77: VSWR response, λ/2 cable, indoor, VNA.

Figure 78: Smith Chart response, extender cable #1, indoor, VNA.

Figure 79: Extender cable #1.

Figure 80: Smith Chart response, extender cable #2, indoor, VNA.

Figure 81: Extender cable #2.

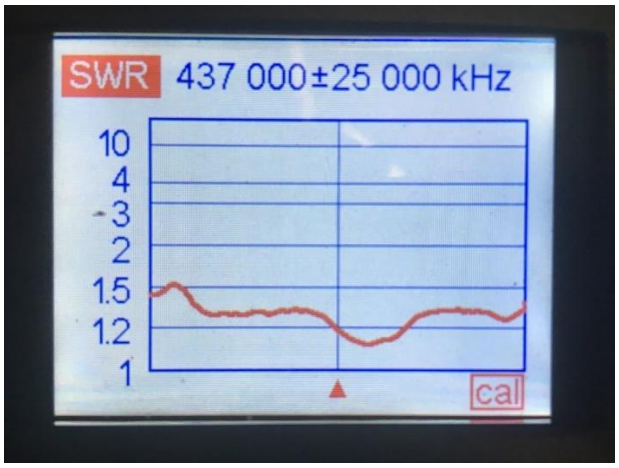

Figure 82: VSWR response, λ/2 cable, indoor, antenna analyzer.

Figure 83: R/X response, λ/2 cable, indoor, antenna analyzer.

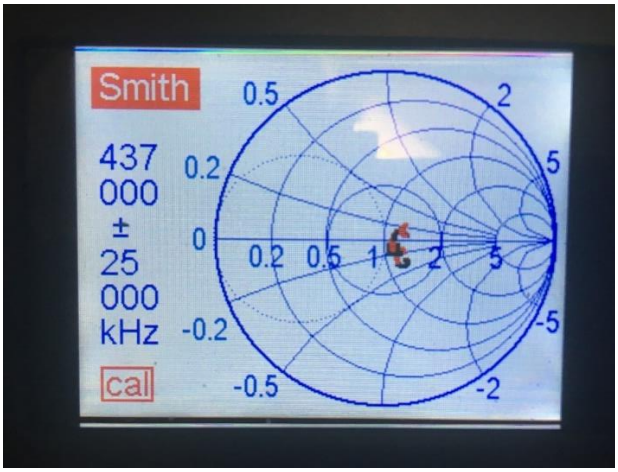

Figure 84: Smith Chart response, λ/2 cable, indoor, antenna analyzer.

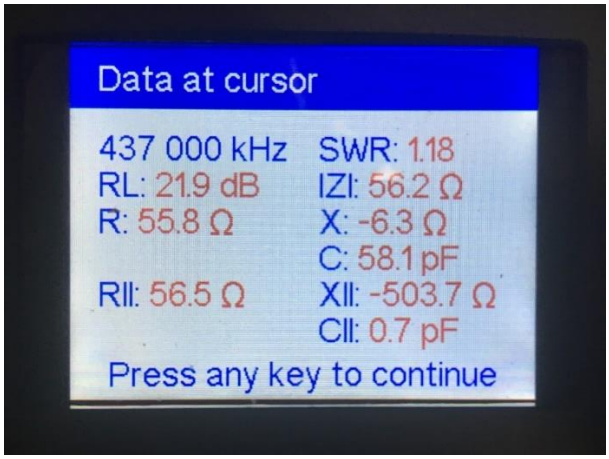

Figure 85: Data snapshot at 437 MHz, λ/2 cable, indoor, antenna analyzer.

Figure 86: VSWR response, λ/2 cable, outdoor, antenna analyzer.

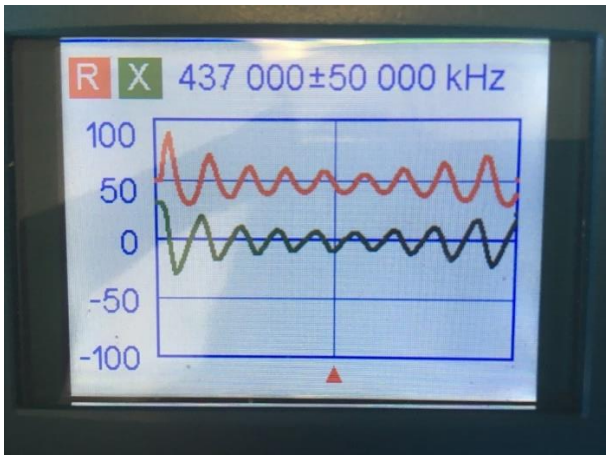

Figure 87: R/X response, λ/2 cable, outdoor, antenna analyzer.

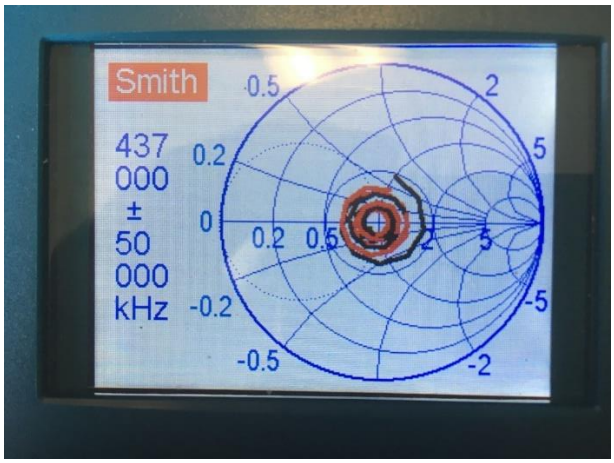

Figure 88: Smith Chart response, λ/2 cable, outdoor, antenna analyzer.

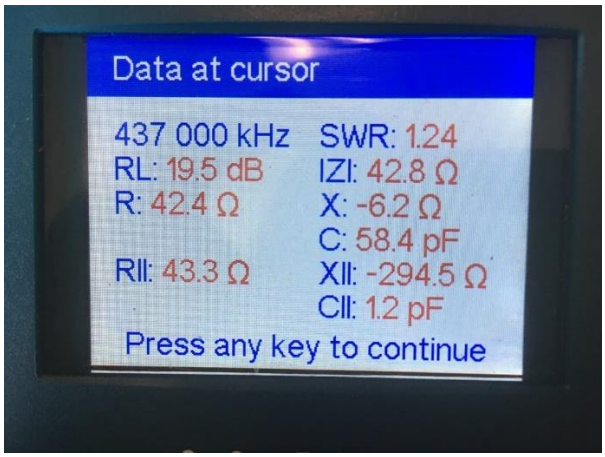

Figure 89: Data snapshot at 437 MHz, λ/2 cable, outdoor, antenna analyzer.

Figure 90: Data snapshot at 437 MHz, extender cable #1, outdoor, antenna analyzer.

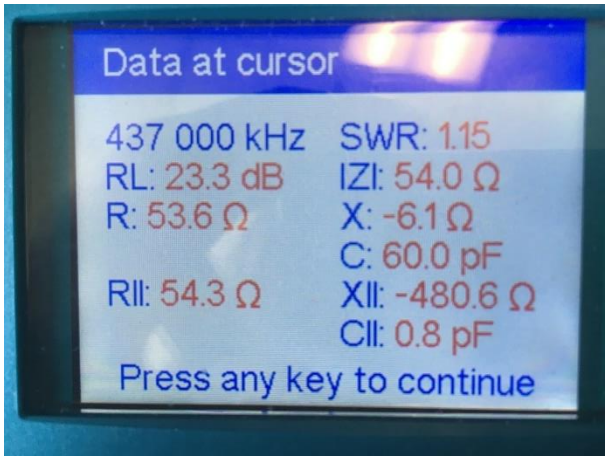

Figure 91: Data snapshot at 437 MHz, extender cable #2, outdoor, antenna analyzer.

Table 1: Qualitative test results for the return loss test.

Parameter of Interest	Observation
DUT responsive to the environment?	Yes
Outdoor reading stable?	Yes
Continuity, Test Equipment to Satellite Mock-up Body	Pass (0.04 Ω)
Optimal Arm Length, Indoor Test (mm)	150
Optimal Arm Length, Outdoor Test (mm)	165

Table 2: Test result summary - outdoor measurements, 437 MHz +/-50MHz, readings recorded at 437 MHz.

Cable	0.5 λ	Extender #1	Extender #2
Return Loss (dB)	19.5	25.2	23.3
Z (Ohm)	42.4-6.2j	53.7-4.3j	53.6-6.1j

10.2.8 Discussion

Based on the results presented in the last section, the DUT has performed as expected:

- It was verified that the VNA and the antenna analyzer can be substituted for each other. This is based on the Z_{in}=55.3-6.0j and RL=-22 dB measured by the VNA, and Z_{in}=55.8-6.3j and RL= -21 dB measured by the antenna analyzer for the same test article on the benchtop. These results are shown in Figure 76 and Figure 82.
- It was also verified that the antenna is tunable, because pruning it was proven to be an effective tool in moving its resonance to the frequency of interest. As desired, the antenna impedance was also observed to be around 50 Ω resistive after tuning, around 437 MHz, the frequency of interest.
- The effect of adding extra cable length to the electrical half wavelength feeder was observed to be minimal, causing at most few Ohms of change in the measured input

impedance. This is relevant because this is the expected behaviour if the antenna input impedance is resistive, as looking into the feed block.

- The addition of the spacecraft mock-up did have some impact on the results, but not to an extent which would be problematic, as a largely resistive input impedance around 50 Ω was obtained for this test configuration as well.
- One interesting, unexplained observation was that the R/X graph observed on the antenna analyzer between the indoor and outdoor test has changed, going from a flat response indoors to more of an oscillatory one outdoors when the spacecraft body was added. The reason for this may be external radiated signals received by the antenna and processed by the antenna analyzer as part of the response.

10.3 Coarse Antenna Pattern Test

10.3.1 Test Objective

The main objective of this test is to verify the radiation pattern of the ORCASat antenna coarsely matches that of a dipole. As secondary objectives, the impact of the lossy ferry choke balun construction on the antenna, and the return loss performance of the antenna in the anechoic chamber are also of interest.

10.3.2 Equipment Used

The equipment required for the coarse antenna pattern test is listed below:

- Sigilent SVA1015X spectrum analyzer
- Rigol DSG815 RF signal generator
- RigExpert AA-1000 antenna analyzer
- Coaxial cables
- Coaxial adapters
- Anechoic chamber
- Com-Power AC-220 Hybrid Combilog log periodic antenna
- Com-Power ATAC-110 Combilog antenna attachment
- Com-Power ATTS-110 Antenna support
- SMA SOLT calibration kit
- String

- Protractor
- Electrical tape
- Satellite mock-up
- Pipe adapter for satellite mock-up
- Fibreglass pole, 60”
- Hose clamps
- Blade type screwdriver
- Tape measure (25’ min.)
- Sheet metal scissors
- Multimeter
- Multimeter leads
- Driver kit

10.3.3 Test Setup

The setup for the coarse antenna pattern test is shown in Figure 92.

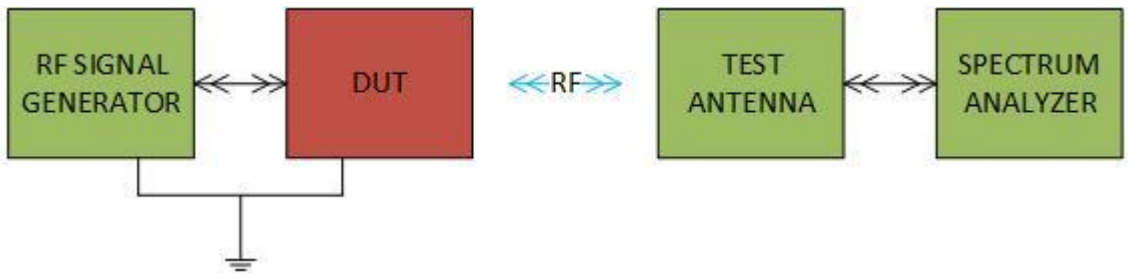

Figure 92: Electrical test setup for gain pattern measurement in the E and H plane.

10.3.4 Test Procedure

10.3.4.1 Pattern Measurement

1. Configure the test setup in Figure 92.
    a. Mount the test article in the satellite mock-up, after having made sure that the arms from the outdoor part of the return loss test have been installed, and the test article has been outfitted with a balun of a single turn.
    b. Mount the pipe adapter on the nadir face of the mock-up and use the hose clamps to fasten the fibreglass tube to the stand of the positioner of the anechoic chamber.

c. Feed a coaxial test lead trough the fiberglass tube and attach it to the test article and the RF signal generator. Also attach the DUT ground connection to the shield of the test lead.
d. Mount the DUT on the pole and cover up the mounting structure with absorbers facing the test antenna.
e. Arrange the test antenna on its tripod, pointed towards the DUT. Make sure that the planes of the two antennas match. Cover the bottom section of the tripod with absorbers as well, facing the DUT.
f. Record the distance between the tip of the test antenna and the ram face of the spacecraft. Make sure that the antennas are in each other's far fields, using the far field equation (Equation #13). Also make sure that strategically placed absorbers are used as much as possible to minimize any reflections in the chamber.

2. Start with the E plane antenna pattern measurements. Position the DUT such that the ram face points at the test antenna. Use the string fastened between the DUT and the test antenna and the protractor to verify accurate pointing.
3. Configure the signal generator to output a 0dBm signal at 437 MHz and enable it.
4. Configure the spectrum analyzer for 437 MHz centre frequency, no input attenuation, a reference level of -20 dBm, a span of 5 MHz and the LNA enabled. Use the “Peak” function to place a marker on the received tone, and record the power measured.
5. Rotate the DUT in the E plane clockwise by 10 degrees and repeat the previous step.
6. Repeat the previous step until data has been collected over 360 degrees.
7. Repeat from Step 2 but interchange the transmit and the receive antenna.
8. Continue with the H plane antenna pattern measurement. Rotate the test antenna and the DUT 90 degrees and repeat from Step 2 but in the H plane.
9. Skip to the next section and complete it, and then repeat from Step 1 in this section but use two turns of coax over the ferrite.
10. Plot the results in dB in a normalized manner in a polar coordinate system.

10.3.4.2 Return Loss Verification

1. Calibrate the antenna analyzer over a frequency range of 437 +/- 50 MHz, using the test setup shown in Figure 73 for the return loss test procedure.
2. Use the antenna analyzer to measure the input return loss of the DUT in the anechoic chamber. Take captures of the R/X, VSWR and Smith Chart plots, as well as a data snapshot at 437 MHz.

10.3.5 Expected Outcomes

The expected outcomes for the coarse gain pattern test are listed below:

- The expected result is that radiation pattern obtained will match that of a centre fed half wavelength dipole, introduced by Figure 9 earlier in this thesis. A match is only expected shape wise as no attempt is made in this test to characterize the absolute gain of the dipole, due to the frequency limitations of the anechoic chamber available at UVic.
- It is also expected that the return loss measurement results will be like the results obtained outdoors in the Return Loss test.

10.3.6 Limitations and Assumptions

The limitations and assumptions for the coarse gain pattern test are listed below:

- The anechoic chamber at UVic is only designed for measurements down to 1 GHz, so the results may be severely impacted by reflections.
- The positioning of the DUT is done manually, so the readings may not be taken exactly at the angles specified.
- The mounting of the DUT in the anechoic chamber may have an adverse effect on the shape of the pattern compared to free space.
- The spacecraft mock-up is not the same as the final spacecraft, so deviations between the test article and the final device may produce different results.
- The setup in the anechoic chamber did not allow for an easy way to place the DUT to the far field of the test antenna. The DUT was at 4.16 m instead of the 4.68 m distance defining the far field of the test antenna.

- This distance was computed in the same manner as shown in Section 9.4.3, but with the largest dimension (the reflector) of the test antenna as D_{max}.

- Due to operator error during the test, return loss test data has not been collected for a single turn choke balun.

10.3.7 Test Results

The physical configuration of the DUT and the test antenna for the anechoic chamber measurements are illustrated in Figure 93 to Figure 98. The test results for the return loss related measurements are shown in Figure 99 to Figure 102, and the result for the coarse gain pattern test are shown in Figure 103 to Figure 118. It is noted that the distance from the ram face of the DUT to the tip of the test antenna was measured to be 4.16m. It is also noted that the antenna pattern plots in this section were produced by, with resources from the MATLAB Antenna Toolbox.

Figure 93: DUT ram view, E plane measurement.

Figure 94: Test antenna, E plane measurement.

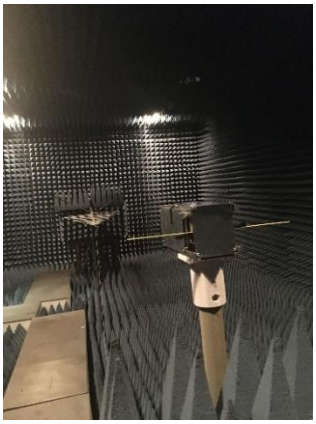

Figure 95: Range setup, E plane measurement.

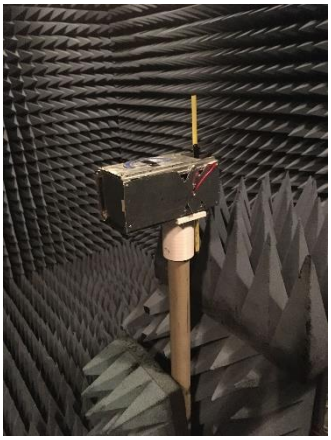

Figure 96: DUT ram/nadir view, H plane measurement.

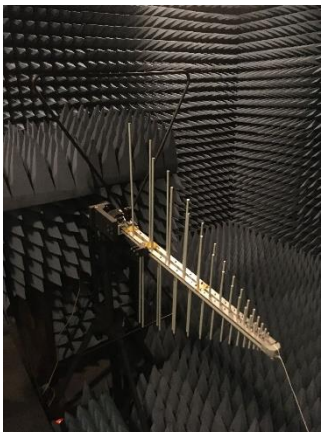

Figure 97: Test antenna, H plane measurement.

Figure 98: Range setup, H plane measurement.

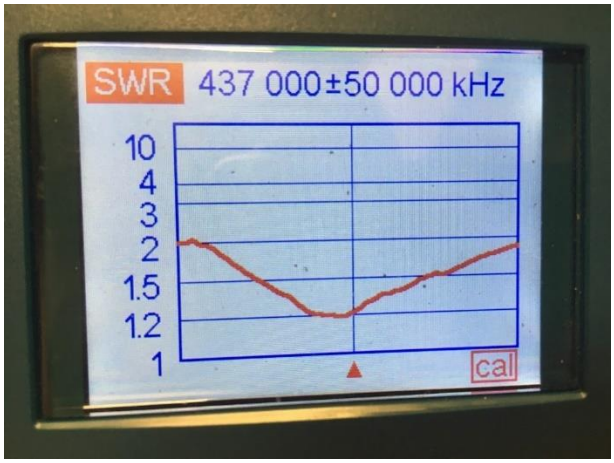

Figure 99: VSWR response, 18" cable, anechoic chamber, analyzer, double turn choke.

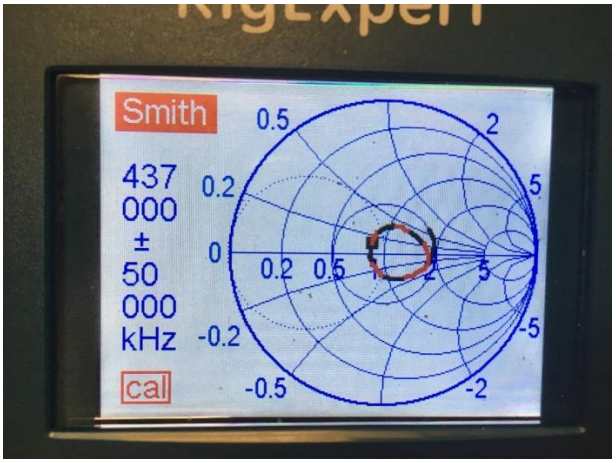

Figure 100: Smith Chart response, 18" cable, anechoic chamber, analyzer, double turn choke.

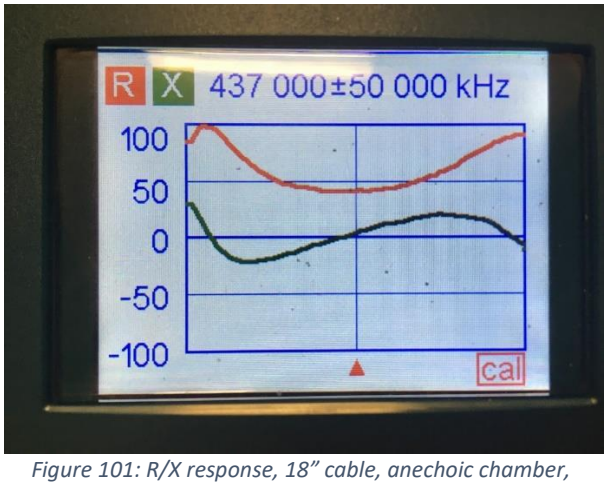

Figure 101: R/X response, 18" cable, anechoic chamber, analyzer, double turn choke.

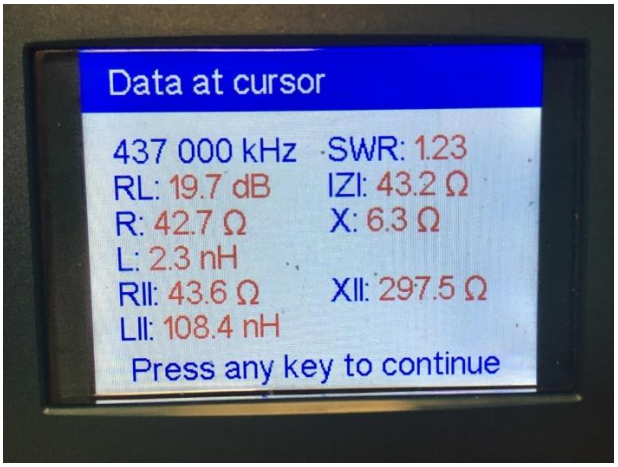

Figure 102: 437 MHz data snapshot, 18" cable, anechoic chamber, analyzer, double turn choke.

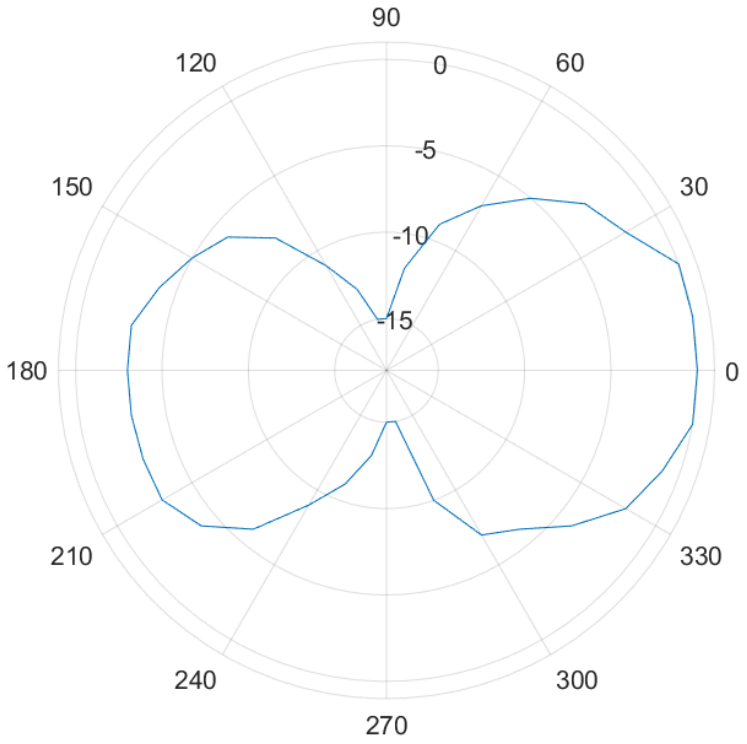

Figure 103: Measured E plane pattern plot, TX, single turn choke.

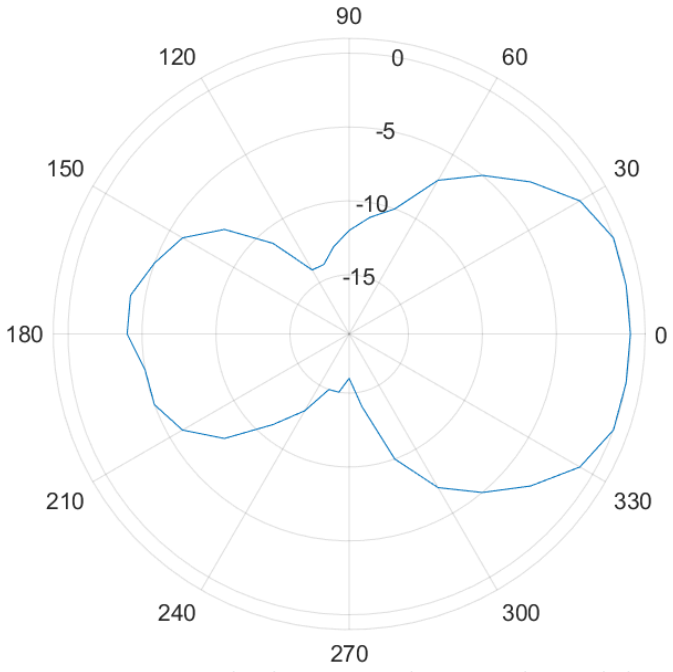

Figure 104: Measured E plane pattern plot, RX, single turn choke.

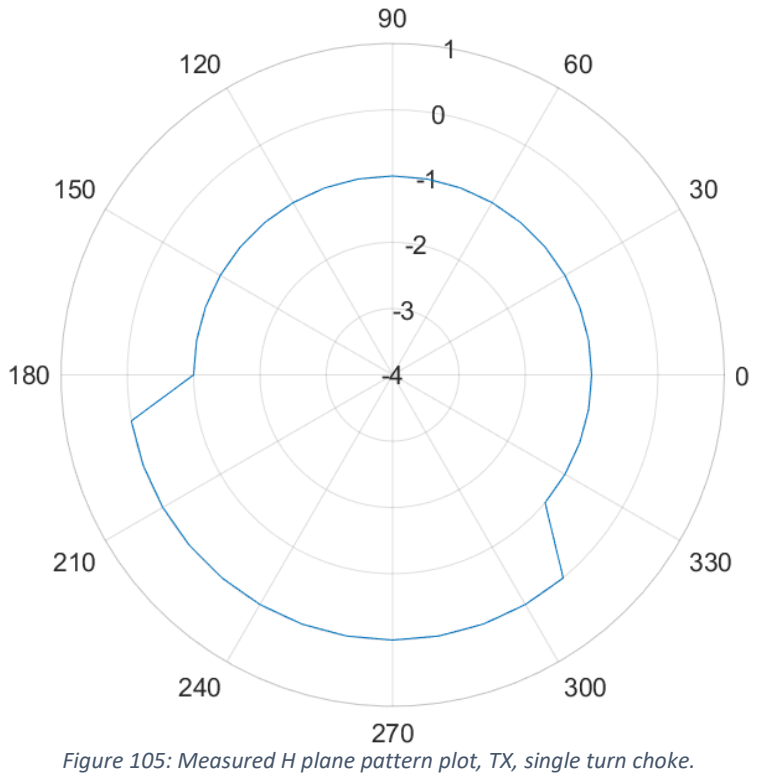

Figure 105: Measured H plane pattern plot, TX, single turn choke.

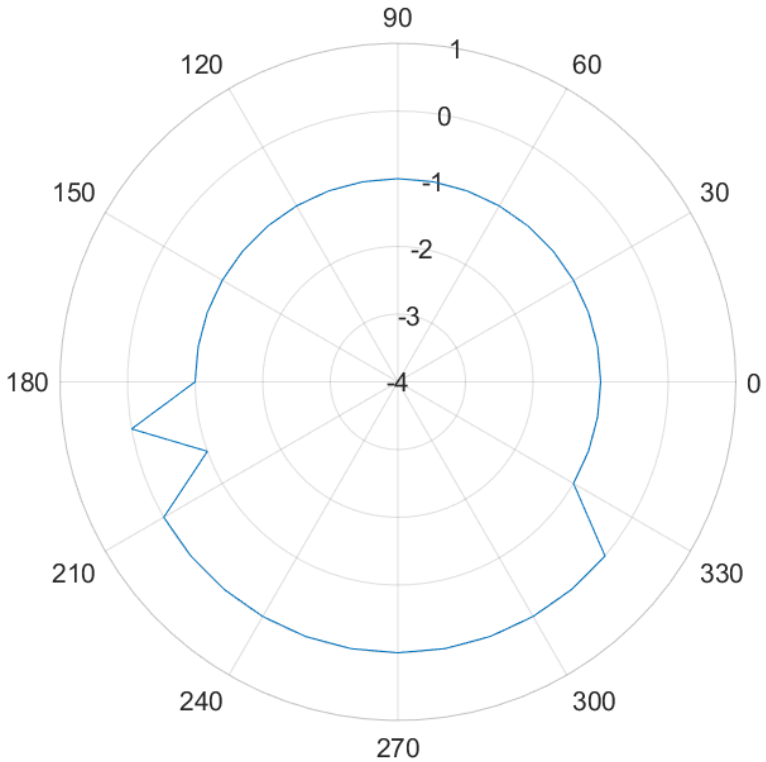

Figure 106: Measured H plane pattern plot, RX, single turn choke.

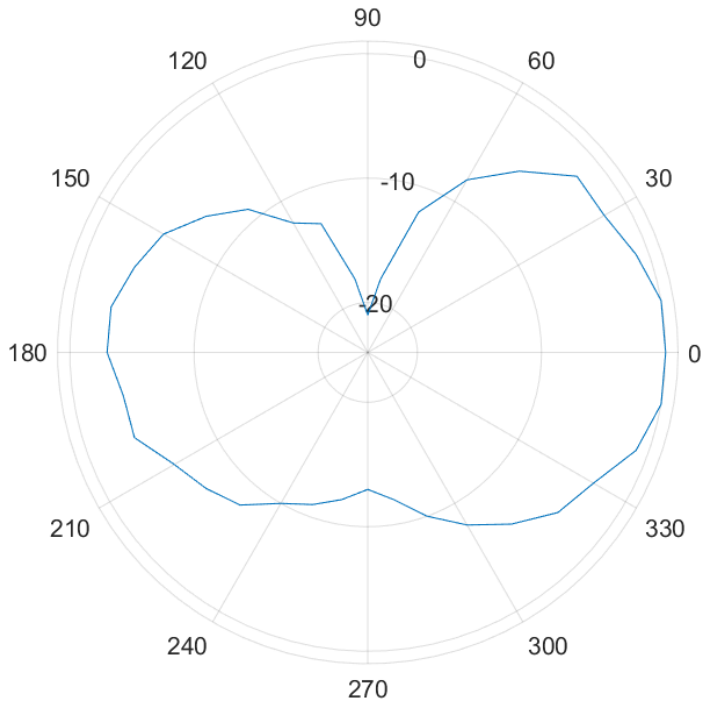

Figure 107: Measured E plane pattern plot, TX, double turn choke.

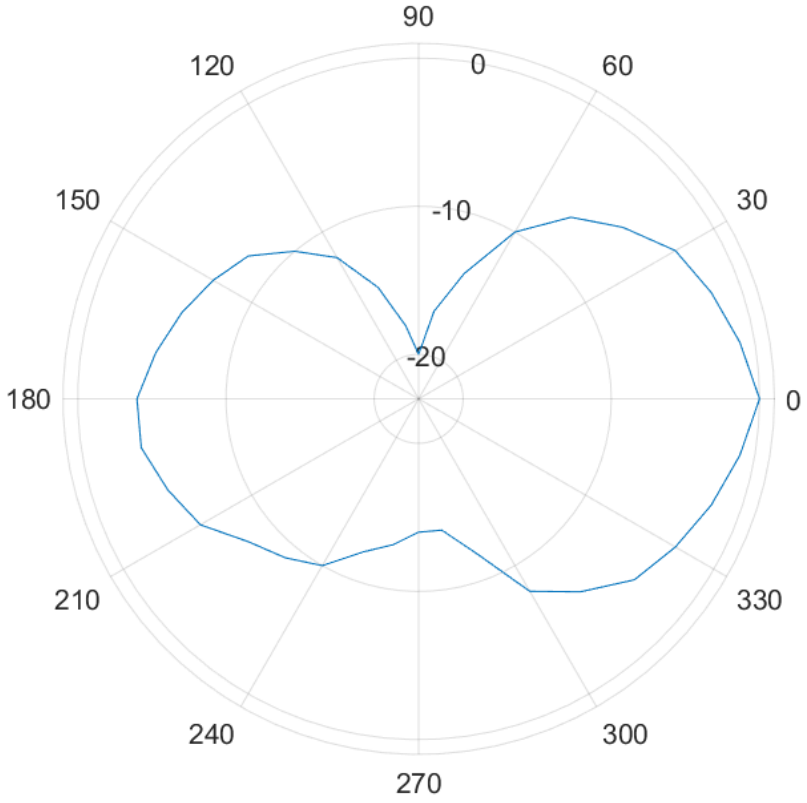

Figure 108: Measured E plane pattern plot, RX, double turn choke.

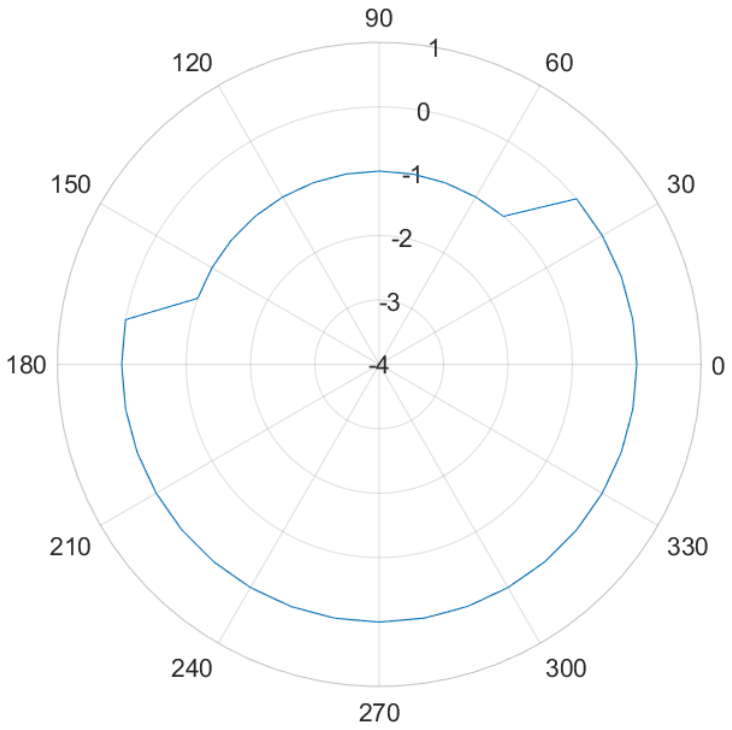

Figure 109: Measured H plane pattern plot, TX, double turn choke.

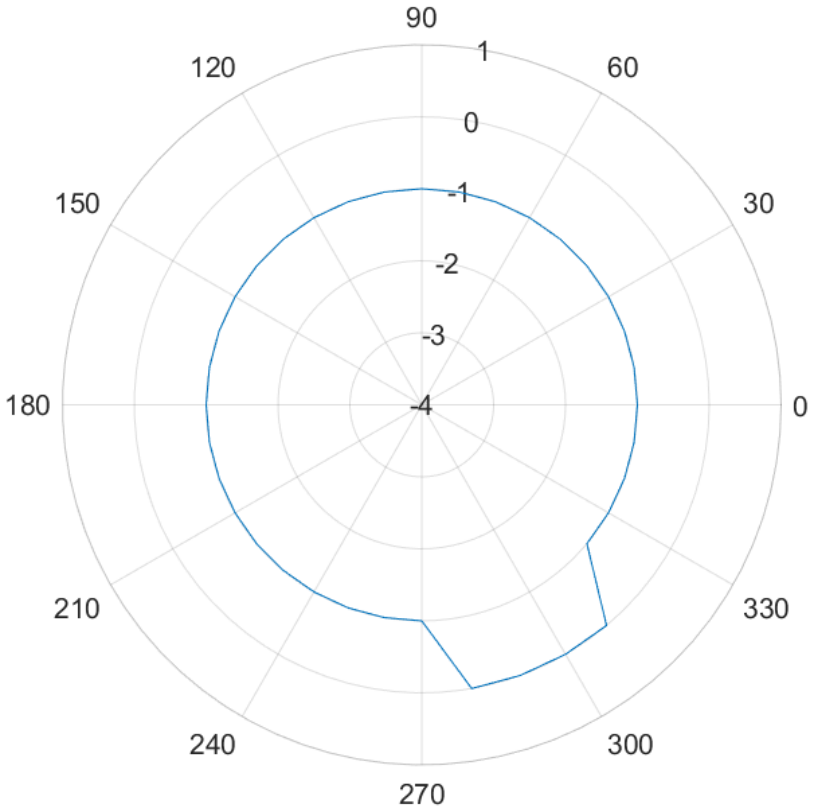

Figure 110: Measured H plane pattern plot, RX, double turn choke.

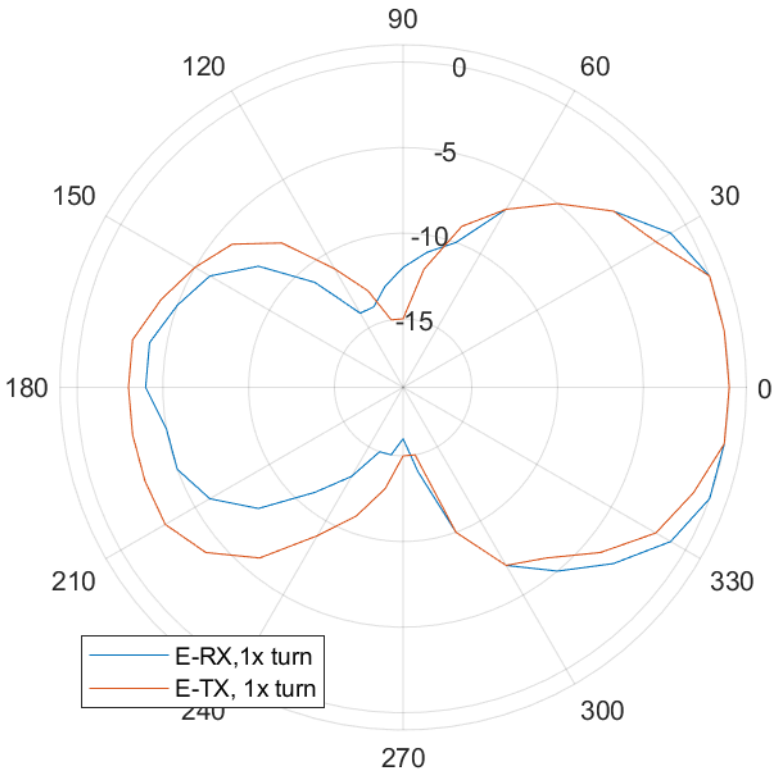

Figure 111: Measured E plane pattern plot, RX vs. TX, single turn choke.

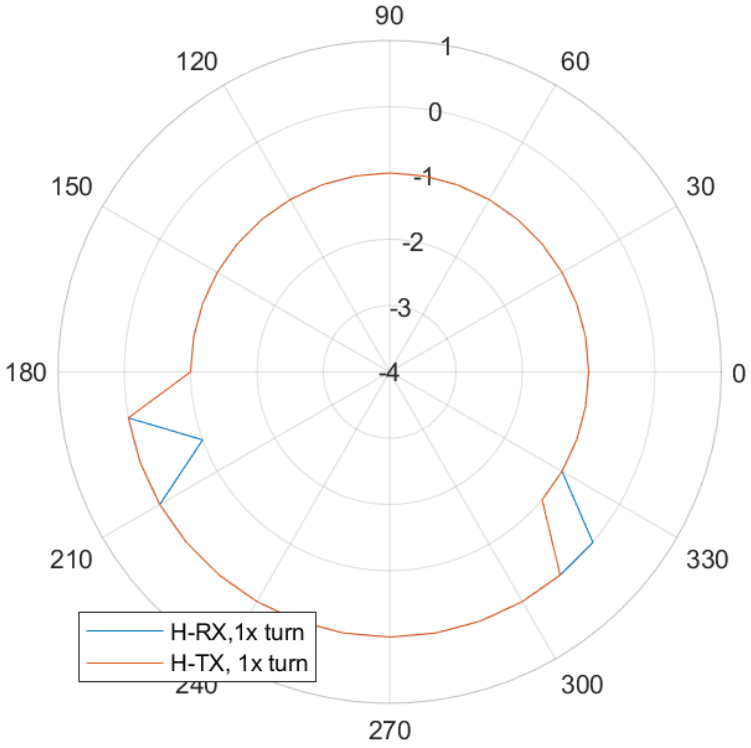

Figure 112: Measured H plane pattern plot, RX vs. TX, single turn choke.

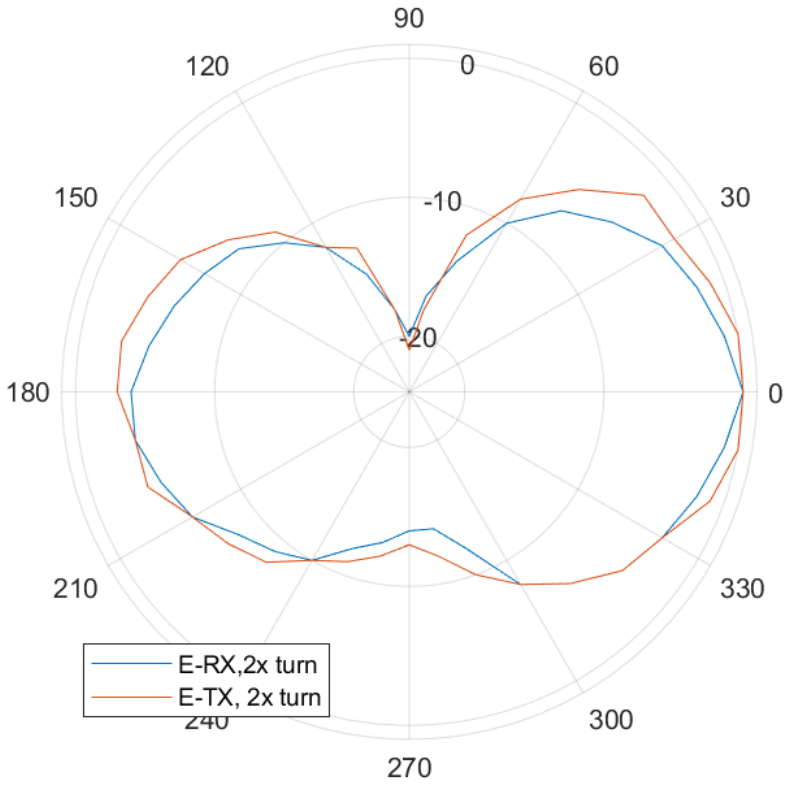

Figure 113: Measured E plane pattern plot, RX vs. TX, double turn choke.

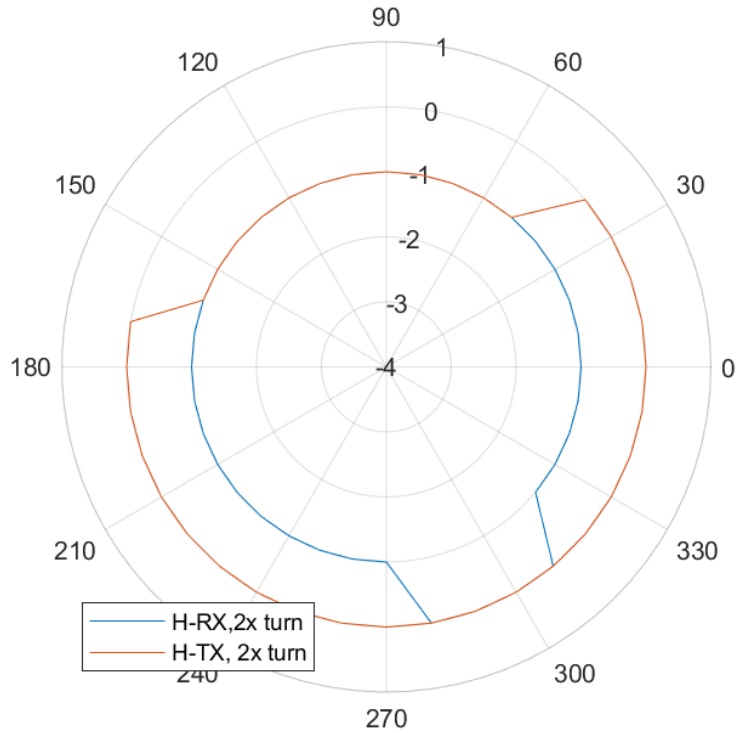

Figure 114: Measured H plane pattern plot, RX vs. TX, double turn choke.

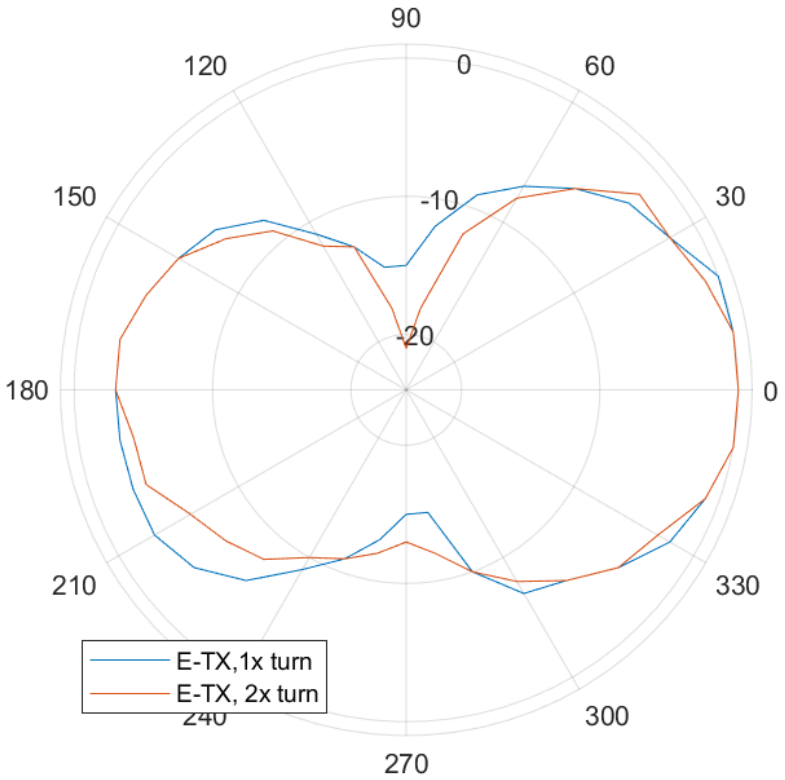

Figure 115: Measured E plane pattern plot, TX, 1 vs. 2 turn choke.

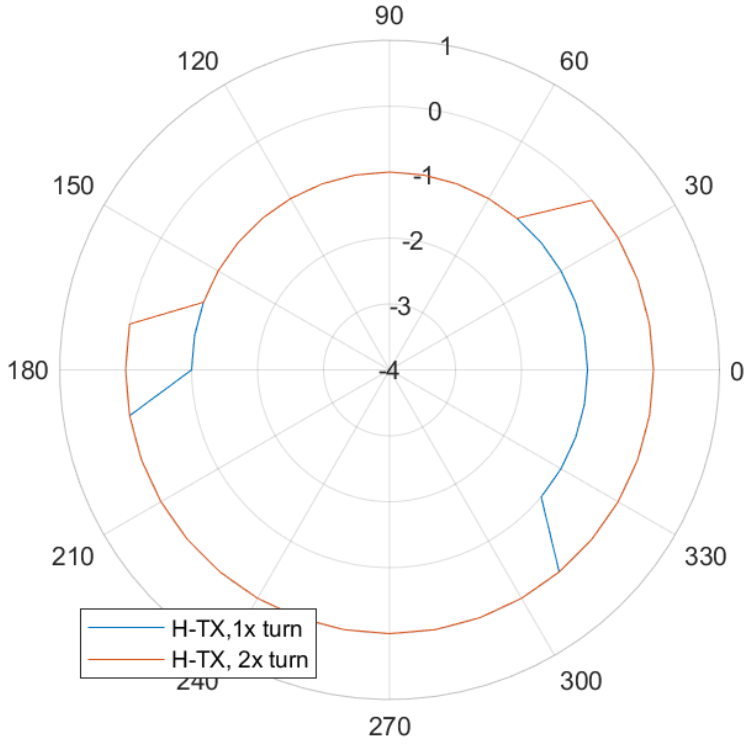

Figure 116: Measured H plane pattern plot, TX, 1 vs. 2 turn choke.

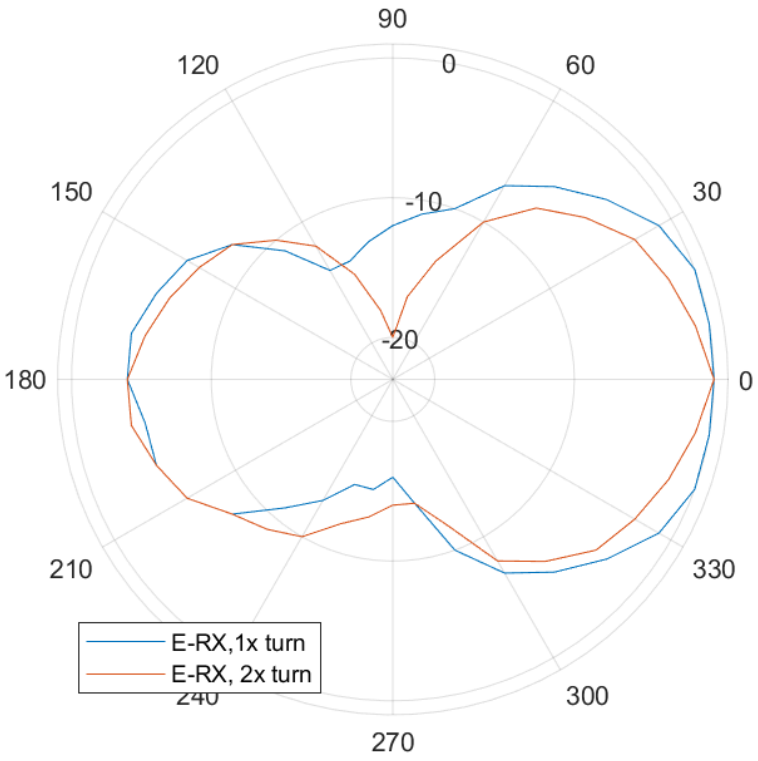

Figure 117: Measured E plane pattern plot, RX, 1 vs. 2 turn choke.

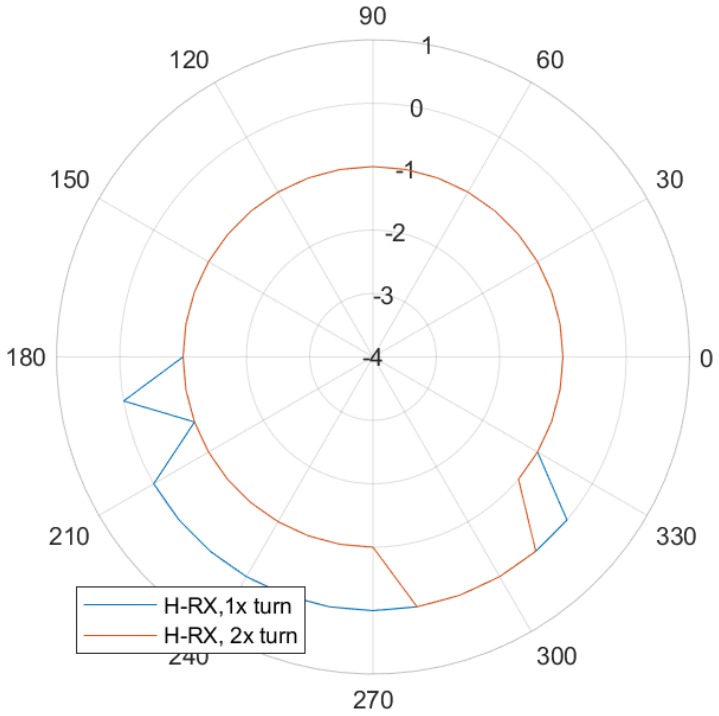

Figure 118: Measured H plane pattern plot, RX, 1 vs. 2 turn choke.

10.3.8 Discussion

The test results verify that the performance of the antenna is as expected:

- It has been verified that the pattern of the test article roughly matches what is expected for a dipole shape-wise. This is regardless of the number of choke turns employed, or if the test article is used for receiving or transmitting. The relevant figures confirming this are those showing the measured antenna patterns in Figure 103 to Figure 118.
- It has been determined that an extra turn on the choke balun does not offer an improvement in the radiation pattern. This is shown by the measured antenna patterns in Figure 115 to Figure 118. These patterns are matching within a few dB, which can easily be explained by the limitations of this experiment, explained in Section 10.3.6.
- It has been determined that the antenna is more directive towards the ram face of the spacecraft, which may be attributed to the effects of the spacecraft body. Among others, this can be clearly seen in Figure 103 and Figure 104.
- It has been verified that the return loss related response, when measured in the chamber, does not show any significant deviation from the measurements taken outside. This further supports the validity of the test results presented for the return loss test. Unfortunately, return loss data for the single turn choke was not collected due to human error, however, this is deemed to have limited impact on the overall outcome of this test because this data has been collected as part of the indoor and outdoor return loss tests earlier, and the results do not seem to deviate between the those and the measurements taken with a choke of two turns.
- It has also been observed that the R/X graph for this test in the chamber does not show the same oscillatory behaviour as observed outdoors. This can be seen by a comparison between Figure 87 and Figure 101. The fact that the oscillations vanish in the RF quiet environment of the anechoic chamber further support the theory put forward in Section 10.2.8 that the antenna analyzer response was impacted by radiated signals picked up by the DUT. This is also supported by the fact that the R/X graph in Figure 83 did not show oscillatory response either. Data for that was collected indoors, where the offending signal is attenuated compared to outdoor measurements.

10.4 Coarse Absolute Gain Test

10.4.1 Test Objective

The objective of this test is to obtain a coarse estimate of the gain of the dipole antenna of the ORCASat TT&C subsystem by measurement, to an extent which is practical given the characteristics of the anechoic chamber at the University of Victoria.

10.4.2 Equipment Used

The equipment required for the coarse absolute gain test is listed below:

- HP8720C vector network analyzer
- Coaxial cables
- Coaxial adapters
- Anechoic chamber
- Com-Power AC-220 Hybrid Combilog log periodic antenna
- Com-Power ATAC-110 Combilog antenna attachment
- Com-Power ATTS-110 Antenna support
- SMA SOLT calibration kit
- Satellite mock-up
- Pipe adapter for satellite mock-up
- Plastic sawhorse
- Fibreglass pole
- 18 AWG tie wire
- Wire cutters
- Tape measure (25’ min.)
- Driver kit
- Multimeter
- Multimeter leads

10.4.3 Test Setup

The test setup for VNA calibration is shown in Figure 119. The test setup for the coarse absolute gain measurement is shown in Figure 120. The plan indicating the physical layout of the DUT and the test antenna in the anechoic chamber to maximize the distance between them is shown in Figure 121. This is to ensure that the antennas are in each others far fields.

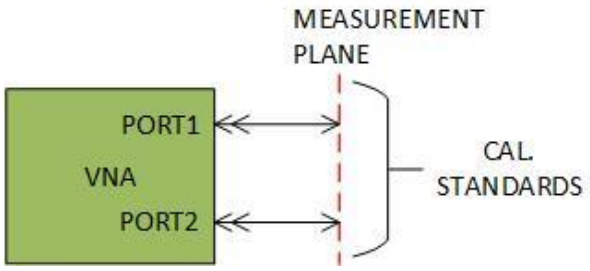

Figure 119: Test setup for VNA calibration.

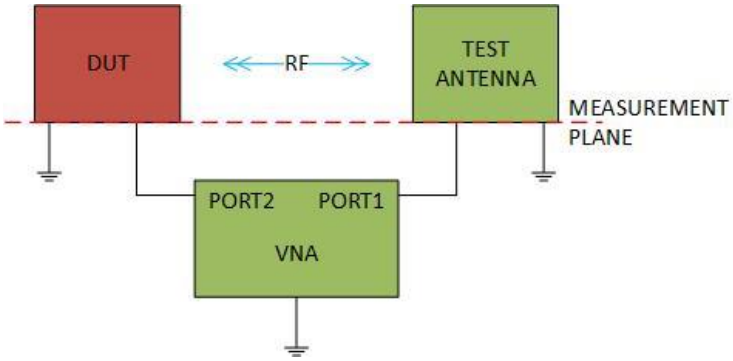

Figure 120: Test setup for coarse absolute gain measurement.

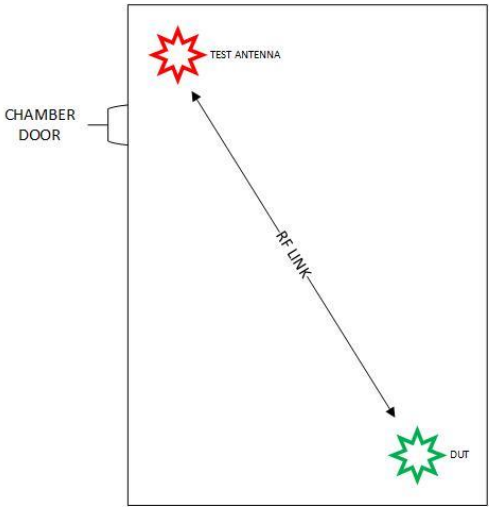

Figure 121: Optimal anechoic chamber arrangement to obtain maximum link distance.

10.4.4 Test Procedure

1) Configure the test setup in Figure 119.
    a) Make sure that the coaxial test cables, adapters etc. are the same as they will be for the gain measurement.

b) Configure the VNA for the maximum drive power level and for the 415 to 475 MHz frequency range.
c) Do a full 2 port calibration of the VNA.

2) Configure the test setup in Figure 120 and Figure 121.
   a) Make sure that the DUT is comprised of the antenna PCB mounted inside of the mock-up, featuring the tape arms pruned to length in the return loss test, and a double turn choke wound from the maximum coaxial cable length that the spacecraft will be able to fit (18”).
   b) Mount the test antenna on its tripod at the location indicated and route its feeder under the absorbers to the VNA.
   c) Mount the DUT on the fiberglass pole at the location indicated. Route the coaxial test lead inside the pole, and make sure that the mock-up is grounded to the VNA ground by continuity measurement. Use the tie wire to secure the pole to the sawhorse. Cover the DUT support with absorbers facing the test antenna as much as possible and route the test cable to the VNA under the absorbers.
3) Record the distance between the tip of the test antenna and the ram face of the spacecraft. Position the DUT such that the face with the direction of maximum radiation from the coarse gain pattern test points at the test antenna. Make sure that the plane of the antennas matches.
4) Photograph the DUT and the test antenna in their final configuration used for the test. Make sure to also include a photo showing the entire chamber with the DUT and the test antenna installed.
5) Measure and record the return loss, Smith Chart response and VSWR of the test antenna and the DUT at 437 MHz using the VNA.
6) Make sure that the antennas are in each other's far fields.
7) Configure the VNA to display a log-magnitude plot of S21. Record the magnitude of S21 at 437 MHz
8) Repeat from the last step, but this time measure and record S12 log-magnitude.

10.4.5 Expected Outcomes

The expected outcomes of the coarse absolute gain test are as follows:

- It is expected that the gain of the dipole will be around 2 dBi, as introduced earlier in this document.
- It is expected that the return loss of the test antenna around 437 MHz will be, based on the data from the manufacturer shown in.
- It is expected that the return loss of the DUT will be like the value measured as part of the coarse gain pattern test and the return loss test.

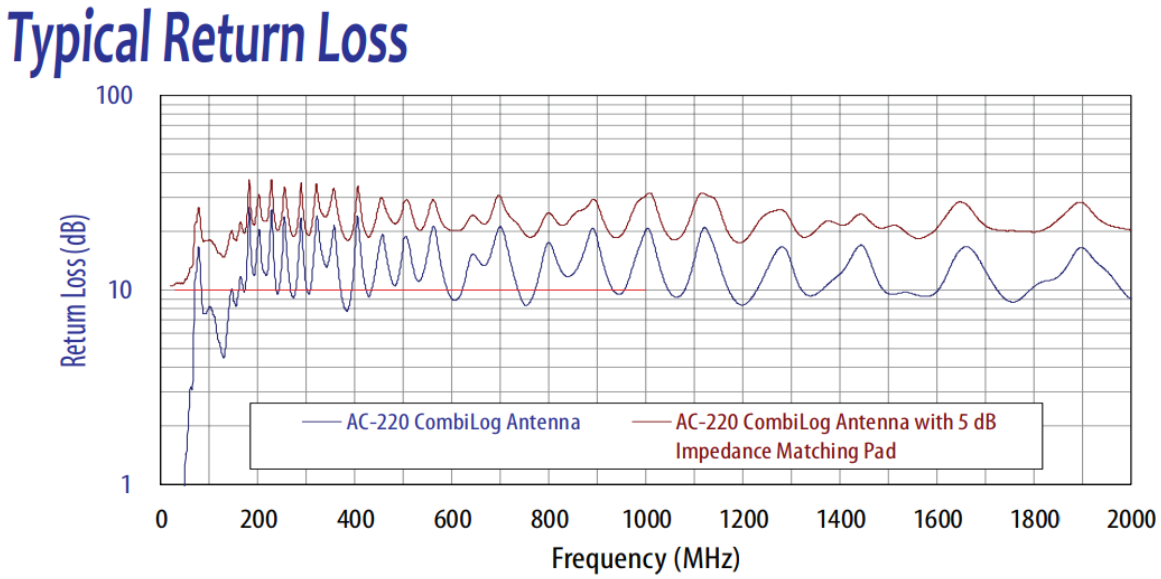

Figure 122: Test antenna return loss against frequency. Adapted from [52].

10.4.6 Limitations and Assumptions

The limitations and assumption of the coarse absolute gain test are as follows:

- The anechoic chamber at UVic is only designed for measurements down to 1 GHz, so the gain data obtained may be severely impacted by reflections.
- The mounting of the DUT in the anechoic chamber may influence the measured gain, when compared to free space.
- The test article is not the final spacecraft, so deviations between the test article and the final device may produce different results.
- The antenna/DUT positioner of the chamber has not been used, and it has been moved out of the way as much as possible and covered with absorbers. However, the presence of these undesired obstacles in the chamber this may still adversely impact the results.

10.4.7 Test Results

The physical configuration of the anechoic chamber is shown in Figure 123 to Figure 125. The VNA captures are shown in Figure 126 to Figure 133. The raw test data is summarized in Table 3.

Figure 123: DUT set up for gain measurement.

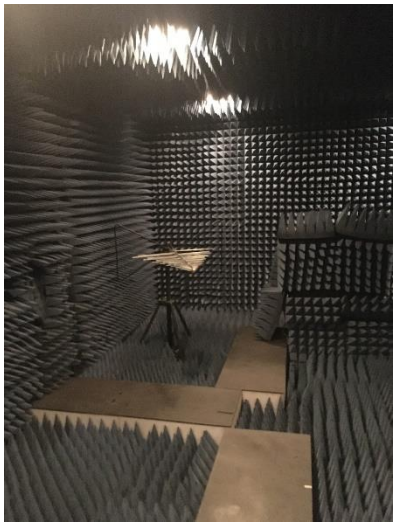

Figure 124: Test antenna set up for gain measurement.

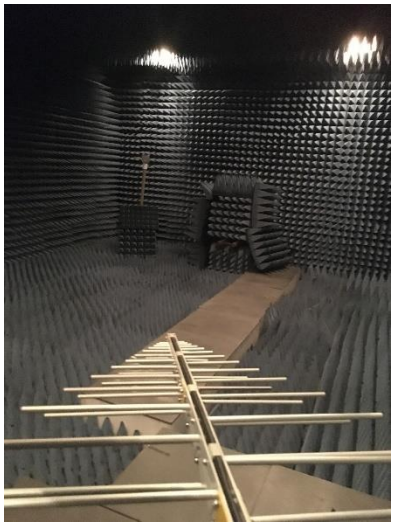

Figure 125: Range set up for gain measurement.

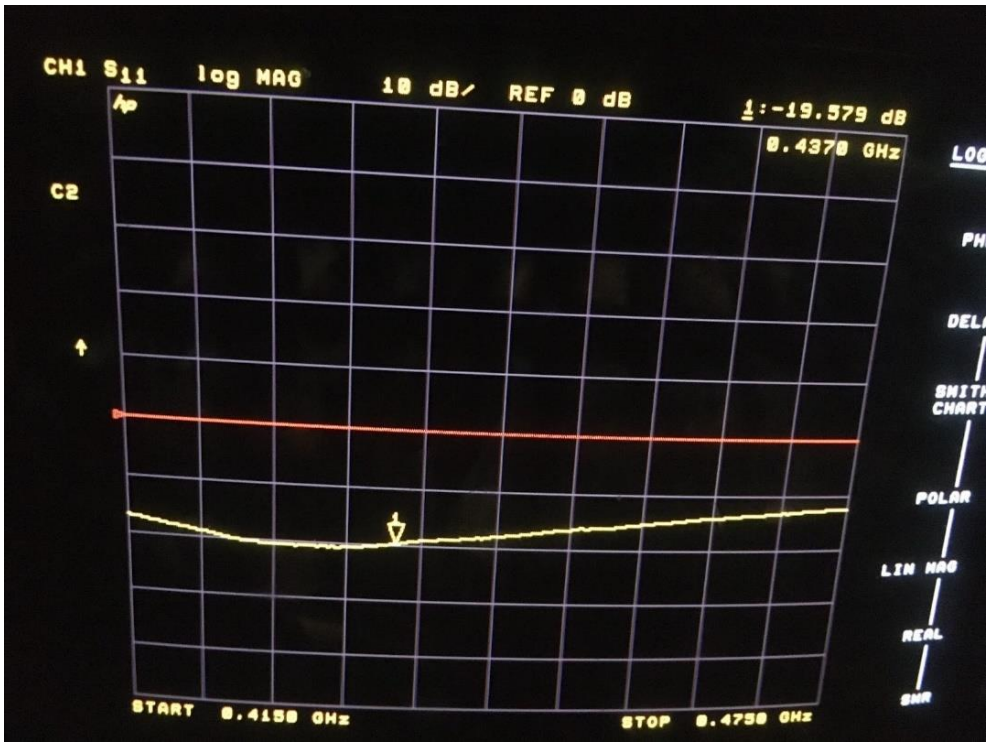

Figure 126: DUT return loss at 437 MHz.

Figure 127: DUT Smith Chart capture 437 MHz.

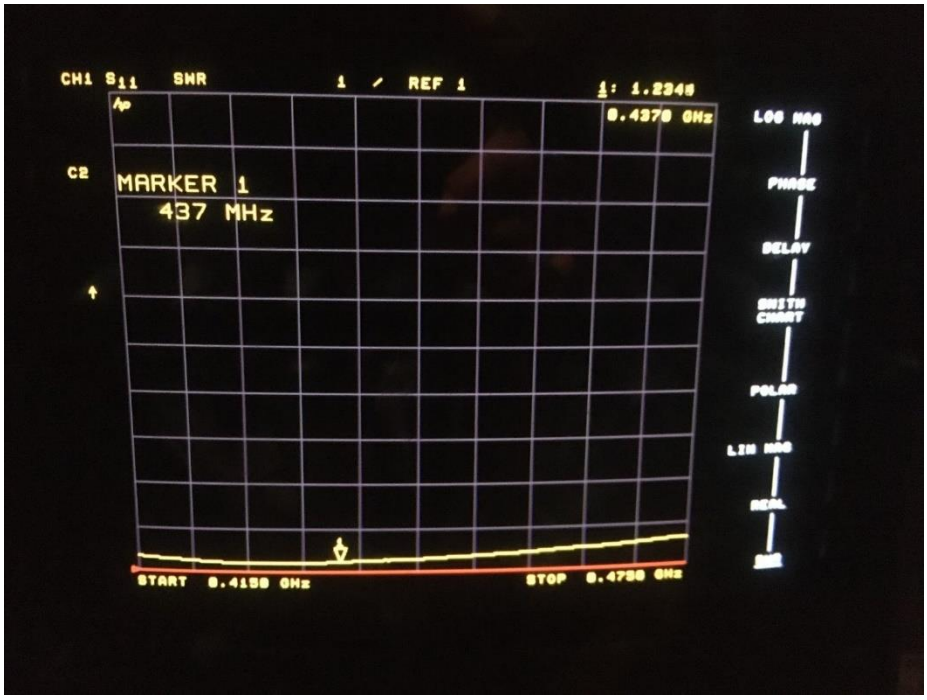

Figure 128: DUT VSWR at 437 MHz.

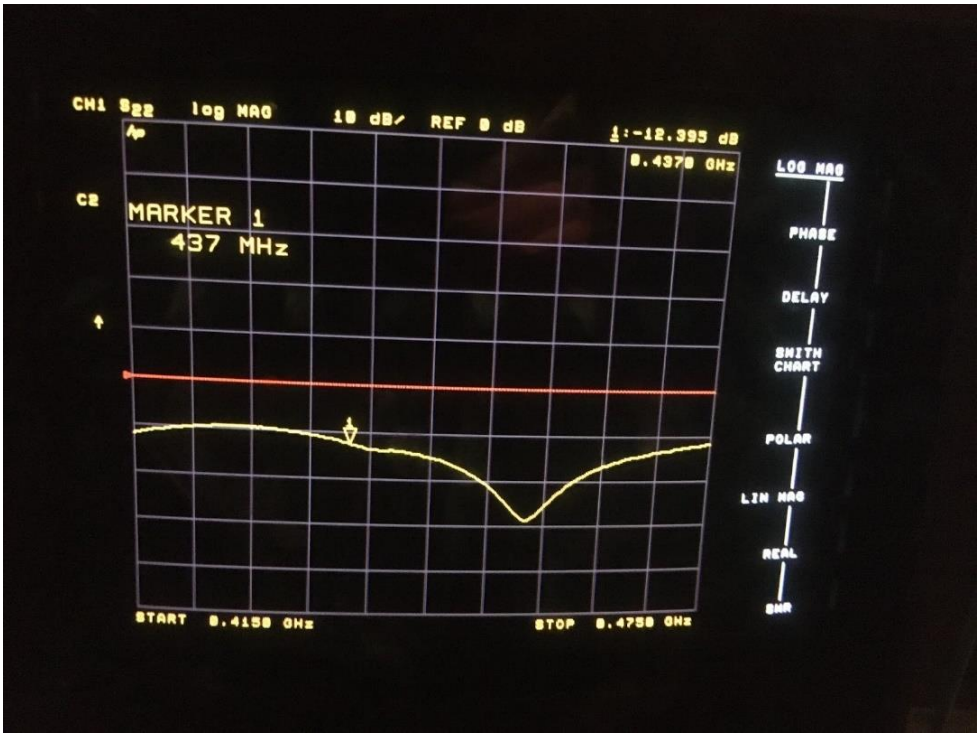

Figure 129: Test antenna return loss at 437 MHz.

Figure 130: Test antenna Smith Chart captures 437 MHz.

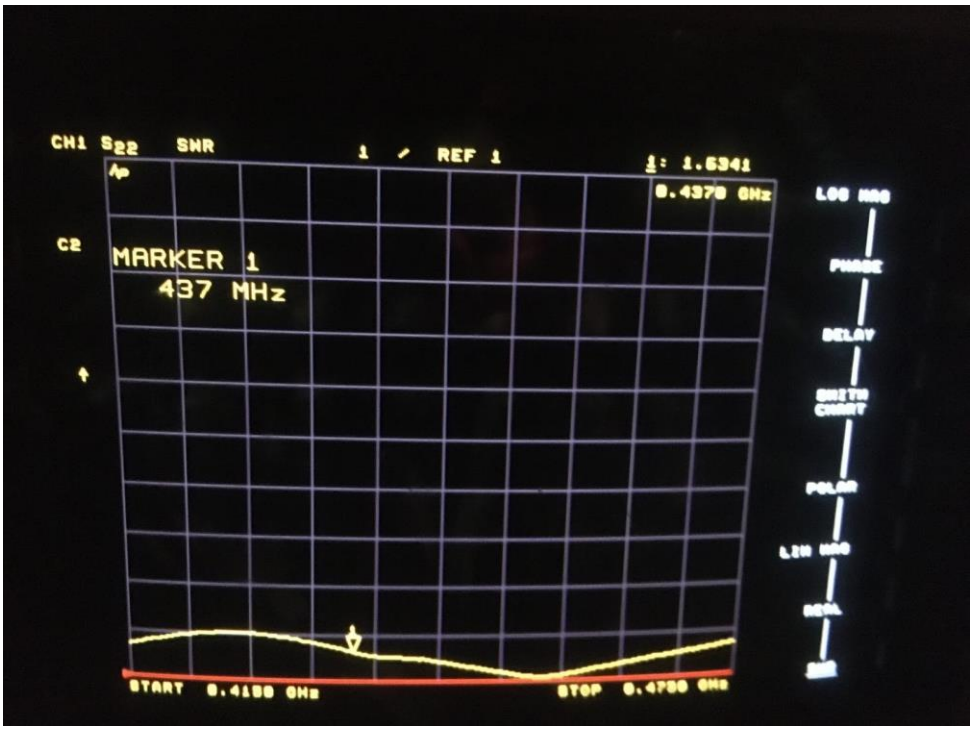

Figure 131: Test antenna VSWR at 437 MHz.

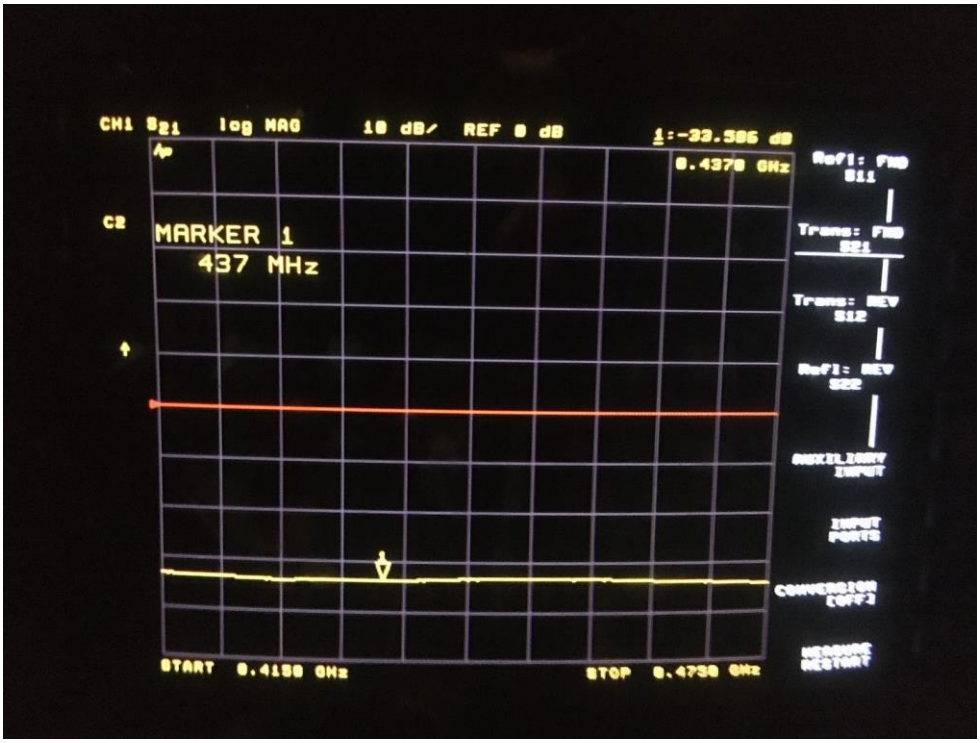

Figure 132: S21 measurement to determine the gain at 437 MHz.

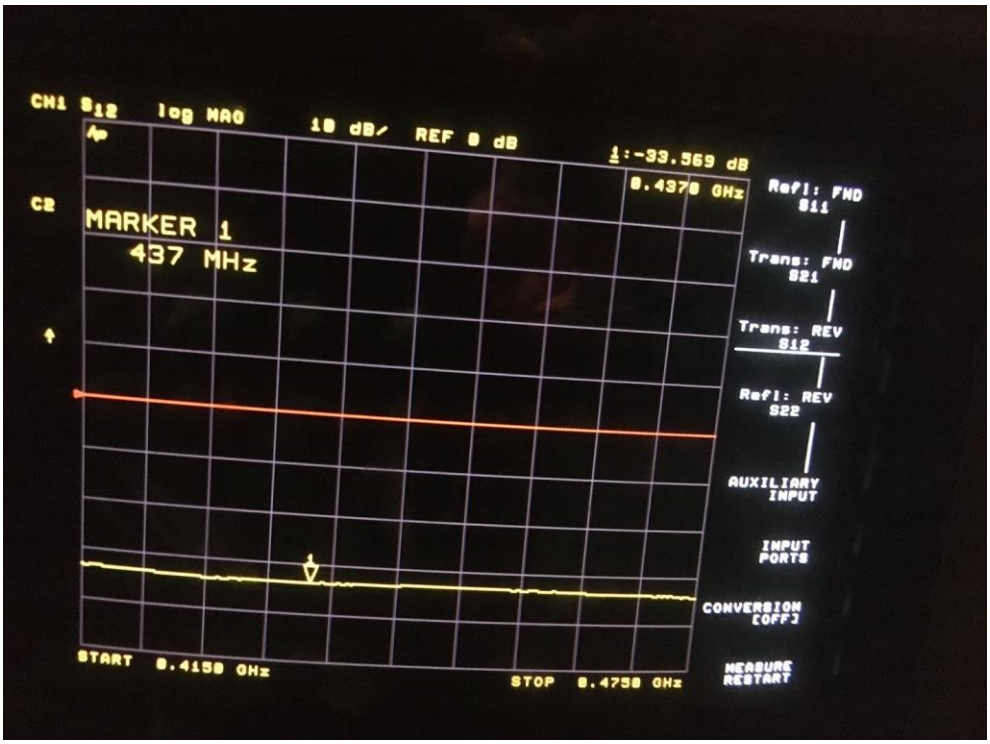

Figure 133: S12 measurement to determine the gain at 437 MHz.

Table 3: Raw test data summary. All measurements all 437 MHz. Note that for this test, the DUT was attached to VNA Port #1 and the test antenna for Port #2 for all measurements.

Quantity	Value
Test Antenna Return Loss (dB)	-12.4
Test Antenna VSWR (no unit)	1.6
Test Antenna Input Impedance (Ω)	
DUT Return Loss (dB)	-19.6
DUT VSWR (no unit)	1.2
DUT Input Impedance (Ω)	
Distance From Test Antenna to DUT (m)	5.98
|S21|, DUT Transmitting (dB)	-33.6
|S12|, DUT Receiving (dB)	-33.6

10.4.8 Discussion

The collection of the raw test data has been achieved without any notable setbacks. However, for this data to be meaningful, further data processing is required. To determine an estimate of the absolute gain G_{DUT} of the antenna, a link budget needs to be calculated. Due to the SOLT calibration, only four parameters are required, if no consideration is given to the match between the VNA and the DUT, and the VNA and the test antenna. This simplified link budget is given by the equations below.

$$|S_{21}| = G_{test} - L_{path} + G_{DUT} \tag{17a}$$

$$G_{DUT} = |S_{21}| - G_{test} + L_{path} \tag{17b}$$

In the formulas above, G_{DUT} is the parameter of interest, |S21| (or |S12| if the transmitter and receiver is reversed) is the measured parameter, the magnitude of the forward/reverse gain of the "network", while G_{test} and L_{path} are the gain of the test antenna, and the free space path loss, respectively.

The value of G_{test} can be estimated from Figure 134 as ~6.5 dBi, while the value of the path loss can be computed from the measured distance from the test antenna to the DUT, using the formula below [53], where d is distance in km, and f is frequency in MHz.

$$L_{path}(dB) = 20\log_{10}(d) + 20\log_{10}(f) + 32.44 \tag{18a}$$

$$L_{path}(dB) = 20\log_{10}\left(\frac{5.98}{1000}\right) + 20\log_{10}(437) + 32.4 \tag{18b}$$

$$L_{path}(dB) = 40.8\ dB \tag{18c}$$

Based on this, the measured gain of the DUT is computed below. There is no need to distinguish between the transmit and receive gain, as |S12| = |S21| based on the measurements shown in Figure 132 and Figure 133. This is expected as antennas are reciprocal.

$$G_{DUT} = |S_{21}| - G_{test} + L_{path} \tag{19a}$$

$$G_{DUT} = |-33.6\ dB| - 6.5\ dBi + 40.8\ dB \tag{19b}$$

$$G_{DUT} = 0.7\ dBi \tag{19c}$$

The resulting gain for the test article, 0.7 dBi is 1.46 dB lower than the ideal dipole gain quoted as 2.16 dBi earlier in this thesis. To determine if this number is acceptable, the EIRP produced by the ORCASat TT&C subsystem needs to be computed, when using this gain. Since the feed losses are included in the gain of the antenna, the EIRP is computed as below. This computation shows that given the gain, the antenna designed meets the EIRP requirement, if the RF front end produces its nominal 31.5 dBm output power [47].

$$EIRP = P_t + G_{DUT} = 31.5\ dBm + 0.7\ dBi = 32.2\ dBm = 2.2dBW > -3.5dBW \tag{20}$$

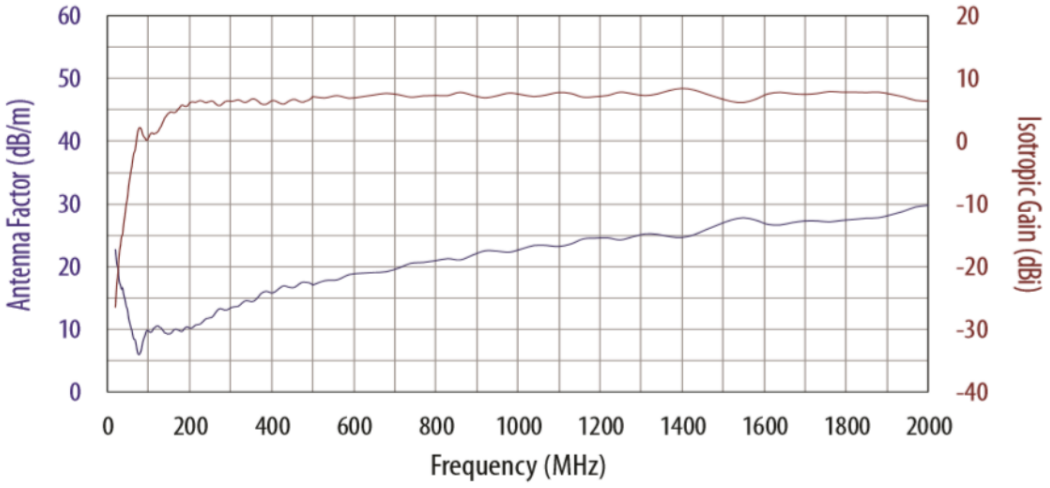

Figure 134: Gain as a function of frequency for the test antenna. Adapted from [52].

11 Conclusions and Future Work

11.1 Conclusions

In this thesis, the design, manufacturing, assembly and testing of an antenna for the ORCASat nanosatellite was presented. First, some key theoretical concepts relevant to the work in this thesis were introduced. Then, a literature review was conducted, and the state of the art for CubeSat dipole antenna design was considered. Following this, in light of the state of the art, as well as other project related consideration, a methodology was conceptualized. After this, previous work on ORCASat design was reviewed, and the root cause preventing successful delivery of a functional dipole previously was identified as the presence of ground planes in the earlier porotype. Next, considering the state of the art, the requirements and constraints, as well as and the lessons learned from previous mistakes, a deployable tape spring dipole design was conceptualized. Alternatives for the various blocks of this dipole were considered, and the best option for each block was selected based on the requirements and constrains for this projects, as well as practical considerations. The design selected for implementation was manufactured and assembled, and its performance was initially evaluated as part of an informal commissioning test consisting of return loss, VSWR and input impedance measurements in various configurations. This informal test quickly revealed that the prototype functions as designed. To formally verify this performance against the requirements at the beginning of this thesis, a verification test campaign was conceptualized and executed. This consisted of return loss, gain pattern and absolute gain measurements. It was determined that the antenna features a return loss of -19.6 dB and an input impedance of 43.0 + 7.0 j Ω at 437 MHz with a bandwidth more than what is required to cover the 435.0-438.0 MHz allocation, while offering pattern which matches the pattern expected from an ideal dipole in the E and H planes, with a peak gain of 0.7 dBi. It has also been determined that this gain is sufficient to meet the EIRP requirement of -3.5dBW. Thus, the project requirements have been met, while the constraints have been observed, and therefore the project has successfully been completed, delivering a viable antenna for the flight of the ORCASat nanosatellite, show in in Figure 135 and Figure 136.

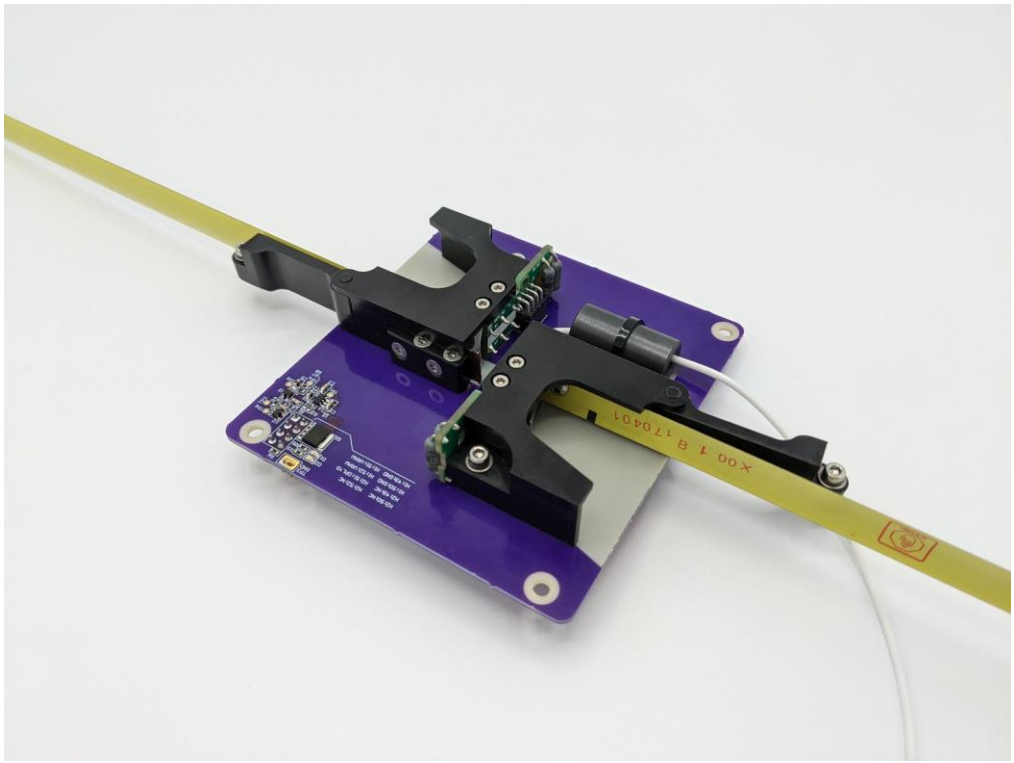

Figure 135: Full antenna prototype, side view. Courtesy of A. Doknjas.

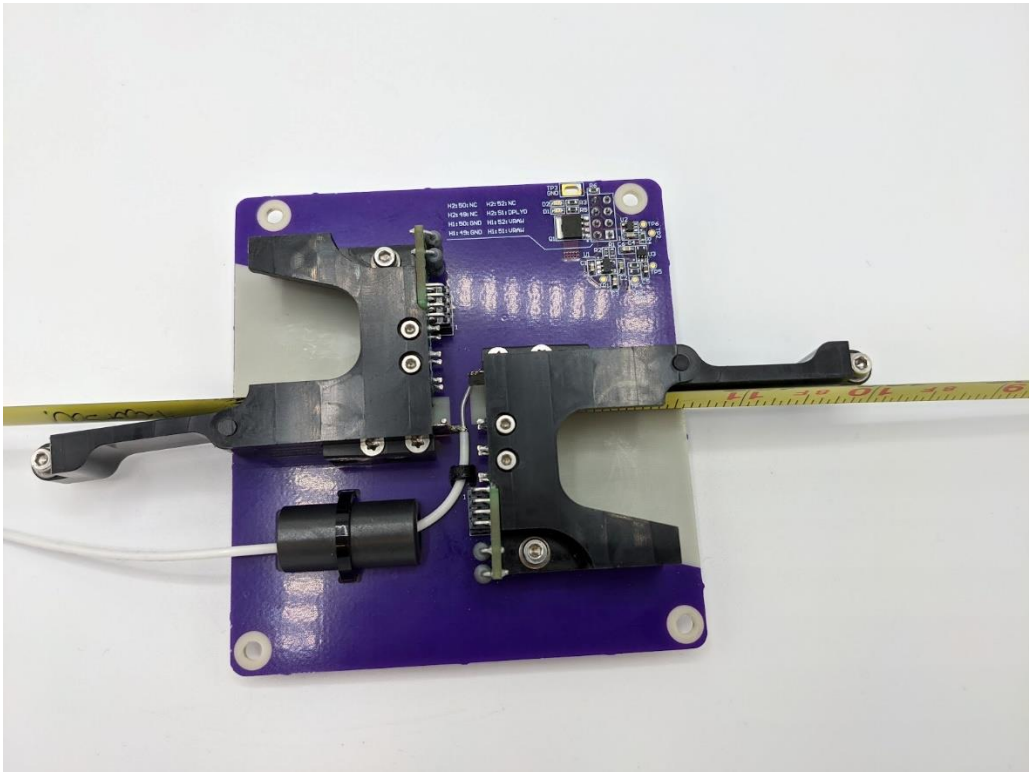

Figure 136: Full antenna prototype, top view. Courtesy of A. Doknjas.

11.2 Future Work

The project which is the topic of this thesis has not been completed with the delivery of the first working prototype and this document. Additional work will be needed to prepare the antenna for flight as part of ORCASat. The keys steps and considerations for the completion of work is outlined below.

1. The performance of the antenna needs to be professionally verified in test facilities which are designed for use at the frequency of operation of ORCASat. This is deemed necessary to remove any risk from using an anechoic chamber which is not rated for the frequency of operation of the ORCASat communication system. To undertake this testing, a more realistic mock-up of the spacecraft bus will also be required. The facility selected for this testing is Antenna Test Lab Co. of Rayleigh, North Caroline, due to their favourable pricing and suitable equipment. The testing will be undertaken in Q1 2022. At the time of this thesis, the availability of this facility was confirmed, and a quote was obtained for the testing services, which is included in Appendix F-1.
2. The coaxial cable feeding the antenna needs to be swapped out for a thicker cable. It was determined that there is no measurable benefit from the use of a double turn choke, so there is no longer a need to fit multiple turns of the same coax trough the ferrite. This means that a higher diameter, lower loss cable can be used. This cable will need to be custom manufactured by a commercial entity for use in ORCASat as well. This will ensure that only known materials (e.g. no heat shrink of unknown composition) is used in the antenna, and there won't be any outgassing issues. As well, this will avoid the need to strip and cut fragile and thin coax in-house. This cable will have to be incorporated into the test article which will be used for testing at the facilities of Antenna Test Lab Co.
3. A method will need to be devised and implemented to allow the bleed-off of the charge accumulating on the antenna arm connected to the centre of the coaxial feed during flight. The RF path to the transceiver front end is DC blocked, so if this is not undertaken, a high static charge may build up on the antenna, resulting in possible malfunctions.

4. Another revision of the antenna PCB will need to be designed and manufactured. While this is not critical, this will allow the removal of the adjustable feed gap, and the incorporation of charge bleed off, thus making the antenna a better product.

12 References

[1] Union of Concerned Scienties, "UCS Satellite Database," 1 May 2021. [Online]. Available: https://www.ucsusa.org/resources/satellite-database. [Accessed 19 October 2021].

[2] E. Kulu, "What is a CubeSat & other picosatellites," 2021. [Online]. Available: https://www.nanosats.eu/cubesat. [Accessed 19 October 2021].

[3] Canadian Space Agency, "Canadian CubeSat Project - Inforgraphics," 26 November 2018. [Online]. Available: https://asc-csa.gc.ca/eng/multimedia/search/image/search/cubesat-illustrations. [Accessed 27 November 2021].

[4] Canadian Satellite Design Challenge Management Society, "About Us," 2021. [Online]. Available: https://www.csdcms.ca/index.php/about-us. [Accessed 19 October 2021].

[5] Canadian Space Agency, "Ex-Alta 1: University of Alberta's first CubeSat," 06 June 2017. [Online]. Available: https://www.asc-csa.gc.ca/eng/satellites/cubesat/ex-alta-1.asp. [Accessed 19 October 2021].

[6] Innovation, Science and Economic Development Canada, "Authorized and Approved Canadian Satellites," 9 August 2021. [Online]. Available: https://www.ic.gc.ca/eic/site/smt-gst.nsf/eng/sf05343.html. [Accessed 19 October 2021].

[7] Candian Space Agency, "What is the Canadian CubeSat Project," 21 April 2021. [Online]. Available: https://www.asc-csa.gc.ca/eng/satellites/cubesat/what-is-the-canadian-cubesat-project.asp. [Accessed 19 October 2021].

[8] Canadian Space Agency, "Selected teams," 18 June 2020. [Online]. Available: https://www.asc-csa.gc.ca/eng/satellites/cubesat/selected-teams.asp. [Accessed 19 October 2021].

[9] National Aeronautics and Space Administration Goddard Space Flight Center, "Orbiting Configurable Artificial Star (ORCAS)," [Online]. Available: https://asd.gsfc.nasa.gov/orcas/about/. [Accessed 4 December 2021].

[10] University of Victoria Centre for Aerospace Research, *ORCASat Mission & System Requirements,* Unpublished.

[11] NanoRacks, "Technical Resources," 29 May 2018. [Online]. Available: https://nanoracks.com/wp-content/uploads/Nanoracks-CubeSat-Deployer-NRCSD-IDD.pdf. [Accessed 27 November 2021].

[12] C. A. Balanis, Antenna Theory - Analaysis And Design, Hoboken, NJ: John Wiley & Sons, Inc., 2005.

[13] D. M. Pozar, Microwave Engneering, Hoboken, NJ: John Wiley & Sons Inc., 2005.

[14] U. Editor, "Microwaves101.com," [Online]. Available: https://www.microwaves101.com/encyclopedias/light-phase-and-group-velocities. [Accessed 3 November 2021].

[15] J. Brown, "Audio Systems Group," January 2019. [Online]. Available: http://audiosystemsgroup.com/RFI-Ham.pdf. [Accessed 29 October 2021].

[16] W. Maxwell, "Some Aspects of the Balun Problem," *QST,* vol. LXVII, no. 1, pp. 38-40, 1983.

[17] M. Getzlaff, Fundamentals of Magnetism, Berlin, Germany: Springer-Verlag, 2008.

[18] Fair-Rite Products Corp., "61 Material Data Sheet," [Online]. Available: https://www.fair-rite.com/61-material-data-sheet/. [Accessed 4 November 2021].

[19] Fair-Rite Products Corp., "Round Cable EMI Suppression Cores (2661480002)," [Online]. Available: https://www.fair-rite.com/product/round-cable-emi-suppression-cores-2661480002/?__cf_chl_jschl_tk__=pmd_iia0b2krYFLul0zDfV_NU8zVR6IcGOMZe6N9AoTfxVw-1635531787-0-gqNtZGzNAlCjcnBszQi9. [Accessed 29 October 2021].

[20] S. Abulgasem, F. Tubbal, R. Raad, P. I. Theoharis, S. Lu and S. Iranmanesh, "Antenna Designs for CubeSats: A Review," *IEEE Access,* vol. 9, pp. 45289-45324, 2021.

[21] G. D. Krebs, "Gunter's Space Page," [Online]. Available: https://space.skyrocket.de/index.html. [Accessed 28 November 2021].

[22] E. Kulu, "Nanosats Database," [Online]. Available: https://www.nanosats.eu/. [Accessed 27 November 2021].

[23] M. Swartwout, "The Database," [Online]. Available: https://sites.google.com/a/slu.edu/swartwout/cubesat-database#h.2uocnm7j8arf. [Accessed 28 November 2021].

[24] B. Klofas, "CubeSat Communications System Table," 22 November 2018. [Online]. Available: https://www.klofas.com/comm-table/. [Accessed 28 November 2021].

[25] M. Rupprecht, "Status of active Satellites on Amateur Radio Frequencies," 18 August 2021. [Online]. Available: https://www.satblog.info/status-2/. [Accessed 28 November 2021].

[26] M. Wakita, "Satellite Frequency List," 26 November 2021. [Online]. Available: http://www.ne.jp/asahi/hamradio/je9pel/satslist.htm. [Accessed 28 November 2021].

[27] M. P. Schroer, "NPS-SCAT: A CubeSat Communications System Design, Test and Integration," Naval Postgraduate School, Monterey, CA, 2009.

[28] A. Spanakis-Misirlis, "A UHF half-wave dipole antenna for the AcubeSAT mission," Aristotle Space and Aeronautics Team, Thessaloniki, 2020.

[29] K. Schraml, A. Narbudowicz, S. Chalermwisutkul, D. Heberling and M. J. Ammann, "Easy-to-deploy LC-loaded dipole and monopole antennas for cubesat," in *11th European Conference on Antennas and Propagation*, Paris, France, 2017.

[30] N. Hansen, "Toward High Data Rate CubeSat Telecommunication," Dalhousie University, Halifax, Nova Scotia, 2019.

[31] J. C. Gómez, "Communication link design at 437.5 MHz for a nanosatellite," Aalto University, Espoo, Finland, 2013.

[32] A. G. Cappiello, "Design, Implementation, and Analysis of Electrical System Architecture for CubeSat to Ground Communications," Old Dominion University, Norfolk, VA, 2019.

[33] M. Cody K., "NPS-SCAT communications system : design, test, and integration of NPS' first CUBESAT," Naval Postgraduate School, Monterey, California, 2010.

[34] G. D. Krebs, "CP 2, 4," [Online]. Available: https://space.skyrocket.de/doc_sdat/cp-2.htm. [Accessed 28 November 2021].

[35] D. Ford, "NPS-SCAT," [Online]. Available: https://in-the-sky.org/spacecraft.php?id=39389. [Accessed 28 November 2021].

[36] M. Kishimoto, T. L. D. Malmadayalage, A. Maskey, P. Lepcha, D. C. Withanage, Y. Kakimoto, Y. Sasaki, H. R. Shrestha, G. Maeda, T. Yamauchi, S. Kim, H. Masui and M. Cho, "Improvement of Communication System for 1U CubeSat," Utah State University, Logan, UT, 2020.

[37] A. E. Lyerly and P. W. Pachowicz, "Antennas for Academic CubeSats: VHF thru S-Band, What, How and Why," Utah State University, Logan, UT, 2020.

[38] Arrow Electonics, "CX2078NL," [Online]. Available: https://www.arrow.com/en/products/cx2078nl/pulse-electronics-corporation. [Accessed 28 November 2021].

[39] M. Lankinen, "Design and Testing of Antenna Deployment System for Aalto-1 Satellite," Aalto University, Espoo, Finland, 2015.

[40] European Space Agency, "Aalto-1: The Finnish Student Nanosatellite," [Online]. Available: https://directory.eoportal.org/web/eoportal/satellite-missions/a/aalto-1. [Accessed 1 December 2021].

[41] I. P. Bernardino, "Electrical Design of Radio Antenna for the TT&C Subsystem of the ORCASat Nanosatellite," Técnico Lisboa, Lisbon, Portugal, 2021.

[42] Planet Labs Inc., "Planet Releases OpenLST, An Open Radio Solution," 6 August 2018. [Online]. Available: https://www.planet.com/pulse/planet-openlst-radio-solution-for-cubesats/. [Accessed 2 December 2021].

[43] American Radio Relay League, Inc, "Baluns: What They Do And How They Do It," in *The ARRL Antenna Compendium Vol. 1*, Newington, CT, American Radio Relay League, Inc, 1985, pp. 157-164.

[44] Palomar Engineers, "Coax Feed Line Common Mode Chokes (1:1)," [Online]. Available: https://palomar-engineers.com/antenna-products/1-1-balun-kits. [Accessed 29 October 2021].

[45] Palomar Engineers, "Slip On Ferrite Beads," [Online]. Available: https://palomar-engineers.com/ferrite-products/ferrite-beads/1-1-Current-Balun-p213373384. [Accessed 29 October 2021].

[46] O. Duffy, "Pawsey Balun – what is it good for?," [Online]. Available: https://owenduffy.net/blog/?p=14882. [Accessed 4 December 2021].

[47] Qorvo, "RFFM6406," [Online]. Available: https://www.qorvo.com/products/p/RFFM6406. [Accessed 4 November 2021].

[48] Qorvo, "RFXF0009H 45 - 1200 MHz 1:1 SMT Transformer," [Online]. Available: https://www.qorvo.com/products/p/RFXF0009H#documents. [Accessed 29 October 2021].

[49] NASA, "Outgassing Data for Selecting Spacecraft Materials Online," March 2017. [Online]. Available: https://outgassing.nasa.gov/. [Accessed 4 November 2021].

[50] Digi-Key Electronics, "415-0027-036," [Online]. Available: https://www.digikey.ca/en/products/detail/cinch-connectivity-solutions-johnson/415-0027-036/457088?s=N4IgTCBcDaICwEYCsBaADGsB2dBmAbCALoC%2BQA. [Accessed 29 October 2021].

[51] L. Buzas, "Antenna," 29 September 2021. [Online]. Available: https://gitlab.com/ORCASat/ttc/antenna. [Accessed 29 October 2021].

[52] Com-Power, "Hybrid Combilog Antenna AC-220," [Online]. Available: https://www.com-power.com/products/antennas/combilog-antennas/ac-220. [Accessed 9 November 2021].

[53] ElectronicsNotes, "Free Space Path Loss: details & calculator," [Online]. Available: https://www.electronics-notes.com/articles/antennas-propagation/propagation-overview/free-space-path-loss.php. [Accessed 9 November 2021].

[54] Wikipedia, the free encyclopedia, "International Space Station," [Online]. Available: https://en.wikipedia.org/wiki/International_Space_Station. [Accessed 19 January 2022].

[55] AMSAT UK, "AMSAT-IARU Link Model Rev 2.5.5," [Online]. Available: http://www.amsatuk.me.uk/iaru/AMSAT-IARU_Link_Model_Rev2.5.5.xls. [Accessed 19 January 2022].

[56] M2 Antenna Systems Inc., "436CP42UG, 420-440 MHZ," [Online]. Available: https://www.m2inc.com/FG436CP42UG. [Accessed 19 January 2022].

[57] J. R. Wertz and W. J. Larson, Space Mission Analysis and Design, New York, NY: Springer, 2010.

13 Appendix A

13.1 A-1 Link Budget Analysis for EIRP Requirement

The link budget below is prepared under the following assumptions:

- Generic CubeSat in circular International Space Station (ISS) orbit with 51.64 degree inclination, and 460 km orbital height, the maximum orbital height the ISS may assume [54]
- Worst case situation for the link from the perspective of the link distance with the computation of the link budget for minimum commonly accepted elevation angle at which CubeSats are communicated with
- Operation in the centre of the UHF amateur satellite allocation, with linearly polarized spacecraft and circularly polarized ground station antenna to limit polarization loss
- Consideration for atmospheric and ionospheric loss according to values suggested by the International Amateur Radio Union (IARU) for CubeSat links in the band of interest [55]
- Top of the line Yagi antenna at the ground station, designed specifically for amateur satellite operations (gain and beam width used for noise computation from common example, M2 Antenna Systems 436CP42UG [56])
- Noise in beam computed for worst case scenario from compounded effect of terrestrial noise, galactic noise, and Sun noise assuming that Sun is in beam. Galactic and terrestrial noise contribution is weighed by amount of beam solid angle overlapping with ground and space at elevation angle specified
- Uncoded 2-FSK modulation is assumed with E_b/N_0 specified for a bit error rate (BER) of 10^{-5}, with 9600 bps data rate which is common for CubeSats

Downlink Budget		
Description of Parameter	**Value**	**Unit**
Satellite Transmit EIRP	-3.50	dBW
Minimum Elevation Angle	5.00	degrees
Maximum Orbit Height	460.00	km
Earth Equatorial Radius	6,378.14	km
Slant Range	1,971.66	km
Carrier Frequency	436.50	MHz
Speed of Light in Vacuum	3.00E+08	m/s
Wavelength	0.69	m
Free Space Path Loss	151.14	dB

Polarization Loss	3.00	dB
Atmospheric Loss	2.1	dB
Ionosphere Loss	0.4	dB
Isotropic Signal Level at Ground Station	-160.14	dBW
Boltzmann Constant	1.38E-23	J/K
Boltzmann Constant	-228.60	dBW/(Hz*K)
Ground Station Receive Antenna Gain	18.90	dBic
Receiver Equivalent Noise Temperature, Sun Case	807.9	K
Receiver Figure of Merit (G/T)	-10.17	dB/K
Signal to Noise Power Density	58.29	dB-Hz
Data Rate Rb	9,600.00	bit/s
Data Rate Rb	39.82	dB-Hz
Required Link Eb/N0	13.30 [57]	dB
Eb/N0	18.47	dB
Downlink Margin	5.17	dB

14 Appendix B

14.1 B-1 Antenna Deployer Housing

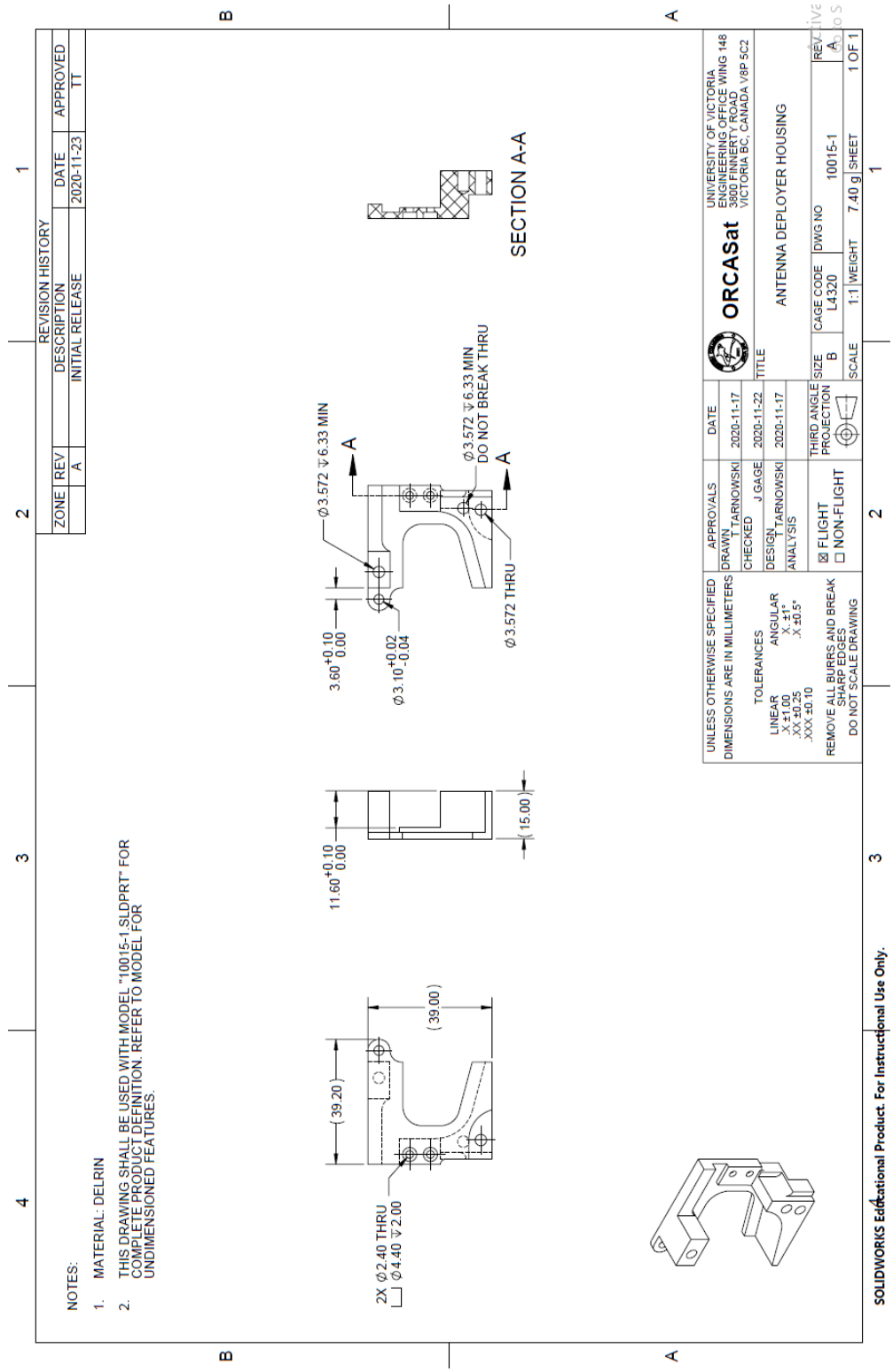

REVISION HISTORY				
ZONE	REV	DESCRIPTION	DATE	APPROVED
	A	INITIAL RELEASE	2020-11-23	TT

NOTES:

1. MATERIAL: DELRIN
2. THIS DRAWING SHALL BE USED WITH MODEL "10016-1.SLDPRT" FOR COMPLETE PRODUCT DEFINITION. REFER TO MODEL FOR UNDIMENSIONED FEATURES.

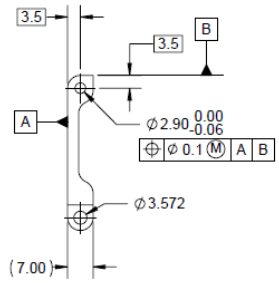

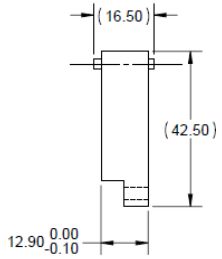

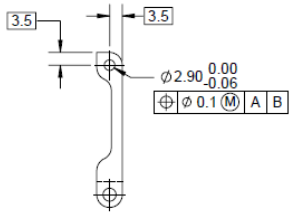

UNLESS OTHERWISE SPECIFIED	APPROVALS	DATE
DIMENSIONS ARE IN MILLIMETERS	DRAWN T TARNOWSKI	2020-11-17
TOLERANCES	CHECKED J GAGE	2020-11-22
LINEAR .X ±1.00 .XX ±0.25 .XXX ±0.10 ANGULAR X. ±1° .X ±0.5°	DESIGN T TARNOWSKI	2020-11-17
REMOVE ALL BURRS AND BREAK SHARP EDGES DO NOT SCALE DRAWING	ANALYSIS	
☒ FLIGHT ☐ NON-FLIGHT	THIRD ANGLE PROJECTION	

ORCASat
UNIVERSITY OF VICTORIA
ENGINEERING OFFICE WING 148
3800 FINNERTY ROAD
VICTORIA BC, CANADA V8P 5C2

TITLE: ANTENNA DEPLOYER DOOR

SIZE	CAGE CODE	DWG NO	REV
B	L4320	10016-1	A
SCALE 1:1	WEIGHT 3.23 g	SHEET 1 OF 1	

14.2 B-2 Burn Wire Mechanism

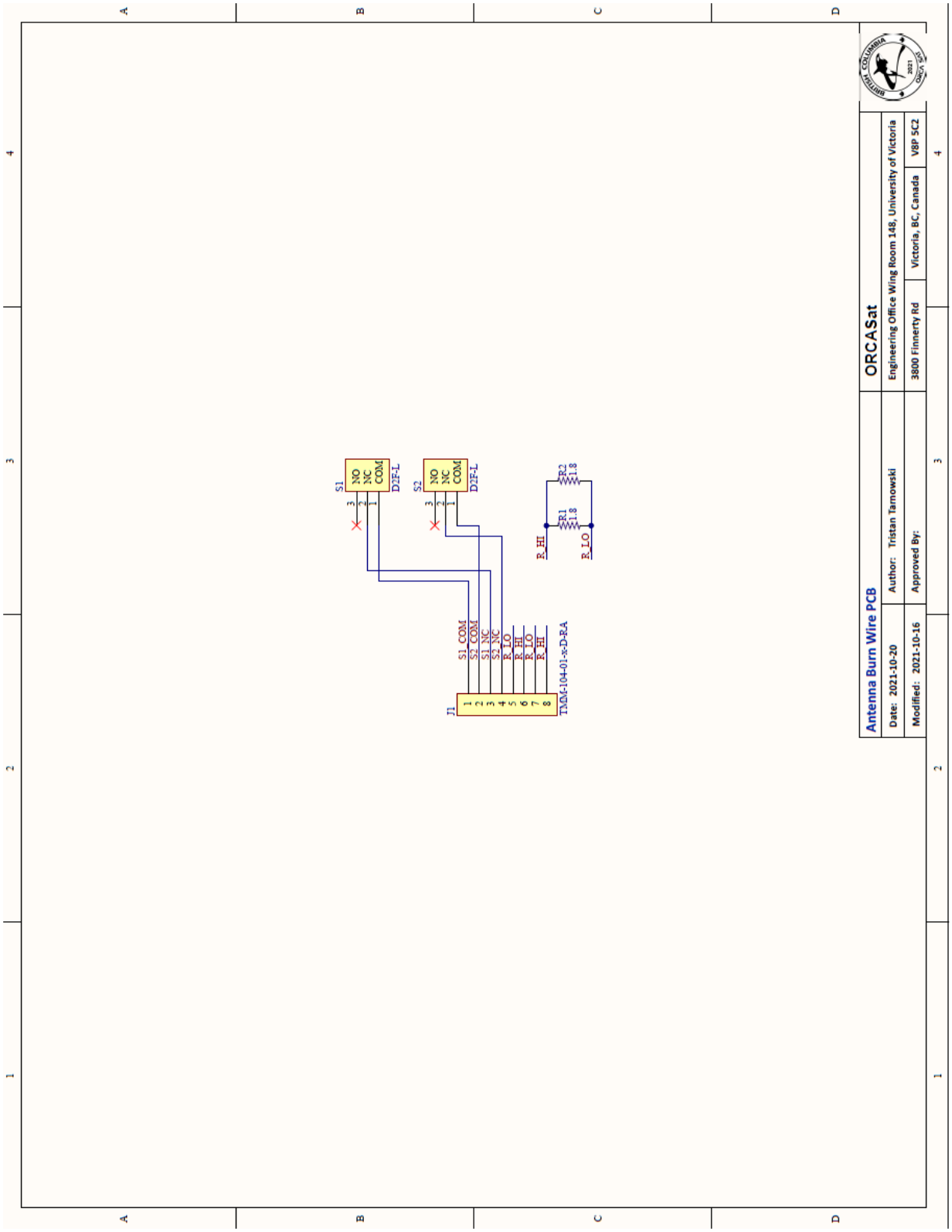

14.3 B-3 Antenna Deployment Circuit

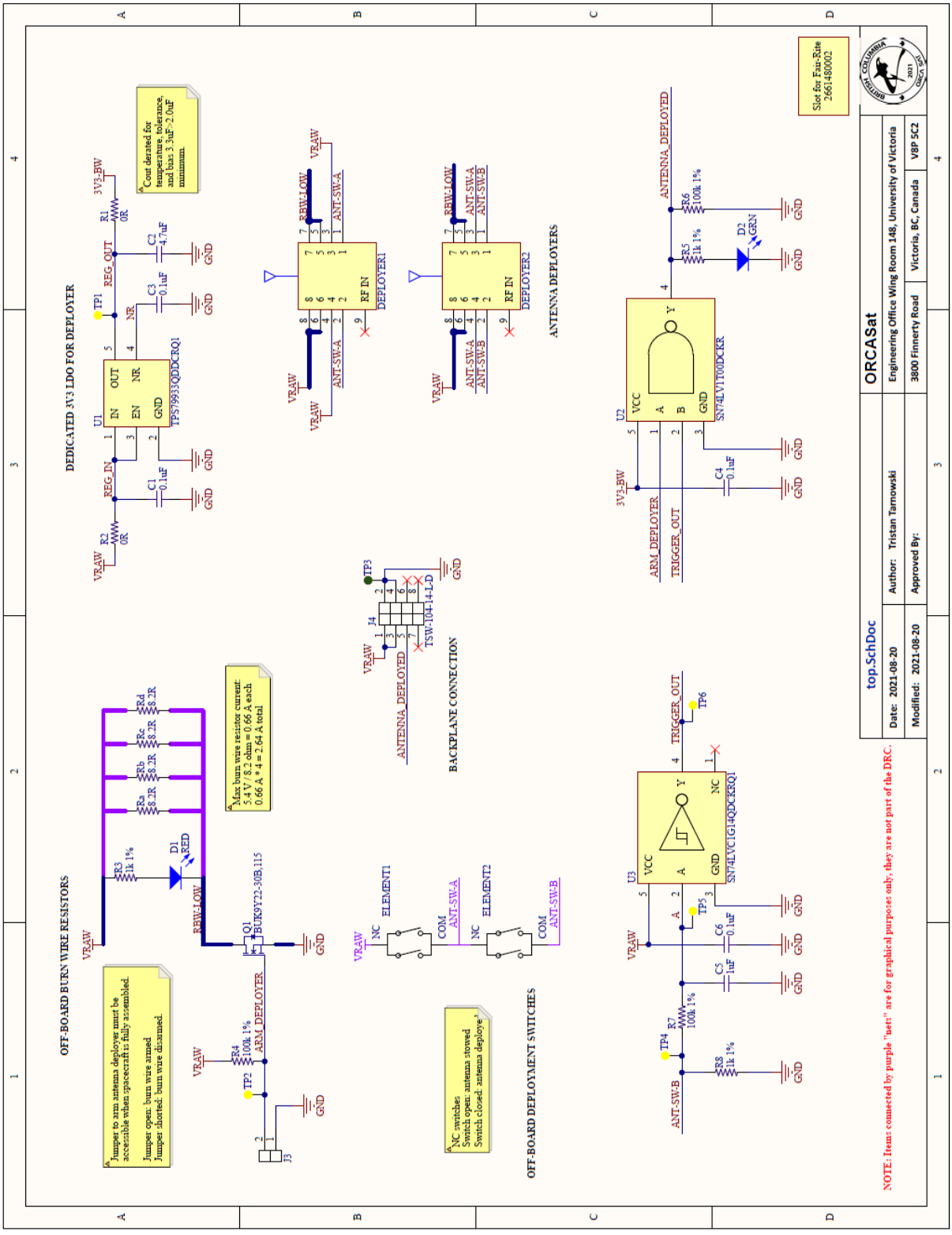

14.4 B-4 TT&C Mechanical Interface Control Document

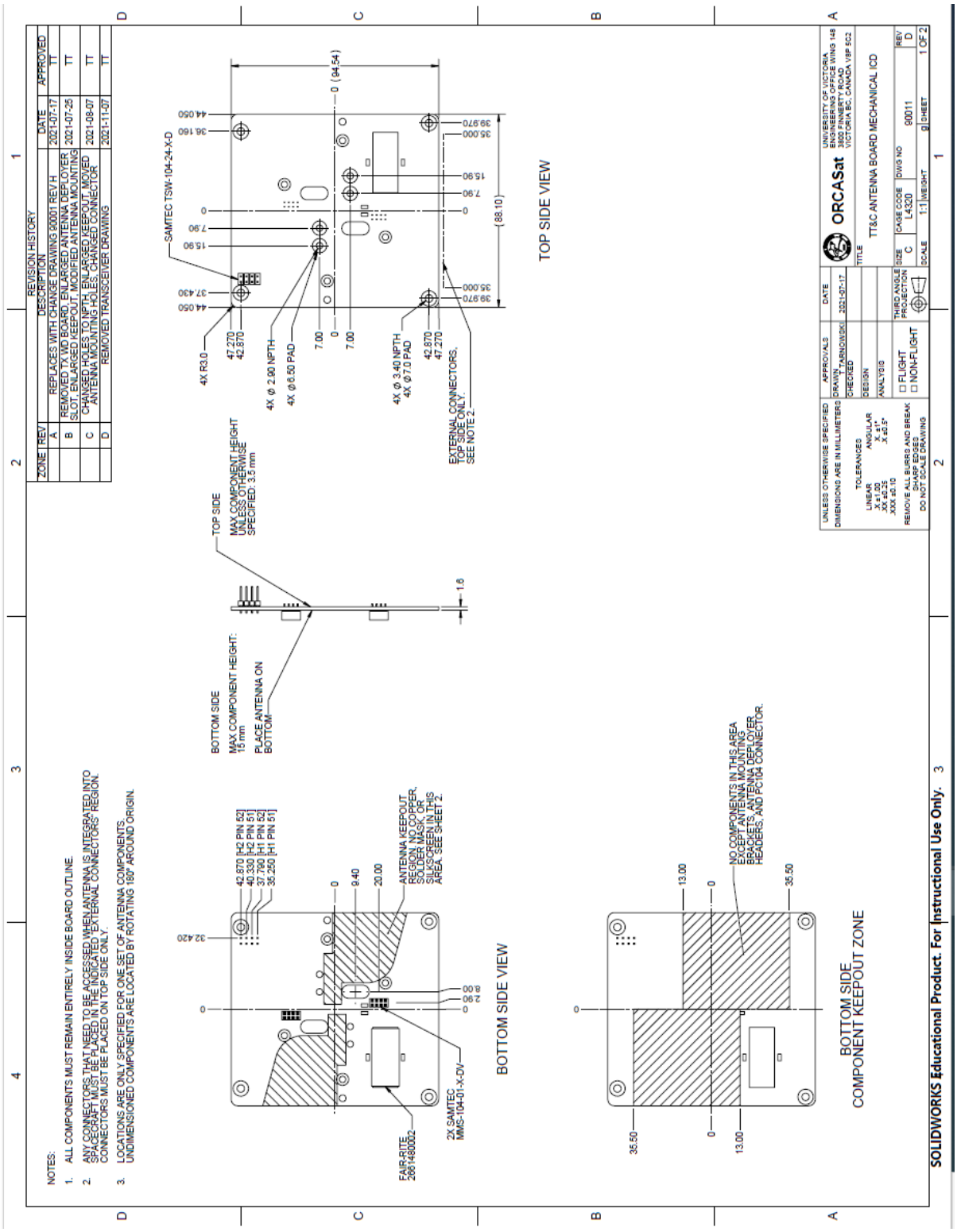

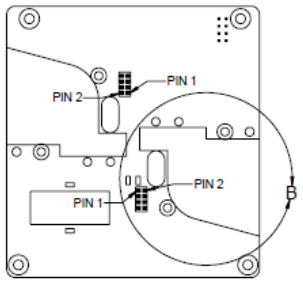

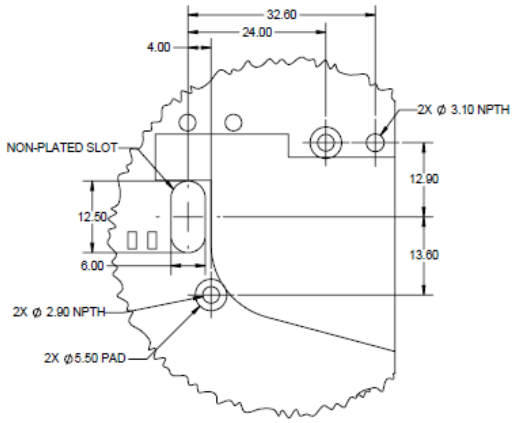

DETAIL B
ANTENNA DEPLOYER FOOTPRINT - HOLES
SCALE 2 : 1

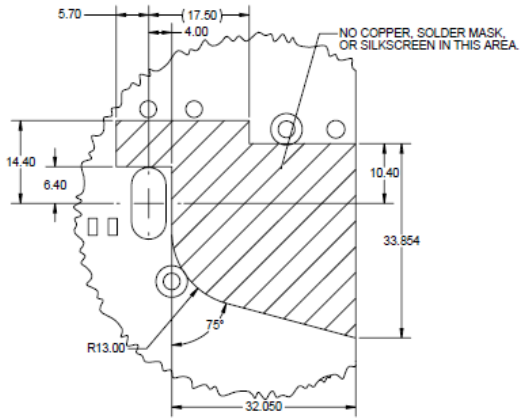

DETAIL B
ANTENNA DEPLOYER FOOTPRINT - KEEPOUT REGION
SCALE 2 : 1

SIZE	CAGE CODE	DWG NO	REV
C	L4320	90011	D
SCALE 1:1	WEIGHT g	SHEET	2 OF 2

REVISION HISTORY				
ZONE	REV	DESCRIPTION	DATE	APPROVED
	A	INITIAL RELEASE	2021-11-07	TT

NOTES:

1. ALL COMPONENTS MUST REMAIN ENTIRELY INSIDE BOARD OUTLINE.
2. ANY CONNECTORS THAT NEED TO BE ACCESSED WHEN TRANSCEIVER IS INTEGRATED INTO SPACECRAFT MUST BE PLACED IN THE INDICATED 'EXTERNAL CONNECTORS' REGION. CONNECTORS MUST BE PLACED ON BOTTOM SIDE ONLY. CONNECTORS MAY BE REARRANGED WITHIN SPECIFIED REGION.
3. POUR WITH CHASSIS GND. REMOVE SILKSCREEN AND SOLDER MASK.
   KEEP SOLDER MASK 0.25 mm AWAY FROM CONTACT AREA.
   KEEP COMPONENTS AND OTHER NETS 1 mm AWAY FROM CONTACT AREA

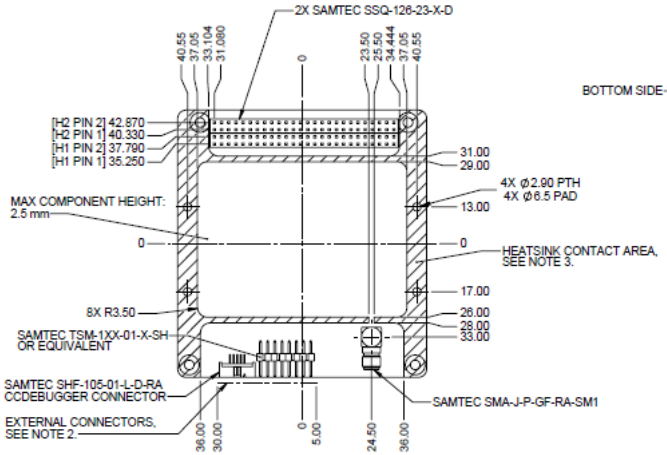

BOTTOM SIDE VIEW

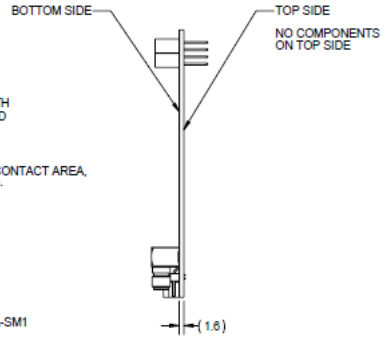

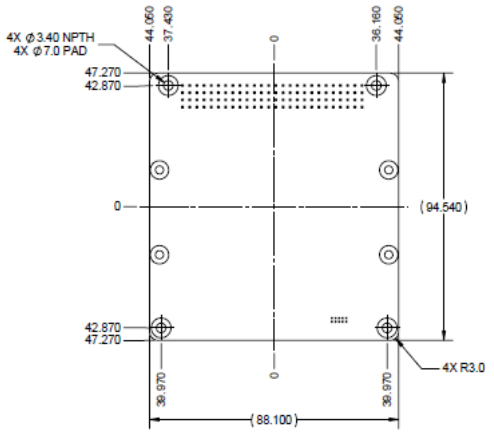

TOP SIDE VIEW

UNLESS OTHERWISE SPECIFIED	APPROVALS	DATE	ORCASat	UNIVERSITY OF VICTORIA ENGINEERING OFFICE WING 148 3800 FINNERTY ROAD VICTORIA BC, CANADA V8P 5C2
DIMENSIONS ARE IN MILLIMETERS	DRAWN T TARNOWSKI	2021-11-07		
TOLERANCES LINEAR .X ±1.00 .XX ±0.25 .XXX ±0.10 ANGULAR .X ±1° .X ±0.5°	CHECKED		TITLE	TT&C TRANSCEIVER MECHANICAL ICD
	DESIGN			
	ANALYSIS			
REMOVE ALL BURRS AND BREAK SHARP EDGES DO NOT SCALE DRAWING	☐ FLIGHT ☐ NON-FLIGHT	THIRD ANGLE PROJECTION	SIZE C / CAGE CODE L4320 / DWG NO 90014 / REV A	
			SCALE 1:1 / WEIGHT g / SHEET 1 OF 1	

15 Appendix C

15.1 C-1 COTS Inductive Choke Baluns

15.1.1 Baluns with Z_0=50 Ohm:

Manufacturer	Manufacturer Part Number	Technology	Outgassing Data?	Power Rating (W)	Turn Ratio	Frequency Range (MHz)	Typical Insertion Loss (dB)	Supply Chain?	Price
Macom	TP-101	Wire	must request	3	1	0.5-1500	0.5	Richardson	231.94 USD
Macom	MABA011115	Wire	must request	2	1	5-3000	0.6	No stock	Does not matter
Mini-Circuits	SYTX1-52HP-15W+	Wire	upscreen upon request	15	1	20-520	0.7	Special order	Does not matter

15.1.2 Baluns with Z_0=75 Ohm:

Manufacturer	Manufacturer Part Number	Technology	Outgassing Data?	Power Rating (W)	Turn Ratio	Frequency Range (MHz)	Typical Insertion Loss (dB)	Supply Chain?	Price
Macom	MABA-011085	Wire	must request	2	1	5-1225	0.6	Not available	Does not matter
Macom	MABA-011013	Wire	must request	2	1	45-1200	0.8	Digi-Key	4.04 CAD
Macom	MABA-011014	Wire	must request	2	1	45-1201	0.9	Digi-Key	4.04 CAD
MiniRF	MRFXF6713-1	Wire	must request	2	1	45-1800	0.6	Not available	Does not matter
MiniRF	MRFXF5R17	Wire	must request	3	1	5-700	0.4	RFMW	2 USD
MiniRF	MRFXF5R16	Wire	must request	3	1	5-700	0.4	RFMW	2.15 USD
MiniRF	MRFXF6713	Wire	must request	2	1	45-1800	0.4	RFMW	2.37 USD
MiniRF	MRFXF0035	Wire	must request	2	1	45-1218	0.5	RFMW	1.75 USD
MiniRF	MRFXF5702	Wire	must request	2	1	45-1200	0.4	RFMW	1.95 USD
MiniRF	MRFXF0024	Wire	must request	2	1	45-1218	0.4	RFMW	1.75 USD
MiniRF	MRFXF0032	Wire	must request	2	1	45-1200	0.4	RFMW	1.75 USD
Mini-Circuits	TRC1-1-122-75+	Wire	upscreen upon request	2	1	2-1250	0.5	Mini-Circuits	1.99 USD
Mini-Circuits	TRC1-1K122-75+	Wire	upscreen upon request	2	1	20-1250	0.9	Mini-Circuits	9.95 USD
Qorvo	RFXF0009H	Wire	no	2	1	45-1200	0.5	RFMW	4.16 USD
Mini-Circuits	ADTL1-12+	Wire	upscreen upon request	2	1	20-1200	1	Mouser	9.52 CAD
Mini-Circuits	NCS1-521+	LTCC	upscreen upon request	2	1	223-520	4.08	Mouser	3.92 CAD
Mini-Circuits	NCS1.5-232+	LTCC	upscreen upon request	2	1.5	400-2300	1.2	Mini-Circuits	0.99 USD
Macom	MABA-011115	Wire	must request	2	1	5-3000	0.8		Does not matter

15.2 C-2 Coaxial Cable Selection

Part Number	Jacket OD (mm)	Static Min. Bend Radius (mm)	Attenuation (dB/m)	Shielding (single, double etc.)	Direct NASA Outgassing Table Reference?
RG-188 A/U	2.60	15	0.57	single	yes
RG-142 A/U	4.95	30	0.35	double	no
RG-303 /U	4.30	25	0.31	single	no
RG-316/U	2.50	15	0.56	double	yes

16 Appendix D

16.1 D-1 Antenna Feed Drawings

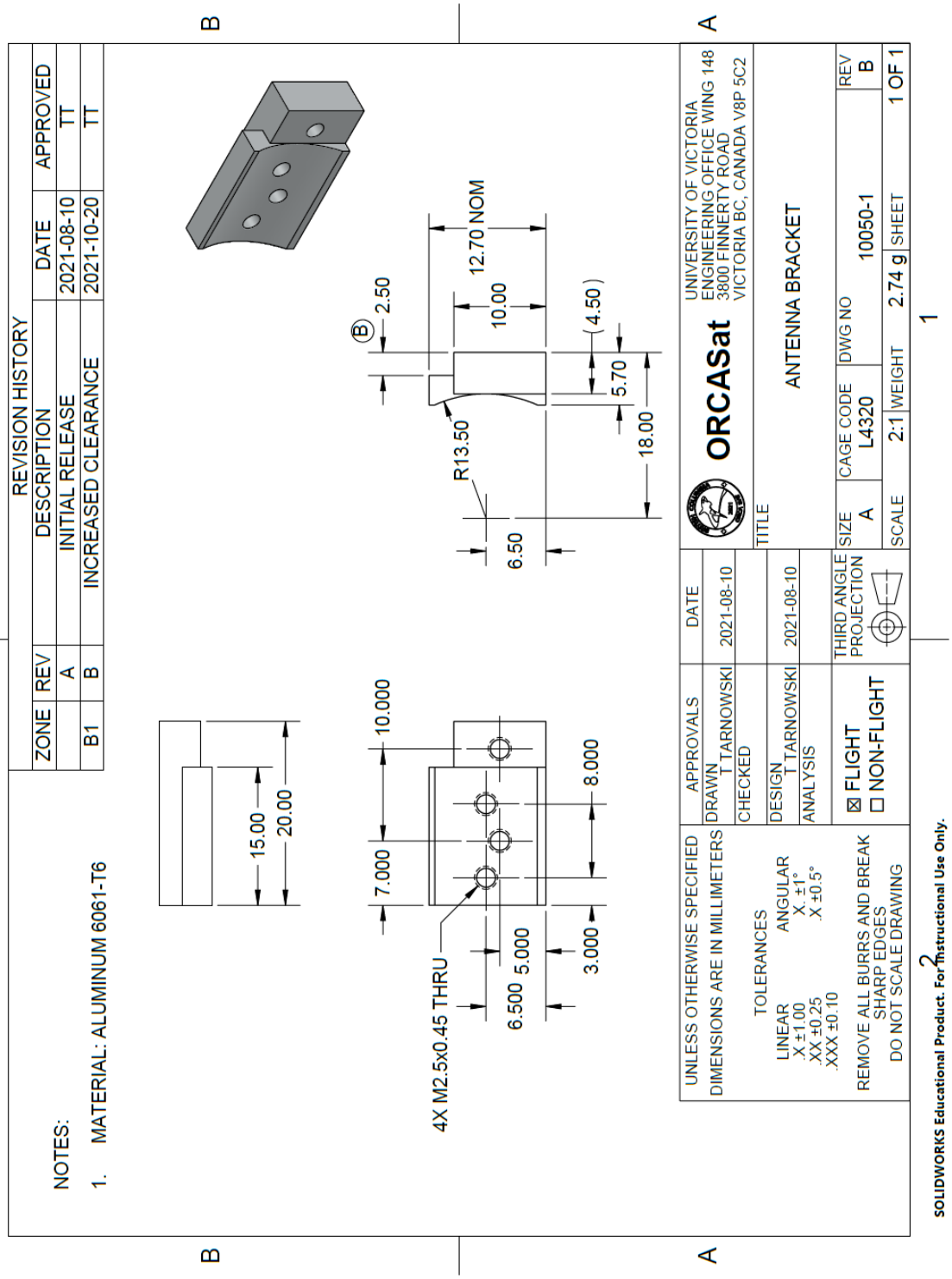

REVISION HISTORY				
ZONE	REV	DESCRIPTION	DATE	APPROVED
	A	INITIAL RELEASE	2021-08-10	TT
B2	B	INCREASED CSINK DIAMETER	2021-10-20	TT

NOTES:

1. MATERIAL: DELRIN

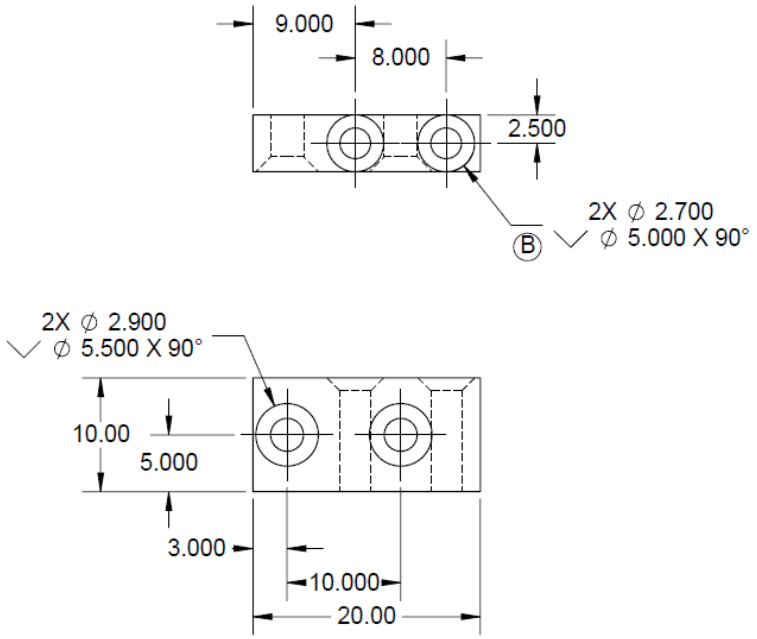

UNLESS OTHERWISE SPECIFIED DIMENSIONS ARE IN MILLIMETERS TOLERANCES LINEAR: .X ±1.00, .XX ±0.25, .XXX ±0.10 ANGULAR: X. ±1°, .X ±0.5° REMOVE ALL BURRS AND BREAK SHARP EDGES DO NOT SCALE DRAWING	APPROVALS / DATE DRAWN T TARNOWSKI 2021-08-10 CHECKED DESIGN T TARNOWSKI 2021-08-10 ANALYSIS ☒ FLIGHT ☐ NON-FLIGHT THIRD ANGLE PROJECTION	ORCASat UNIVERSITY OF VICTORIA ENGINEERING OFFICE WING 148 3800 FINNERTY ROAD VICTORIA BC, CANADA V8P 5C2 TITLE ANTENNA MOUNTING BLOCK SIZE A | CAGE CODE L4320 | DWG NO 10051-1 | REV B SCALE 2:1 | WEIGHT 1.11 g | SHEET 1 OF 1

NOTES:

1. MATERIAL: COPPER 110 SHEET, 0.010 INCHES THICK

REVISION HISTORY				
ZONE	REV	DESCRIPTION	DATE	APPROVED
	A	INITIAL RELEASE	2021-10-06	TT

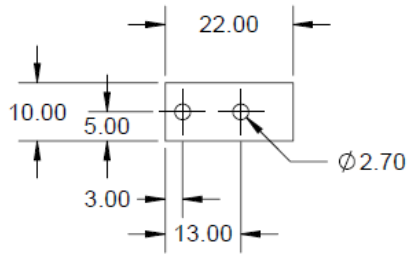

UNLESS OTHERWISE SPECIFIED DIMENSIONS ARE IN MILLIMETERS TOLERANCES LINEAR .X ±1.00 .XX ±0.10 .XXX ±0.05 ANGULAR X. ±1° .X ±0.5° REMOVE ALL BURRS AND BREAK SHARP EDGES DO NOT SCALE DRAWING	APPROVALS / DATE DRAWN T TARNOWSKI 2021-10-06 CHECKED DESIGN T TARNOWSKI 2021-10-06 ANALYSIS ☒ FLIGHT ☐ NON-FLIGHT	THIRD ANGLE PROJECTION

ORCASat

UNIVERSITY OF VICTORIA
ENGINEERING OFFICE WING 148
3800 FINNERTY ROAD
VICTORIA BC, CANADA V8P 5C2

TITLE: COPPER FOIL

SIZE	CAGE CODE	DWG NO	REV
A	L4320	10059-1	A

SCALE	WEIGHT	SHEET
1:1	0.47 g	1 OF 1

REVISION HISTORY				
ZONE	REV	DESCRIPTION	DATE	APPROVED
	A	INITIAL RELEASE	2021-11-15	TT

NOTES:

1. MATERIAL: STEEL, POLYURETHANE COATED
2. MODIFIED FROM STARRETT PART NUMBER KTS12-XX-N.
3. ACTUAL LENGTH DETERMINED BY TUNING WHEN INSTALLED IN SPACECRAFT.

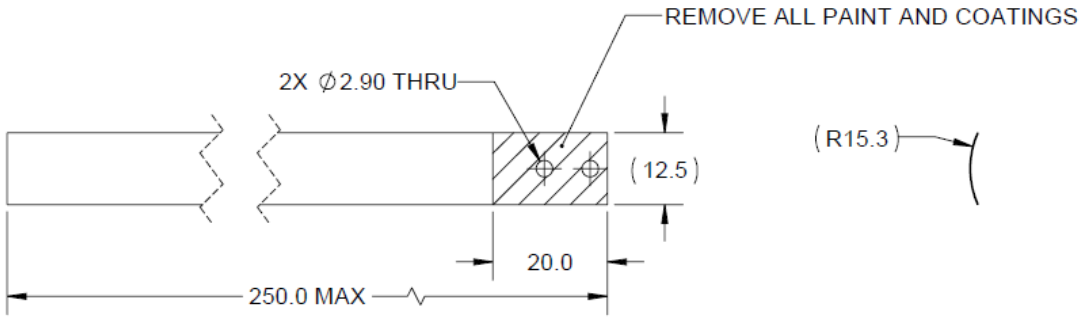

UNLESS OTHERWISE SPECIFIED DIMENSIONS ARE IN MILLIMETERS TOLERANCES LINEAR .X ±1.00 .XX ±0.25 .XXX ±0.10 ANGULAR X. ±1° .X ±0.5° REMOVE ALL BURRS AND BREAK SHARP EDGES DO NOT SCALE DRAWING	APPROVALS	DATE	ORCASat UNIVERSITY OF VICTORIA ENGINEERING OFFICE WING 148 3800 FINNERTY ROAD VICTORIA BC, CANADA V8P 5C2	
	DRAWN T TARNOWSKI	2021-11-15	TITLE ANTENNA ARM	
	CHECKED			
	DESIGN T TARNOWSKI	2021-11-15		
	ANALYSIS			
	☒ FLIGHT ☐ NON-FLIGHT	THIRD ANGLE PROJECTION	SIZE A / CAGE CODE L4320 / DWG NO 10065-1 / REV A	
			SCALE 1:1 / WEIGHT 3.18 g / SHEET 1 OF 1	

16.3 D-3 Antenna Feed Assembly Procedure

1. Cut the coaxial cable to the desired length with a razor blade. Verify that end away form the connector has a clean cut.
2. Mark the coaxial cable 20 mm away from the cut end.
3. Add ferrite onto the cable and put on gloves.
4. Strip the jacket off from the 20 mm mark. Check that shield is intact after stripping.
5. Carefully unweave the shield, all the way to the jacket. Make sure no pieces of it are ripped out.
6. Straighten shield wires and roll them into a single conductor on one side of the cable
7. Mark 10 mm from the end of the cable and strip the dielectric off.
8. Check that all the strands of the centre conductor remain, and no strands of it are cut off or left in the stripped dielectric.
9. Roll the strands of the centre conductor into a single conductor and set the cable aside.
10. Mount the Delrin blocks. Make sure their edges are parallel to the solder mask before torquing them down.
11. Clean the copper tabs with isopropyl alcohol.
12. Tin the edges of the copper pieces (edges facing each other in assembly). Hold them horizontally during tinning so the solder does not bunch up on one end.
13. Tin the centre conductor of the cable.
14. Solder the centre conductor of the cable to the further copper tab. Do this on a flat surface so that the solder does not bunch up.
15. Make sure that the rolled-up shield does not have to pass under the centre conductor of the cable.
16. Tin the shield of the cable.
17. Solder the shield to the other copper tab while making sure that the shield does not protrude underneath the copper tab.
18. Clean the copper tabs with isopropyl alcohol.
19. Clean the aluminum pieces with isopropyl alcohol.

20. Bolt the aluminum to the Delrin with the copper in-between.
21. Stress relive the coax, with the connection point of the zip tie on the other side of the board.
22. Clean the antenna arms with isopropyl alcohol. Mount them to the aluminum.
23. Mount the antenna deployers and the burn wire PCBs.
24. Mount and fix the ferrite in its slot with a zip tie.
25. Measure continuity between arms to ensure that there is no short circuit between them due to assembly problems.

17 Appendix E

17.1 E-1 Raw Data for Antenna Patterns3

E Plane, Single Turn Choke RX (left) and TX (right)

Angle (degrees)	Measured Amplitude (dBm)
0	-31
10	-31
20	-31
30	-32
40	-34
50	-36
60	-38
70	-41
80	-42
90	-43
100	-44
110	-45
120	-45
130	-42
140	-39
150	-37
160	-36
170	-35
180	-35
190	-36
200	-36
210	-37
220	-39
230	-42
240	-44
250	-46
260	-46
270	-47
280	-45

Angle (degrees)	Measured Amplitude (dBm)
0	-31
10	-31
20	-31
30	-33
40	-34
50	-36
60	-38
70	-40
80	-43
90	-46
100	-46
110	-44
120	-42
130	-39
140	-37
150	-36
160	-35
170	-34
180	-34
190	-34
200	-34
210	-34
220	-35
230	-37
240	-40
250	-42
260	-44
270	-46
280	-46

290	-41
300	-38
310	-36
320	-34
330	-32
340	-31
350	-31
360	-31

290	-41
300	-38
310	-37
320	-35
330	-33
340	-32
350	-31
360	-31

H Plane, Single Turn Choke RX (left) and TX (right)

Angle (degrees)	Measured Amplitude (dBm)
0	-33
10	-33
20	-33
30	-33
40	-33
50	-33
60	-33
70	-33
80	-33
90	-33
100	-33
110	-33
120	-33
130	-33
140	-33
150	-33
160	-33
170	-33
180	-33
190	-32
200	-33

Angle (degrees)	Measured Amplitude (dBm)
0	-33
10	-33
20	-33
30	-33
40	-33
50	-33
60	-33
70	-33
80	-33
90	-33
100	-33
110	-33
120	-33
130	-33
140	-33
150	-33
160	-33
170	-33
180	-33
190	-32
200	-32

210	-32
220	-32
230	-32
240	-32
250	-32
260	-32
270	-32
280	-32
290	-32
300	-32
310	-32
320	-32
330	-33
340	-33
350	-33
360	-33

210	-32
220	-32
230	-32
240	-32
250	-32
260	-32
270	-32
280	-32
290	-32
300	-32
310	-32
320	-33
330	-33
340	-33
350	-33
360	-33

E Plane, Double Turn Choke RX (left) and TX (right)

Angle (degrees)	Measured Amplitude (dBm)
0	-30
10	-31
20	-32
30	-33
40	-35
50	-37
60	-40
70	-44
80	-47
90	-50
100	-48
110	-45
120	-42

Angle (degrees)	Measured Amplitude (dBm)
0	-31
10	-31
20	-32
30	-33
40	-33
50	-36
60	-39
70	-43
80	-49
90	-52
100	-49
110	-44
120	-43

130	-40
140	-38
150	-37
160	-36
170	-35
180	-34
190	-34
200	-35
210	-36
220	-38
230	-39
240	-40
250	-42
260	-43
270	-44
280	-44
290	-42
300	-38
310	-36
320	-34
330	-33
340	-32
350	-31
360	-30

130	-40
140	-38
150	-36
160	-35
170	-34
180	-34
190	-35
200	-35
210	-37
220	-38
230	-39
240	-41
250	-42
260	-43
270	-44
280	-43
290	-41
300	-39
310	-37
320	-35
330	-34
340	-32
350	-31
360	-31

H Plane, Double Turn Choke RX (left) and TX (right)

Angle (degrees)	Measured Amplitude (dBm)
0	-33
10	-33
20	-33
30	-33
40	-33

Angle (degrees)	Measured Amplitude (dBm)
0	-33
10	-33
20	-33
30	-33
40	-33

50	-33
60	-33
70	-33
80	-33
90	-33
100	-33
110	-33
120	-33
130	-33
140	-33
150	-33
160	-33
170	-33
180	-33
190	-33
200	-33
210	-33
220	-33
230	-33
240	-33
250	-33
260	-33
270	-33
280	-32
290	-32
300	-32
310	-32
320	-33
330	-33
340	-33
350	-33
360	-33

50	-34
60	-34
70	-34
80	-34
90	-34
100	-34
110	-34
120	-34
130	-34
140	-34
150	-34
160	-34
170	-33
180	-33
190	-33
200	-33
210	-33
220	-33
230	-33
240	-33
250	-33
260	-33
270	-33
280	-33
290	-33
300	-33
310	-33
320	-33
330	-33
340	-33
350	-33
360	-33

18 Appendix F

18.1 F-1 Quote for Professional Antenna Test Services

ANTENNA TEST LAB
Experience. Expertise. Insight.

Cost Estimate

[redacted]

Cost Estimation Number CE3471B

To:	Ship To:
University of Victoria Satellite Design Team Victoria, BC Canada	Antenna Test Lab Co 2210 East Millbrook Rd Unit 113 Raleigh, NC 27604

Date	Requested By	Approved By	Terms
10/19/2021	[redacted]	[redacted]	NET 30

LINE	DESCRIPTION	Rate	QTY	PRICE
1	NRE setup for 375 to 500 MHz antenna testing. Results will include 251 frequencies in 500 kHz steps, with gain in dBi for all directions and patterns. Total gain will be reported along with gain from two orthogonal components. All test data will be supplied in easy to use Excel spreadsheets.	$175.00	1	$175.00
2	Evaluate antenna (integrated on 100x100x227 mm cubesat mockup): 3D spherical gain pattern, with 10 degree resolution (703 "direction" theta/phi grid), calculate and provide radiation efficiency vs frequency and peak gain vs frequency graphs.	$350.00	1	$350.00
3	Perform swept VSWR / Return-Loss testing. Your test results data will include the same frequency steps as above, with return loss and VSWR. All test data will be supplied in easy to use Excel spreadsheets.	$75.00	1	$75.00
4	Tune antenna to 437 MHz by length trimming, before patterning.	$150.00	1	$150.00
5	*** Customer is responsible for all shipping and import/export charges and will prepare and supply all return shipping paperwork and package labels in emailed PDF form ***			
6				
7				
8				
9				
10				
			TOTAL	$750.00

NOTES:

Customers may make their own desktop 3-dimensional plots (at any test frequency) with the software available at...
http://antennatestlab.com/antenna-education-tutorials/plotting